HOST UNIVERSITY: The University of Edinburgh

FACULTY: College of Science & Engineering

DEPARTMENT: School of Engineering

Academic Year 2019-2020

EXPERIMENTAL STUDY ON THE EFFECT OF CHAR FALL OFF ON THE HEAT TRANSFER WITHIN LOADED CROSS-LAMINATED TIMBER COLUMNS EXPOSED TO RADIANT HEATING

Laura Schmidt

Promoter(s): Dr Rory Hadden and Assoc. Prof. Dilum Fernando

Master thesis submitted in the Erasmus+ Study Programme

International Master of Science in Fire Safety Engineering

Disclaimer

This thesis is submitted in partial fulfilment of the requirements for the degree of *The International Master of Science in Fire Safety Engineering (IMFSE)*. This thesis has never been submitted for any degree or examination to any other University/programme. The author(s) declare(s) that this thesis is original work except where stated. This declaration constitutes an assertion that full and accurate references and citations have been included for all material, directly included and indirectly contributing to the thesis. The author(s) gives (give) permission to make this master thesis available for consultation and to copy parts of this master thesis for personal use. In the case of any other use, the limitations of the copyright have to be respected, in particular with regard to the obligation to state expressly the source when quoting results from this master thesis. The thesis supervisor must be informed when data or results are used.

Read and approved,

Laura Schmidt

Brisbane, April 30th, 2020

Total word count: 19,986

Abstract

An experimental investigation of the impact of char fall off on the in-depth heat transfer in medium-scale cross-laminated timber (CLT) members under radiant heating was undertaken. The response of bare CLT columns, which showed debonding of char without exception under both heating conditions (20 and 50 kW/m²), was compared to CLT columns with a glass fibre reinforced polymer (GFRP) layer that effectively prevented all char fall off. Loss of uncharred cross-section, mass loss, thermal penetration depths, in-depth temperatures and the rate of heating were shown to increase in samples that experienced char fall off. This implies a strong effect of char fall off regarding residual structural capacity of engineered timber members in fire conditions that is not accounted for in any numerical analysis or design tools.

A heat transfer model was developed to analyse the influence of different properties of the GFRP composite and the char layer on the evolution of the in-depth temperature profile in the CLT. The numerical results indicated high importance of the surface absorptivity and the formation of an air gap between the glasss fibre layer and the charred timber surface. However, none of the investigated properties alone showed the same effect on the heated depth as that observed in the experimental study. This highlights the need for further research to understand the mechanisms causing char fall off and its consequences for the in-depth heat transfer in engineered timber.

Abstract (Kurzfassung)

Die Auswirkungen der Ablösung verkohlter Holzschichten auf die Wärmeübertragung in Brettsperrholz (Cross-laminated timber, CLT) im Brandfall wurden in einer experimentellen Studie untersucht. Alle Brettsperrholz-Bauteile zeigten Kohleablösungen sowohl unter 20 als auch unter 50 kW/m² Bestrahlung. Der Effekt wurde mit einer Kontrollgruppe verglichen, in der ein glasfaserverstärkter Kunststoff (GFRP) auf der beheizten Oberfläche Kohleablösungen aus der Matrix des Verbundwerkstoffs effektiv verhinderte. Holzkohleablösungen verstärkten den Verlust tragfähigen Querschnitts, Massenverlust, hitzebeinflusste Tiefe, Temperaturen im Querschnitt und die Aufheizgeschwindigkeit. Dies deutet auf einen starken Einfluss von Holzkohleablösungen auf die verbleibende Tragfähigkeit von Holzbauteilen im Branfall hin, der allerdings in Design und Dimensionierung von Holztragwerken bisher nicht beachtet wird.

Der theoretische Einfluss verschiedener GFRP- und Holzeigenschaften auf den Wärmetransport in CLT wurde mit einem numerisches Verfahren untersucht. Die Ergebnisse deuten auf einen starken Einfluss des Oberflächenabsorptionsvermögens sowie der entstehenden Luftschicht zwischen GFRP und Holzoberfläche hin. Keiner der untersuchten Parameter erwirkt jedoch denselben Effekt, der in den Experimenten gemessen wurde. Dies deutet darauf hin, dass dringender Forschungsbedarf bezüglich der Mechanismen hinter der Ablösung der Kohleschicht und ihrer Auswirkungen auf das Brandverhalten von Holzwerkstoffen besteht.

Declaration of Covid-19 Impact

The uncertainties related to the future developments of the Coronavirus situation put us all to the test, some days more than others, some of us more than others. I believe there is no one who didn't suffer from any mental burden of the current situation. To my knowledge, all my loved ones stayed healthy and alive to this day. I can take solace in the fact that my birth country has an excellent healthcare system and I managed to sleep better again from the day that I knew that my parents and my sister were back home and together. I am, however, blessed with friends from all over the world that I hold close to my heart. Friendship means compassion, and listening takes a toll on anyone with empathy easily in times like these. But especially now, when we can't give each other a hug, listening and decency are more important than ever. We are not talking about abstract statistics. Behind all those numbers on the news, there are people, and I have trouble to fade out their personalities, or maybe I don't want to. This section could get quite personal quite quickly, and this document is likely to be published or passed on in a professional context.

I feel fortunate because I had a comfortable place to stayed self-isolated since March 13th, 2020. A good internet connection and VPN from several universities allowed me to access most needed materials online, almost as if I had been working at university. Only the access to some literature has been restrained since university libraries limited their services or could not get a hold of hard copies due to rapidly changed policies.

Most of my experimental work was finished before I stayed in self-isolation. I would have done some more calibrations to study the heat flux I was applying more accurately. This would have improved the quality of the herein presented work. Apart from that, I would really have liked but did not need to test some samples with altered properties, like a different kind of glass fibre, or perform some tests at other heat fluxes. Instead, I took the time to do a more thorough analysis of the already collected data. That allowed for a deeper understanding of the phenomena of interest.

Since travel between Brisbane and Edinburgh became impossible, my first supervisor and I were not able to have a single face-to-face meeting since December 2019. However, this also meant we were already quite practised in meeting online at the time of the Covid19-restrictions. It was more challenging to exchange knowledge with other members of the Fire groups of the Universities of Edinburgh and Queensland. Several online presentations made up for some of this. It would definitely have been valuable to get more perspectives on my work. In the current situation, I just look forward to the day when I can present my completed work to my colleagues and hear their thoughts then – as our research work will be developing continuously in any case.

Project Status Declaration

School of Engineering – Incident Management

Project Status Declaration

This form is to be used in unforeseen circumstances necessitating the immediate cessation of practical project work during semester. It acts as a record of the current status of practical work (whether it be laboratory based, computational, or fieldwork). Due to circumstances, ***no further practical work is to be continued, regardless of the type of work or current status***. This ensures equality of opportunity for all students, regardless of the type of work being undertaken.

The form must be completed during a meeting with the student, and verified by the student, supervisor, and either the thesis examiner, or a second supervisor. **Any practical work beyond that stated in this form will not be considered in the final project assessment.**

A copy of the signed form must be included in the final project submission.

Name: Laura Schmidt _____ Student number: s2006212 _____

Work completed

All items of wholly, or partially completed work must be listed, indicating the percentage completion for each task. Reference can be made to an attached project plan if appropriate. **Please take care to provide a full detailed list of all work done.**

- 19 experiments of CLT columns in loading frame with radiant panel (12 CLT columns without glass fibre reinforced polymer, 7 CLT columns with glass fibre reinforced polymer) (100% completed)
- Rudimentary heat flux calibration of the radiant panel to determine distance between samples and radiant panel for tests (100% completed)
- Measurements of char depths and remaining depths of cross section (10% completed)

Project Status Declaration Page 1 of 2

Work not commenced

Any items of outstanding work that have not been started should be listed here.

- Proper heat flux calibration of the radiant panel to determine exact heat flux over exposed area and variation applied during tests (0% completed)
- Heat flux calibration of the radiant panel over time to determine fluctuations over time and duration to reach steady heat flux (0% completed)
- Sanity check of LVDT and string gauge displacement data (0% completed)
- Additional experiments with altered samples or setup (e.g. different glass fibre thickness, different heat fluxes). 6 more CLT columns would have been available for an extension of the experimental matrix. (0% completed)

Plans for completing project submission

State revised plans for producing the final project submission in the absence of any additional practical work beyond that already listed. For example, this may include literature based research, or more in-depth analysis of results already obtained. Dates for completion of each element should be given.

The last test of the experimental matrix was completed on March 4th, 2020. Therefore the thesis work will not be greatly affected.
The remaining time until April 30th, 2020 will be used to complete in-depth analysis of the already obtained data, a literature review and writing up of the thesis.

Declaration

To the best of our knowledge, this form is an accurate record of the project status and revised

completion plans on 18.03.2020 _____ (date)

Student: L. Schmidt _____ (Signature)

Supervisor: _____

Second sup./Thesis examiner: _____

Acknowledgements

The four months spent on this Master thesis were an amazing finish to the two most inspiring years of my whole university studies. The IMFSE and its people created an outstanding learning environment. I would especially like to thank my supervisors Dr Rory Hadden and Associate Professor Dilum Fernando for their guidance with this thesis project. I feel very fortunate about all the knowledge and experience you shared with me. The trust and encouragement with which you let me explore my ideas independently and your enthusiasm which with you got involved are genuinely appreciated.

The School of Civil Engineering and the Fire Safety Engineering research group at the University of Queensland provided this project with support from technical staff and access to laboratory facilities. There are many people without whom this work would have been impossible. I would especially like to acknowledge the help of Stewart Matthews, Dr Van Thuan Nguyen, Jeronimo Carrascal, and Shane Walker with the experimental aspects of this thesis. The inspiring discussions with and the practical help from the Fire Safety Engineering research group enriched this work and made it infinitely more enjoyable. Thank you Ian Pope, Dr Felix Wiesner, Abdulrahman Zaben, Hangyu Xu, Jaime Cadena, Luis Yerman Martinez, Hons Wyn and Dr David Lange. I am also thankful for the support from the UQ Composites group.

The entire IMFSE group taught me a lot about friendship and collegiality. My friends, Antonela and Cathleen, motivate me every day to give my best while loving me for who I am. You were a huge support, not only near the finish line. Thanks Stefanie and Haydn for pointing out how much fun we are having! And Julia, I am deeply grateful for many years of unconditional friendship, and that you are patient enough to stay friends with me, even through the far journeys of my studies. You are with me wherever I go.

Without the support of my family I would certainly not have made it to where I am today. While I know that my travelling, studying and living abroad has often kept us apart for too long, I am very happy that I can make you proud. Thank you for giving me both roots and wings. I will always be home when I'm with you.

Hebt man den Blick, so sieht man keine Grenzen.

Table of contents

List of figures

Notation

Terminology

a	Absorptivity (-)
c_P	Specific heat capacity (J/kgK)
ΔH_p	Heat of pyrolysis (kJ/g)
I_{th}	Thermal inertia (W^2s/m^4K)
k	Thermal conductivity (W/mK)
m	Mass (kg)
$\dot{m}''_{crit}$	Critical mass loss rate
$\dot{m}''_p$	Mass loss rate (kg/s)
$\dot{q}''_{air\ gap}$	Heat flux through air gap (kW/m^2)
$\dot{q}''_{cond}$	Conductive heat transfer per unit area (kW/m^2)
$\dot{q}''_{in}$	Incident heat flux (kW/m^2)
$\dot{q}''_{out}$	Heat flux leaving the solid (kW/m^2)
T	Temperature (°C)
t	Time (s)

Greek letters

α	Thermal diffusivity (m^2/s)
$\delta_{air\ gap}$	Air gap thickness (mm)
ε	Emissivity (-)
ρ	Density (kg/m^3)

Acronyms

CLT	Cross-laminated timber
EP	Epoxy resins
FRP	Fibre reinforced polymer
GF	Glass fibre
GFRP	Glass fibre reinforced polymer
Gypro	Generalized pyrolysis model
HFT	Hybrid Fibre Reinforced Polymer Timber
MUF	Melamine-urea-formaldehyde
PUR	Polyurethane
TGA	Thermogravimetric analysis

Chapter 1 Introduction

The objective of the fire safety design for buildings is to guarantee life safety and property protection. To deliver that, fire safety strategies incorporate fundamental principles such as egress unaffected by the fire and structural integrity during and after the duration of the fire. Compartmentation and structural integrity are the two essential components of fire safety strategies for buildings that ensure the safe evacuation of occupants over extended periods and the life safety of fire service personnel.

Over the past decades, the demand for timber construction has seen a renaissance worldwide with a newly added interest in high-rise timber structures due to timber's potential for more sustainable construction. Naturally grown wood is often processed into wood composites, called "engineered timber". By minimizing defects and variability of mechanical properties, engineered timber products achieve increased dimensional stability and more homogeneous and predictable mechanical properties. One of the most commonly used types of engineered timber is cross-laminated timber (CLT) made from several layered timber boards (lamellae) that are stacked crosswise, i.e. with fibre-directions alternating at 90° for enhanced dimensional properties. Typically, CLT consists of three to seven layers that are glued together under pressure. Cross-laminated timber is used internally and externally for load-bearing walls and floor elements [1]. However, the lack of understanding of the complex behaviour of these products under fire conditions limits their applicability, especially in mid- and high rise buildings [1], [2].

Re-introducing timber as a construction material for modern buildings fundamentally changes the hazards compared to non-combustible construction materials like steel or concrete [3], the dominant construction materials of the twentieth century. Wood is an organic charring material, unlike steel and concrete, and undergoes complex combustion reactions that are not fully understood to-date. It is known that heated timber thermally decomposes mainly by releasing water,

combustible and non-combustible gases and forming a solid char residue. The burning of the combustible gases releases additional energy that will increase the fire growth within compartments with exposed timber members. It can also affect the potential for spread of fire to other compartments or adjacent buildings.

The mechanical properties of structural timber elements gradually reduce as the timber heats up, with significant irreversible strength reductions already starting from moderate temperatures around 65 °C [4]. To maintain structural integrity, it is therefore desirable to keep as much of the timber structure at low temperatures for as long as possible. For this reason, the transfer of heat inside the timber needs to be reduced as much as possible.

In loaded timber members, the thermal and mechanical degradation are linked, which increases the complexity of the structural analysis of heated timber elements. Together with the reduction of the cross-section of fire exposed timber members due to the combustion of the timber itself, the loss of load-bearing capacity might endanger the required structural performance for fire safety. Eventual self-extinction of the structure is critical to limit fire spread to the compartment of origin and to reduce the damage of the load-bearing elements to a minimum. The movable fuel in the compartment needs to be consumed and the fire starved before self-extinction of exposed timber members can occur. That means the timber structure is required to survive burnout which entails that structural integrity is maintained for sufficient durations, even at elevated temperatures typical of compartment fires.

The natural solid char is one product of the combustion process of timber. This residue, left at the surface after oxidation of the combustible gases, reduces the heat exposure of the underlying timber sections [5]. Like a thermal insulator, the char reduces the heat flux into the underlying timber and lowers the depth that experiences heating. As less and less timber thermally decomposes, the production of combustible gases reduces. This can eventually promote self-extinction of the burning timber structure.

While the formation of a char layer can protect deeper timber sections, the fall-off of charred timber sections exposes the underlying timber structure as additional fuel to the fire, increasing burning rates or the duration of the fire. This effectively delays or prevents the self-extinction and increases the risk of total burnout of the structure. Char fall off also promotes the thermal degradation of the mechanical capacity of greater fractions of the timber cross-section, lowering the load-bearing capacity of the remaining structural section and increasing the risk of structural collapse.

Char fall off is a huge barrier for the design of timber construction, especially as in makes it impossible to ensure adequate fire safety in high-rise timber buildings. The problem of char fall off gained increased attention when exposed engineered timber was investigated increasingly, as char fall off was often seen in connection with the adhesive-lamellae interfaces.

Many failure mechanisms within the timber structure are suspected of causing or promoting char fall off. To date, the phenomenon is still poorly understood and seen as highly stochastic and unpredictable. There are two possible approaches to the problem: It can be attempted to understand char fall off in full detail to be able to predict its occurrence and effects. Alternatively, potential measures to minimize or prevent char fall off can be tested. Comparison with the original timber system can then allow understanding the effect of char fall off on the underlying timber.

Including an additional layer of an inert material like glass fibre mat in the matrix surface of the engineered timber product has potential to hold the char in place even after the char layer detaches from the underlying timber structure. Preventing char fall off allows exploiting the insulating properties of char that reduce the heat transfer through the timber and thereby promote colder in-depth temperatures. Lower temperatures within the timber will decrease the contribution of fuel to the fire and reduce the degradation of mechanical properties. Hindering char fall off will also increase the predictability of the reaction to fire of the timber structure as it minimizes

its stochastic nature.

Glass fibre reinforced polymers (GFRP) are widely used to achieve improved mechanical properties of load-bearing structures at ambient temperatures. The potential of fibre-reinforced composite materials to improve the bending stiffness and strength of timber and make it competitive with steel and concrete has been investigated for decades [6]. A previous experimental study served as a proof-of-concept that non-combustible fibres can also improve the burning behaviour of laminated timber [7]. This thesis will explore the potential of GFRP to obstruct char fall off from cross-laminated timber columns exposed to external radiant heat flux and the implications of retaining the char layer for the propagation of the thermal wave within the timber.

1.1 Aim and objectives

This thesis aims to investigate the thermal effect caused by char fall off on the fire performance of cross-laminated timber, in particular the progression of the thermal wave in-depth of the material. A potential reduction of char fall off through the inclusion of a glass fibre reinforced polymer (GFRP) in the matrix of cross-laminated timber (CLT) will be explored experimentally. This research will enable a deeper understanding of the potential of glass fibre reinforced polymers to mitigate or control hazards introduced by using timber construction.

The following objectives defined this thesis:

- Qualitatively assess the effect of char fall off in structurally loaded CLT columns with and without one layer of GFRP on the exposed surface under fire conditions.
- Quantify differences in the occurrence of char fall off under different external heat fluxes and with and without GFRP.
- Quantify the heated depth through measuring in-depth temperature histories in the loaded CLT columns exposed to high heat fluxes.

- Analyse the impact of the GFRP on the heat transfer within the CLT.
- Investigate the implications for the load-bearing capacity of the CLT columns based on these observations under different heating conditions.

1.2 Scope

The scope of this thesis is to understand the effect of GFRP on one particular timber system. An exemplar medium-scale setup was used to observe char fall off of heated cross-laminated timber columns under the effect of a constant bending load. The impact of char fall off on the thermal penetration was investigated by comparing the system response under external heat fluxes of different magnitude and with and without GFRP.

Chapter 2 Literature Review

This chapter attempts to provide a review of relevant literature regarding the thermal decomposition and combustion of timber. This will allow for a deeper understanding of the important concepts that will be investigated experimentally and numerically in later chapters. Previous findings regarding the phenomenon of char fall off and its implications for the burning of engineered timber will be presented. Then glass fibre reinforced polymers (GFRP) used for strucutral and thermal reinforcement will be introduced. Lastly, different numerical tools of varying complexity will be presented that were proposed by other authors to understand and predict the burning behaviour of timber. The previous work of other authors will be regonized as relevant to the aims and objectives of this thesis and enables the research presented in the following chapters.

Wood is a naturally grown composite material, consisting of a range of different polymers (mainly cellulose, hemicellulose and lignin) forming longitudinal fibres [1], [8]. This makes wood orthotropic: Its mechanical and thermal properties vary with the grain direction. Generally, the two directions considered in timber design are along and orthogonal to the fibre (often referred to as the principal directions) [9]. As a naturally grown material, wood shows variability of properties not only between species or regions of growth but even within the same tree. Variations were found to depend on factors like tree genetics, forest management or environmental conditions [4]. Its inhomogeneity and unpredictability make it difficult to design with solid timber and often require over dimensioning to ensure structural safety.

Engineered timber products are composite materials commonly made from timber boards, veneers or strands and adhesive [1]. One of the most commonly used types of engineered timber is cross-laminated timber (CLT) [4]which this thesis focusses on. Cross-laminated timber is made from sawn panels (lamellae) that are glued together with perpendicularly alternating fibre directions of neighbouring boards. A range of adhesives can be used in the CLT production to bond the individual

timber panels together. The most common adhesives used in CLT production are melamine-urea-formaldehyde (MUF) and polyurethane (PUR) [4], with this thesis focusing exclusively on PUR-bonded CLT. Polyurethane glues are easy to apply and do not require the application of heat to harden. Instead, the moisture in the timber serves as the activating agent [10]. Adhesives generally show lower variability than the timber itself because the production follows specific formulations. However, producers often do not readily provide information on the exact formulations of the used adhesive types [4]. The discontinuity of engineered timber and the possible variation between adhesive properties increase the complexity of the analysis and design, especially for extreme conditions like fire.

The development of engineered timber products opened up new possibilities for timber construction with increased interest in timber construction worldwide. Engineered timber has an excellent strength-to-weight ratio [11], [12] which makes it especially efficient in tall structures or structures with long spans [1]. The cost of engineered timber construction can be competitive with traditional construction materials steel and concrete when costs of labour, material and connections are accounted for [13], [14]. This is an incentive for future investments in timber structures. However, fire safety requirements can significantly increase the cost of timber building in comparison with other construction methods [14]. The presented incentives of timber construction thus motivate for further research to enable safer and still cost-effective timber construction.

2.1 Burning of timber

Many studies have been undertaken to investigate the burning of timber [5], [15], [16]. It is known from these studies that as a combination of natural polymers, timber decomposes mainly by releasing water, combustible and non-combustible pyrolysis gases and forming a solid char residue when exposed to heat.

The thermal decomposition of wood is a function of temperature that has been

investigated by many authors [5], [15], [17]–[20]. Wood is a composite material, consisting of many different components that form different types of layered cell structures, all of which determine the mechanical properties [1]. The various components and cell structures decompose at different temperatures. Timber gradually loses its load-bearing capacity when heated. Moderate temperatures around 65 °C can cause a permanent reduction of the mechanical properties of timber [4]. Experimental conditions strongly impact findings on strength reduction by heating. For example, the loading cases tension and compression lead to a different decline of strength and elastic modulus. This increases the complexity of the structural analysis of heated timber elements [4]. The chemically unbound moisture inside the timber evaporates when it is heated to temperatures above 100 °C. The chemical decomposition under heat (pyrolysis) includes many different, partly interdependent chemical reactions which can affect the load-bearing capacity of timber [5]. The production of combustible pyrolysis gases and a solid residue (char) is most often assumed to take place at 300 °C. At even higher temperatures, the char continues to smoulder and oxidise in the presence of sufficient oxygen[15].

These different phases of decomposition in series have been widely accepted to describe the process of thermal disintegration of wood. There is still a certain degree of disagreement concerning the exact temperature boundaries of these phases. While some authors pick values as low as 200 °C as the critical value above which the timber entails zero residual strength, other refer to the 360 °C-isotherm as an indication of the position of the pyrolysis front [4], [18]. The disagreement could be attributed to the many different components that timber consists off, all of which start to decompose at different temperatures. The content of the individual components can vary, for example, among different species. As in reality, these phases of decomposition may overlap and are not sharply defined, a varying definition of the “onset of pyrolysis” could introduce further deviation. The amount or concentration of pyrolysis gases that can practically be measured or the chosen variation from the ambient condition set as

the criterion to mark the onset of pyrolysis could influence this.

Moreover, when listing single temperature values, it is not always clear if this is the surface temperature of the timber samples (and surface temperatures are nearly impossible to measure accurately) or at specific depths. The density (ρ), specific heat capacity (c_p) and conductivity (k), as well as the moisture content of the timber, were shown to influence the in-depth temperature evolution. These are all highly variable between species but also environmental conditions. A strong influence of the way that the timber temperature is measured could be another factor: Fore example, thermocouple diameter, placement and position can all largely influence the accuracy of measured (in-depth) temperatures. All this can lead to significant variations in the determined critical temperatures for the different decomposition phases of heated timber[a]. Table 1 lists the temperatures and respective degradation phases of heated wood products most highlighted in the relevant literature that will be adopted in the following.

Table 1. Temperature ranges of wood decomposition and pyrolysis at elevated temperatures.

Temperature	Event	Reference
From around 60 °C	Irreversible changes to the strength of timer	[4], [19]
Around 100 °C	Arrest in development of temperatures usually observed due to latent heat evaporate moisture; prolonged heating can convert hemicellulose and lignin into char	[5], [15], [20]
From 150 °C	Exothermic heat generation in timber	[20]
Around 200°C	Mass loss due to slow pyrolysis (mainly non-combustible volatiles); prolonged exposure causes slow-charring	[5], [8], [15]
225 °C	Onset main pyrolysis reactions (combustible volatiles)	[5], [15]
288 °C (550 °F)	Position of the char front {North America}	[5]
300 °C	Onset (rapid) pyrolysis (decomposition of main components); Position char front {elsewhere}	[5], [8], [17], [19]
Above 350 °C	Char oxidation continues (production of non-combustible volatiles and heat, increasing the surface temperature of the timber to values possibly above 700 °C)	[3], [15], [21], [22]

[a] Direct communication with Ian Pope (The University of Queensland) on his recent findings regarding thermocouple errors.

As a thermally thick material, the timber of proportions of interest for structural applications undergoes transient heating with a significant temperature gradient in depth. Therefore, the above presented temperature-dependent processes are likely to take place often concurrently, potentially affecting each other. The zones in which the different processes take place are therefore as indefinite as the temperature boundaries guarding them.

As highlighted above, the burning of timber is a combination of processes. The mass loss rate ($\dot{m}_p''$) given in Equation 3 is a measure of the formation of pyrolysis gases escaping from dry solid timber. The remaining solid residue of decomposed timber is char. Therefore, pyrolysis and charring are coupled, and consequently the burning of the structure can never be seen independently from the char progression.

$$\dot{m}_p'' = \frac{\dot{q}_{in}'' - \dot{q}_{out}''}{\Delta H_p} \quad (1)$$

$$\text{rate of char formation} \approx \frac{\dot{m}_p''}{\rho_{\text{timber}} - \rho_{\text{char}}} \approx \frac{\dot{m}_p''}{\rho_{\text{timber}}} \quad (2)$$

As a function of local temperature, pyrolysis and char formation propagate within the timber with the thermal wave. It is a direct function of the incident heat flux that travels into the solid ($\dot{q}_{in}''$), which is a fraction of the external heat flux received by the surface of the timber.

It is generally acknowledged that an additional external incident heat flux is necessary for sustained flaming, i.e. that thermally thick timber above a certain geometrical threshold will not burn on its own. [5], [23]. Reszka and Torero [24] describe timber as practically inert below 10 kW/m². Combustible pyrolysis gases need to be produced at a sufficient rate to create flammable conditions on the timber surface. The corresponding critical heat flux for piloted ignition is generally given between 10 and 13 kW/m², found in bench-scale experiments [8], [19]. The critical heat flux for non-piloted ignition is listed as 28 kW/m² by Drysdale [8], while Emberley [23] found the heat flux for auto-ignition to be above 30 kW/m².

In contrast, Hottel reported critical heat fluxes of 28 kW/m² for piloted ignition and 63 to 71 kW/m² for auto-ignition. These values are significantly higher than those reported above [8], [23], [26]. The deviation was attributed to differences in the testing apparatus and method [5]. Therefore, the observed difference highlights the potentially strong influence of the surrounding environment, geometry and orientation in timber testing. It also shows that there are design factors that could potentially be manipulated to delay the onset of flaming combustion.

Following the same principle as ignition, combustion reactions will cease below a critical heat flux which has been shown to be as high as 30 kW/m² for solid timber and CLT in small-scale tests [23], [26]. For CLT made from Radiata Pine, which will be investigated in this thesis, Emberley [27] found a critical heat flux for self-extinction of 44.6 ± 0.9 kW/m². Below these values, heat losses will become dominant and the pyrolysis reactions will significantly reduce, eventually leading to self-extinction of the timber. Smouldering combustion of timber will cease below 6 kW/m² [28].

Gorska [29] found different critical incident heat fluxes in medium-scale CLT compartment tests. The authors attribute the deviation to heat losses through the boundaries as the ratio between surface area and volume changes. Therefore a scaled-down test would achieve different temperature gradients in the timber structure than large-scale tests. Similarly, any design varying in size, geometry or ventilation from test scenarios would have different boundary conditions and thereby different heat losses. It is therefore difficult to use strict numerical borders for incident heat fluxes. Only a truly holistic approach can take into account all factors affecting the burning and charring of timber.

The amount of mass flow of combustible gases per unit time below which extinction will happen is a fraction of the "critical mass loss rate" ($\dot{m}''_{crit}$), describing the production of combustible and non-combustible gases. For general wood, Bartlett [5] states critical mass loss rates between 2.5 g/m²s and 5 g/m²s. For CLT, Emberley [23] states 4.0 g/m²s, while Bartlett found [26] 3.5 g/m²s and that a

temperature gradient of 28 K/mm at the char line correlates with this critical mass loss rate for CLT. In another study, Emberley [27] specifically reports 3.65 ± 0.2 g/m²s for CLT made from Radiata Pine, which will be used for the experimental study presented herein.

The incident heat flux is generally seen to be the dominant factor affecting the burning rate of timber, with an effect that is one order of magnitude higher than other studied parameters. In his review on burning of timber, Bartlett [5] found general agreement between authors that increasing the incident heat flux leads to higher burning rates (in an approximately linear relation, as shown in Equation 3) and increased heat penetration depths. Closer investigation of the time-dependency of the burning of timber showed that the external heat flux largely affects the initial burning rate while later steady-state values showed lower sensitivity [30].

The typical development of the burning rate of charring solids like timber shows an initial peak, shortly after ignition. Then the burning rate decreases to a quasi-constant value [5], [23], [31]. Steady-state burning of timber can only take place if the char layer reaches a steady-state thickness.

Char is the residual remaining after the moisture evaporation and pyrolysis of timber. During the thermal decomposition of heated timber turning into char, the thermal material properties change significantly. The different material properties of virgin timber and char, observed by two different authors, are given in Table 2.

The thermal conductivity, density and specific heat capacity of char are approximately halved compared to timber. In an extensive review of different sources, Bartlett [5] states that the density of char is typically five times lower than the density of virgin wood. The deviation between this observation and the listed values could be caused by species-dependent properties as the different components of wood undergo different decomposition processes. For example, higher lignin content results in increased char yield in softwoods [8]. A difference in the initial moisture content of the virgin wood would lead to a higher initial weight per unit volume and a more

considerable weight reduction.

The thermal inertia (I_{th}) is calculated as the product of these three properties and therefore reduces by a factor of 8 in Table 2.

$$I_{th} = k\rho c_p \quad (3)$$

The thickness of the char layer, together with its natural insulating qualities reduce the heat exposure of the underlying timber. This is indicated by the lower thermal inertia, which causes higher surface temperatures and in consequence, higher heat losses at the surface. As a result, the temperature gradient underneath the interface between char and wood is typically steep. In contrast to the above-reported pyrolysis temperature of 300 °C, different authors reported 180 °C at only 6 mm below the char line when quasisteady-state burning rates were reached [19], while depths more than 35 mm below the char surface remained at initial ambient temperatures. [5].

The thermal diffusivity (α) is calculated with the following equation. It is in the same order of magnitude for char as for timber (see Table 2). A lower thermal diffusivity would result in less transfer of heat in the depth of the timber, higher heating times and lower thermal penetrations depths.

$$\alpha = \frac{k}{\rho c_p} \quad (4)$$

Table 2. Material properties of timber and char at ambient temperatures.

Property	Engineered Timber	Timber	Char
	[32]	[33]	[33]
Thermal conductivity (W/mK)	0.14	0.13	0.071 [b]
Density (kg/m^3)	450	470 to 625	200
Specific heat capacity (J/kgK)	2600	1600	670 to1350
Thermal inertia (W^2s/m^4K)	$1.6x10^5$	$1.14x10^5$ [c]	$0.14x10^5$ [d]
Thermal diffusivity (m^2/s)	$1.2x10^{-7}$	$1.48x10^{-7}$	$3.55x10^{-7}$

[b] Measured at 90 °C
[c] Original: 338 $Jm^{-2}K^{-1}s^{-1/2}$
[d] Original: 119 $Jm^{-2}K^{-1}s^{-1/2}$

The (forming) char layer provides an insulating effect for the timber below undergoing pyrolysis. It was established above that as a consequence of increased heat losses from the charred surface and a lower heat transfer in depth, the production and mass flow of pyrolysis gases reduces [18], [31]. Consequently, a growing char layer will continuously reduce the production of combustible pyrolysis gases in the virgin timber layer. Thereby, the burning rate decreases and and delays the onset of pyrolysis in deeper sections of the virgin wood [5]. Eventually, the formation of a char layer can lead to self-extinction of flaming combustion on the surface.

After an initial peak, in the absence of delamination, many authors found steady-state burning at certain heat fluxes [5], [23], [31]. A steady burning is only possible if a constant char layer thickness is achieved. This suggests that the pyrolysis (in depth) and the oxidation (surface) fronts propagate at the same rate. Stagnation of the propagation of heating in-depth would result in self-extinction. Another phenomenon must consume approximately as much of the char layer thickness as is produced by the pyrolysis to create a quasiconstant burning rate.

At sufficiently high temperatures and oxygen concentrations, chemical oxidation of the char occurs. Oxidation reduces the thickness of the char layer, with lower oxygen concentrations resulting in reduced char oxidation [34], [35]. The primary oxidation reaction takes place between solid char and oxygen, i.e. at the char surface or in cracks. Secondary oxidation is a gas phase reaction and releases the majority of energy [21], which can increase the surface temperature by up to 200 °C [22]. Resulting surface tempertures of over 700 °C have been measured [21]. Therefore the exothermic glowing or smouldering combustion of char is an additional heat source that adds energy to the diffusion equation. As said above, at the same time, oxidation reduces the char layer thickness, and thereby lowers the insulation capacity of the char protecting the underlying virgin timber. Char oxidation increases in-depth pyrolysis by supplying additional energy and by increasing in-depth heat transfer through the thinned char layer.

Many authors state that char oxidation takes place only after extinction of flaming combustion, because oxidation of the pyrolysis gases would consume the available oxygen or displace it [30], [35]. This is inconsistent with the often-made observation of steady-state burning which shows, as explained above, that pyrolysis and oxidation of the solid residue, i.e. in other words production and consumption of char, must take place at the same time at least under certain conditions, under which steady-state burning rates were observed. Different sources provide that the rate of char formation becomes constant when ca. 6.4 mm or even 12.7 mm depth of timber has charred [5].

In literature and practice, the progression of thermal decomposition in-depth of timber is commonly referred to as the "charring rate" (mm/min). As discussed above, the char depth is determined by the position of the pyrolysis front within the timber. This is often approximated with the 300 °C–isotherm, which was explained above to be a slightly arbitrarily chosen value out of the temperature range in which thermal decomposition of timber takes place. In experimental testing, the final residual sample thickness is sometimes used to calculate averaged rates of char progression [31]. While measurements of the former allows investigation of the change of burning rate and heat propagation over the duration of heat exposure, the latter only provides an average value over the whole test duration and cannot account for the initial peak in burning rate or other time-dependent changes highlighted above.

Nevertheless, it is common practice and even recommended in design guidance documents to calculate the loss of structural capacity by using fixed "charring rates". Most commonly effective charring rates between 0.6 and 0.8 mm/min are stated for wood [4], [5], [36]. It should be noted that these values apply to solid wood only as they do not account for the specials features of engineered timber like CLT. Few experimental studies on the charring rates of CLT are available [30] and they show larger variation than the values reported for solid wood. Both values higher than 0.8 mm/min and lower than 0.6 mm/min were found for CLT which indicates that the

introduced uncertainties of the CLT production, or the layup of several lamellae, or the use of polymer adhesive might influence the rate of decomposition of timber. The engineering design and manufacturing process of CLT could both positively and negatively affect the average charring rates compared to solid wood.

As these values for "charring rates" are constant over time, and disregard the influence of the many different and changing properties of timber, average charring rates are likely to underpredict initial charring rates and to overpredict the charring in later stages. The guidance provided by the Eurocode was shown to be non-conservative for some heating scenarios [34]. Charring rates seem to be specifically designed to avoid any complex fire dynamics and can therefore hardly be an accurate tool to predict structural fire performance of timber members. Bartlett [34] strongly emphasises the need for heating rate dependent charring rates and points out the significant impact of the initial peak in burning rate especially in compartment fires of typical duration.

Several material properties, as well as other external factors apart from the incident heat flux, were shown to influence the rate at which the in-depth decomposition progresses: Density and moisture content, species and chemical composition, sample size and geometry, and oxygen concentration, char contraction and oxidation [5], [35]. Accelerated char formation was measured along grains perpendicular to the main exposure plane [34], which correlates with higher permeability and higher thermal conductivity along fibres than parallel to them. Bartlett [34] and Hasburgh [10] observed acceleration within natural gaps and groves, like knotholes. Around knots, lower propagation of the pyrolysis front was observed [5]. The ply configuration of CLT (measured independently from the thickness of individual lamellae) was seen to influence overall charring patterns and burning rates [10]. These aspects further increase the uncertainty and local variability of the development of a char layer in engineered timber products.

The thermal decomposition and burning of timber was shown to be an extremely

complex process [34] that is strongly linked with the reduction of mechanical properties [4], [19]. As temperatures within the timber increase to values around 60 °C, the structural capacity starts to decrease and continues to degrade until the timber returns to ambient conditions, i.e. throughout the whole duration of a fire and the subsequent cooling of the structure. Above 200 °C, the thermal decomposition of timber leads to the production of combustible and non-combustible pyrolysis gases as well as a char layer [5], [8], [17], [19]. It was explained above that the rate of char formation is governed by the rate of pyrolysis. Therefore all factors affecting the burning of timber directly influence the production of char [34]. The char and pyrolysis gases can react with oxygen from the surrounding atmosphere in exothermic oxidation reactions, supplying heat to the underlying timber [21], [34]. The critical external heat flux for extinction of flaming combustion of timber was shown to be around 30 kW/m² and 6 kW/m² for smouldering combustion [23], [26], [28].

Initially, the external heat flux strongly influences the burning rate while later on, steady state burning can be reached in the presence of a constant char layer thickness [5], [23], [31]. Especially the lower thermal inertia of char compared to virgin timber insulates the deeper sections of wood by creating a steep temperature gradient below the char-wood interface [5]. For the char layer thickness to remain constant, oxidation reactions reducing the char layer thickness and pyrolysis reactions increasing the char layer thickness need to balance each other. When a sufficient char layer thicknesses is reached, the mass flow rate of combustible pyrolysis gases decreases below the critical value of ca. 3.5 to 4 g/m²s that is required to sustain flaming [23], [26]. This can lead to self-extinction of timber which is an important mechanism to ensure compartmentation and structural integrity, especially in high-rise timber structures [3], [33].

2.2 Char fall off

Hadden et al. [33] and Emberley [37]highlighted that auto-extinction of timber-lined compartments is heavily dependent on the prevention of char fall off. The char layer hinders pyrolysis of deeper layers and can thereby starve the fire of fuel after the movable fuel in the compartment has been consumed. The fall-off of the char layer exposes the underlying timber and thereby adds new fuel to the fire. The stochastic nature of char fall off is a considerable barrier for timber design, especially for tall timber buildings as these entail extended evacuation periods and higher financial losses are connected with burnout of the structure. The formation of char and effects thereof were explained in detail in the previous sections. The impact of char fall off will be discussed in the following.

The terms 'debonding', 'delamination' and 'char fall off' are often used as if interchangeable in literature when authors are in fact referring to very different failure mechanisms. 'Debonding' describes the process of separation between any two bonded joints caused by any type of mechanism. As a natural composite material, wood in itself contains bonding agents that can fail under different critical conditions. Within the composite material CLT, debonding can occur as cohesive failure of timber-timber bonds or adhesive-adhesive bonds. Moreover, CLT is prone to adhesion failure in the adhesive-timber bi-material interface. The same mechanism can be seen for GFRP-to-timber bonds as adhesion failure in the adhesive-GFRP bi-material interface [38]. Moreover, interlaminar failure of GFRP or timber can occur. All these failure modes can be referred to as 'debonding' as the "glue" between cells or materials stops adhering, and the bond breaks. This can be caused by chemical processes, thermochemical influences, thermally or mechanically induced stresses, etc.

The term 'delamination' specifically refers to a separation in the laminate interface between adjacent lamellae and thereby refers to a certain type of debonding. It can be caused by adhesion failure in the bi-material interface or by cohesion failure within the adhesive [38].

Many authors use the terms ‘char fall off’ and ‘delamination’ as synonyms [4], [29], [30] or disregard the many possible failure modes that can result in separation of lamellae [5]. Delamination is always a bi-material debonding failure in this context. Strictly speaking, ‘delamination’ can imply fall-off of char due to adhesion failure in the char-timber interface or in the timber-adhesive interface. Both failure mechanisms are conceivable. The adhesive in the glue line might fail and cause separation between the lamellae before the charring front reaches the timber-adhesive interface, i.e. at temperatures below 300 °C. Depending on the progression of the bi-material failure, this failure mode opens the possibility of fall-off of not fully charred timber pieces or even whole lamellae.

The focus of this thesis is not to investigate the mechanisms behind the falling of char but rather to explore the implications of hindering char fall off and to quantify the protective role of char for exposed timber members (see section 1.2). Therefore, in this thesis, the term ‘char fall off’ will be used consistently to describe the detachment of charred timber pieces from the investigated cross-laminated timber composite column as a whole, regardless of the exact mechanisms behind it.

As discussed above, char has a high insulating capacity and thereby fulfils a protective function for the underlying timber, delaying the onset of mechanical degradation and pyrolysis. When the char falls off, the underlying timber is exposed directly to external heat fluxes. For exposed structural timber the compartment boundary itself is thereby added to the overall fuel load. The loss of the char layer thus affects the fire dynamics.

While it has been shown that self-extinction of intact CLT can occur under critical heating conditions [33], [37], char fall off can prevent or delay the onset of self-extinction of exposed timber in compartment fires [33], even after all movable fuel has been consumed [23]. Char fall off can also occur after the timber itself has already self-extinguished, then raising the potential for re-ignition of the timber structure [27]. Some timber compartment tests even showed secondary flashover due to

delamination of PUR bonded CLT [4].

Fire safety strategies often rely on extended evacuation periods, 'stay put' and/or internal firefighting. All these approaches heavily rely on the assumption that structural stability and compartmentation will be maintained for sufficient times. This generally requires that the structure will survive burn-out of the movable fuel load and eventually self-extinguish, especially in high-rise buildings [3]. When the combustibles in the fire compartment of origin get consumed entirely, the fire needs to extinguish without intervention (starved fuel) within an amount of time that does not allow heat transfer to cause the failure of compartmentation or loss of structural integrity. As char fall off can continually expose the underlying timber structure, it has the potential to increase the loss of load-bearing capacity significantly and compromise compartmentation. The process of char fall off and burning might continue, or accelerate itself, until the whole structure is consumed, causing the collapse and thereby loss of the whole building. This is seldomly considered as an acceptable outcome of a fire safety strategy. Still, engineers often rely on the potential of self-extinction of timber without accounting for the hazards introduced by char fall off.

Char fall off was shown to increase the subsequent burning rate of the underlying timber [5], [17]. This was sometimes attributed to the higher compartment temperatures at the time of fall-off or the previous in-depth temperature increase in the deeper timber layers. Lower charring rates were found for CLT with fewer thicker lamellae which was ascribed to the extended duration of heat penetration through a thicker first lamella. As a consequence, the first adhesive line was heated later and fall off was seen to be delayed as well [17].

Despite the wide recognition of the negative impacts of debonding failures on the fire performance of engineered timber, to date, only very limited research has been peformed that aimed to systematically investigate char fall off. To the knowledge of the author, a conference paper written by Hasburgh [10] is the only publication that presents a scientific approach to the problem. Horizontal CLT panels with a surface

area of 1 m² were exposed to a standard fire in a furnace test. It should be noted that results from calibrated standard furnace tests are not necessarily representative of the real behaviour in natural compartment fires, which are less homogenious. Delamination and related phenomena were observed and the total surface area affected by delamination was quantified in a systematic way [10]. A correlation between occurrence of delamination and adhesive types was found. Melamine formaldehyde and phenol resorcinol adhesives showed significantly less delamination than polyurethane reactive and emulsion polymer isocyianate. Hasburgh [10] suggests that an adhesive that maintained its bonding capacity at the charring temperature of wood would directly improve structural fire resistance by delaying delamination. This statement seems to be based upon the assumptions that adhesive failure is the only cause of fall off events and that only timber pieces of initial ply tickness detach but no "fractions" of the lamella thickness. It is not clarified if these hypotheses are based on empirical data.

The strongly limited findings on char fall off that are available in published literature highlight a strong need for scientific research to investigate relevant phenomena causing char fall off and its impact on the burning of timber. The implications for fire safety of timber structures need to be analysed to address uncertainties and hazards in existing and future timber construction.

In the previous section, the natural process of char formation was found to equip the surface of heated timber with an insulation layer with lower thermal conductivity, density, specific heat capacity and consequently lower thermal inertia [33]. Char fall off was established as one of the main problems making the exploitations of the thermal insulation properties of char and the self-extinction of timber unreliable. If char could be prevented from falling off, the char itself could theoretically improve the fire performance of wood members by providing additional thermal mass to the in-depth heat transfer process and due to its low thermal inertia. The potential of using an inert material, added to the timber matrix, to prevent the loss of the char layer has

been explored previously [7].

2.3 The case for Glass Fibre Reinforced Polymers (GFRP)

Fibre-reinforced polymers are composite materials that consist of a resin matrix and a fibrous reinforcement material which can both be tailored to fulfil specific performance criteria. The fibres can be loosely scattered, continuous filament or woven fabrics either with unidirectional fibres or fibres running in different directions. E-Glass fibre is the most commonly used fibre type providing a high strength-to-weight ratio and high resistance to chemical, corrosive and environmental impacts at low cost [39].

Recent research has shown the potential of glass fibre reinforced polymers (GFRP) to improve the structural performance of load-bearing timber members. These so-called "Hybrid Fiber Reinforced Polymer (FRP)-Timber (HFT) structures" combine the orthotropic properties of both materials to create optimised composite properties [38]. In a preliminary study, GFRP-timber composite walls showed structural performance superior to that of sheathed steel stud walls [40]. Miao [38] investigated four different adhesives for the bonding of HFT composites consisting of unidirectional E-glass fibre fabric with hoop pine veneers.

Additionally to structural improvements, enhanced fire performance of laminated timber was achieved with GFRP. An experimental study showed improved fire performance of a timber-GFRP composite material compared with a pure-timber laminate. Glass fibre mat was used in the former sample type and small-scale tests in a Cone Calorimeter were conducted. Samples with GFRP reached self-extinction of flaming combustion at 50 % of their initial mass while the timber samples without glass fibre mat were almost entirely consumed. Moreover, a faster declining a less fluctuating heat release rate was observed. In-depth temperatures of the GFRP-reinforced samples were kept at much lower values and averaged charring rates were approximately halved for samples with glass fibres (0.52 to 0.68 mm/min) compared

to conventional timber samples (1.13 to 1.46 mm/min). Overall the results showed the potential of improved insulation achieved with the novel GFRP-timber composite system. This was attributed to the glass fibre mat hindering oxidation of the char layer [7] but can also be a direct result of increased integrity of the samples.

In theory, preventing char fall off with the help of a material that will not oxidise when exposed to heat or fire creates a system that follows more closely the assumptions employed already in engineering design. To a certain degree, traditional approaches account for changing material characteristics and loss of mechanical properties. Temperature-dependent reduction factors for structural capacity and the concept of charring rates are applied to timber members under fire conditions. However, these simplified concepts do not directly account for the loss of integrity of the timber structure through debonding caused by heat transfer. Hindering char fall off, effectively delaying, reducing or even preventing it, theoretically brings the composite system closer to these simplifications already applied to timber structures in practice today. Another material that can hold the decomposing timber and underlying timber structure together at elevated temperatures is needed.

Glass fibres are inert and will not oxidise. They can withstand much higher temperatures than timber but tend to soften when exposed to temperatures like those commonly expected in fully developed compartment fires. Bisby and Green [41] summarised several experimental studies on the reduced mechanical capacity of glass fibres at elevated temperatures. Generally, fibres heated to 550 °C showed approximately 50 % reduction in tensile strength compared to the initial capacity at ambient temperatures. One study found a loss of mechanical properties from 400 °C but reported a loss of only 20 % of both strength and stiffness at 600 °C [41]. Significant softening in the range of 800 °C to 1000 °C was seen to be the consensus. Above 1200 °C, only negligible residual strength and stiffness can be expected [41]. In comparison, localised temperatures of 1100 °C can be reached in compartment fires [8]. The char layer was shown to have decreased density compared to virgin timber. If

the glass fibre is not intended to fulfill any structural purposes in case of fire, its only requirement is to maintain enough strength to support the light char layer from falling.

Epoxy resins (EP) are recommended to bond wood and non-wood materials [42], like glass fibre mat. EP can be adapted to a great spectrum of structural applications which makes them the most widely used resins in buildings and non-building structures. Epoxy resins decompose at temperatures from 50 °C to 260 °C which means they will degrade early when exposed to heat from a fire. As EP are combustible, they will contribute the fire when they undergo oxidation. Resin additives can be used to enhance the fire performance of epoxy resins [41] but were not applied within the scope of this thesis to test the potential of GFRP to improve the fire performance under unfavourable conditions. Should the GFRP-timber composite perform well under these conditions, optimisations can be performed in future studies.

The thermal conductivity of fibre reinforced polymers (FRP) are controlled by the resin used for the matrix, the type of reinforcing fibre, the fibre volume fraction and the orientation of the fibres [41]. In unidirectional composites, as those used in this thesis (see Figure 3), all fibres run parallel in the same direction, except for a minimal amout that is necessary to ensure integrity of the fibres as a mat. For the unidirectional case, the transverse thermal conductivity depends on the resin matrix. Polymers generally have low thermal conductivity [43] which makes FRPs good insulators for underlying structural materials when used as external reinforcement [41]. The longitudinal thermal conductivity of unidirectional FRP is determined by the fibres [41].

The resulting thermal conductivities of glass fibre reinforced composites with epoxy as the matrix resin were found by Mallick [43] and are listed in Table 3. It can be seen that the conductivity along the glass fibres is almost ten times higher than across the fibre direction.

Table 3. Thermal conductivities reported for GFRP and epoxy after Mallick [43]**.**

	Epoxy	Unidirectional GFRP with epoxy-matrix	
		Longitudinal direction	Transverse direction
Thermal conductivity (W/m°C)	0.246	3.46	0.35

Not much research regarding the temperature dependency of the thermal conductivity, density or specific heat of fibre reinforced polymers has been published to date. The complex chemical reactions taking place in the matrix of FRP at elevated temperatures make it difficult to quantify the changed rate of heat transfer through the composite material [41]. No relevant data was found that would apply to the herein investigated material combination of glass fibre mat with Ampreg 22 epoxy matrix.

The fire performance of combustible structures is usually evaluated firstly by their reaction to fire, i.e their potential to contribute to the fire growth. Secondly, the loss of load-bearing capacity is assessed for structural members, i.e. their fire resistance. Lastly, the potential for self-extinguishment is addressed [44]. Therefore, the performance of GFRP under fire conditions needs to be quantified based on different parameters depending on the stage of the fire that is of interest. Flammability parameters are an important measure when ignition and flame spread are of interest. Other performance criteria in the early stages of a fire are the generation of smoke and toxic substances which can greatly affect the safety of the evacuation stage. While important, these properties are not considered in the scope of this thesis. Herein, mitigation of char fall off and thermal insulation of CLT members will be the main performance criterion for the GFRP layer. In a real fire, this could improve the load-bearing capacity of the timber structure along with its capacity to provide a barrier for flame and smoke spread.

While any polymer matrix is going to contribute to the burning rate at sufficiently high heat exposure, a higher volume fraction of fibres compared to resin will reduce the provided fuel. Fardis and Khalili [45] stated that as long as sufficient anchorage for the fibres is provided and the bond is not significant for the desired performance of

the FRP, "unbound" fibres could still provide significant confinement. It was shown that after the consumption of the resin matrix by combustion, the remaining fibres can significantly reduce the heat flow into the underlying composite material [41].

2.3.1 The expected effect of GFRP on the fire performance of CLT

The burning of the epoxy matrix might initially increase the burning rate by supplying extra heat to the underlying timber. On the other hand, the glass fibres will not contribute to the burning. They might increase the reflection of heat and thereby increase the surface losses and reduce the in-depth heat transfer. Due to the low thickness of the fibre mat, it can be treated as thermally thin. Therefore the fibre mat itself would probably only add a small delay to the conductive heat transfer based on its thickness. Effects are expected based on the composite action of the glass fibre mat and the underlying char. Even at elevated temperatures, the residual strength of the glass fibres is expected to be sufficient to hold the low-density char in place. The char layer will then create a thermally thick barrier, which could affect the underlying timber as a secondary effect of the glass fibres. This is expected to change the heat transfer and thereby the time scales of the thermal pyrolysis decomposition processes of the underlying timber.

The oxidation of char depends on both combined thermal penetration and available oxygen. The glass fibre mat can potentially decrease oxidation of the char layer due to hindered inflow of oxygen. This could be related to positive surface pressures due to the ongoing pyrolysis reaction creating an outflow of gases. While physically and thermally thin, the glass fibre layer together with the air gap in front of the char layer might reduce the incident heat flow into the char. On the other hand, this insulating effect could also reduce heat losses from the char layer to the surroundings [41], [43]. An increase of the self-insulating capacity of the system might provide conditions that allow for significant potentially self-sustained smouldering of the char below the glass fibre layer.

2.4 Heat transfer modelling

While it is impossible to capture the infinite complexity of combustion processes, heat transfer models are important tools to understand and predict the in-depth temperature evolution of timber members at elevated temperatures. They can be employed to analyse the behaviour and degradation of timber structures under fire conditions. Different models have been proposed that vary in complexity and the accounted phenomena characteristic of the burning of wood. Some models are presented in the following, in order of decreasing complexity.

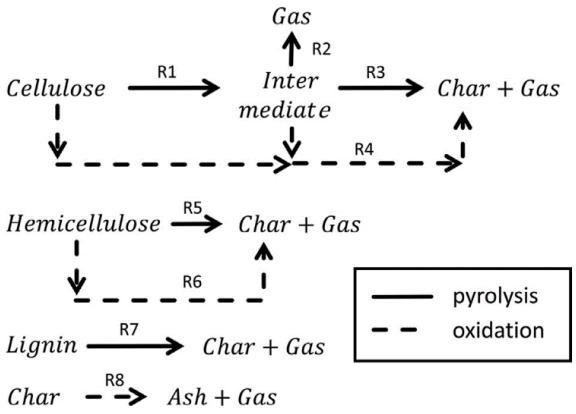

Figure 1. Reaction scheme of the kinetic sub-model implemented by Richter and Rein[46]**.**

Highly complex pyrolysis models aim to capture the decomposition of the main components of wood and their intermediate species and subsequent oxidation of the products with high accuracy. Figure 1 shows the different reactions solved by a pyrolysis model of Richter and Rein [46] as an exemplary emphasis of the level of detail the model developers aimed for. Their models solve conservation equations for energy, species and solid and gaseous mass to most accurately describe temperature profiles, mass fractions and pressures inside decomposing wood. Lautenberger and Pello [47] include four solid phases (wet wood, dry wood, char and ash), seven gaseous species and six reactions in the generalized pyrolysis model (Gpyro). Oxygen diffusion and temperature-dependent specific heat capacities and thermal conductivities of the different wood phases are accounted for. This complex model requires almost 50 input

parameters. Richter and Rein [46] proposed a similar model applicable to a range of different heat fluxes and parallel or perpendicular heating, moisture contents and oxygen concentration. However, the uncertainties of the input material properties significantly lower the accuracy of the model predictions [46] independently of the complexity of the model itself. The increased computational cost of these complex models has not been proven to be justified by higher accuracy of their results [22].

Osorio [44] developed a finite difference model to describe transient one-dimensional heating of semi-infinite timber. Both convective and radiative surface heat losses are accounted for through a linearised total heat transfer coefficient. The timber is divided into three phases (wet, dry and char wood) based on temperature criteria. While the density per phase is constant, specific heat capacity and thermal conductivity are described by temperature-dependent Arrhenius equations. This model does not account for heats of reaction as it assumes external heating to dominate.

Reszka and Torero [24] proposed another simplified semi-infinite heat transfer model that assumes an inert, i.e. non-reacting solid. This model initially over predicts the heating of timber as it does not capture initial influences of moisture evaporation acting as a heat sink or charring of timber. When exothermic reactions in the timber dominate after ignition, the model under predicts the temperatures evolution of the timber. More accurate values are found in the early stages of heating of timber and at low heat fluxes. As none of the exothermic or endothermic reactions taking place during the thermal decomposition of timber are captured, this model can be used in comparison with more complex models to quantify the importance of sub-models accounting for processes like surface oxidation or reaction kinetics.

The most fundamental approach is the analytical solution to the differential heat diffusion equation as derived by Incropera [48]. This approach treats the heated material as inert with constant values for thermal diffusivity, density and specific heat capacity and provides the temperature distribution in a homogeneous medium.

Chapter 3 Materials and Methodology

An experimental methodology was developed to assess the thermal effect of char fall off. Glass fibre reinforced cross-laminated timber columns were compared with bare CLT columns to assess the potential of the GFRP to hinder char fall off and the implications thereof for the thermal degradation of timber. Both sample types were tested under different heat fluxes with a constant bending load. In-depth temperature measurements were undertaken to quantify the temperature evolution within the depth of the timber. The data served to estimate heated depths and charring rates to investigate implications for the loss of load-bearing capacity of CLT under fire conditions.

3.1 Materials and sample preparation

The timber used in the experimental series was cut from one 5-layer cross-laminated timber panel made from Australian Radiata Pine (Pinus radiate) bonded with Polyurethane (PU). This commercially available product was chosen because Radiata Pine is one of the most widely used species in timber construction in Australia. The used timber is thus representative of actual construction products and was readily available. The initial total thickness of the panel was 150 mm with individual lamella thicknesses 45/20/20/20/45 mm.

The thickness of the first lamella was reduced to 20 mm with a Thickness Planer, resulting in a total board thickness of 125 mm. This was done to reduce the heating time and thereby the duration of each experiment for practical reasons. The predominant focus of the experimental study was the heating of the first few centimetres in depth of the timber up to the first adhesive line. A reduced thickness of the first lamella was believed to decrease the test duration but not provide fewer insights based on the findings presented in the literature review in Chapter 2 .

The CLT was cut into columns of 130 mm front width and 790 mm height. Based on the reviewed literature presented in Chapter 2 the sample size seems to affect char

fall off. Medium-scale tests were found to be able to represent mechanically loaded members sufficiently well while a large enough exposed area minimized edge effects. The maximum sample size was limited by the test setup that will be introduced in the following (see section 3.2), the maximum area of constant incident heat flux of the desired magnitude achievable with the radiant panel and practical considerations like sample weight. The sample width was chosen to ensure bending towards to radiant panel for the applied loading case and to minder the risk of out-of-plane buckling. The cutting orientation was chosen such that the fibre direction of the first lamella was vertical for the standing column, i.e. perpendicular to the incident heat flux. Longitudinal fibres are favourable for structural capacities of cross-laminated timber members and are therefore the predominant case in practice.

To allow for in-depth temperature measurements with thermocouples of 1.5 mm diameter (see section 3.3), holes were drilled from both sides of the sample to the centre. The positioning of the thermocouples is discussed in section 3.3. Air gaps between the thermocouple tip and the solid can lead to large deviations between the measurement and the actual solid temperature that the thermocouple is supposed to measure[e]. To ensure direct contact between the tip of the thermocouple and the timber, the last two millimetres of the hole had a diameter of 1.5 mm. The rest of each hole had a diameter of 2 mm to allow easy installation of the thermocouples. A programmable drilling robot with a MatLab script was used to achieve higher accuracy than with a hand-held drill, especially in terms of straightness of the holes and position of the tip of the thermocouple. The main advantage of using the robot was the reduced risk of inserting the drill bit at an angle which can largely influence the final position of the thermocouple tip with respect to the exposed surface, especially for holes with a depth as large as 65 mm.

As an attempt to measure the 'near-surface' temperature, a small indentation was

[e] Direct communication with Ian Pope (The University of Queensland) on his recent findings regarding thermocouple errors.

made in the surface of the CLT columns in which the thermocouple tip was placed. Then the thermocouple shaft was fixed tightly to the timber with two metal staples, with the thermocouple tip carefully ensured to touch the wood just below the surface level. A picture of this approach can be seen in Figure 2. These thermocouple measurements will later be referred to as the 'surface temperature' which refers to the surface of the CLT column, below the glass fibre mat for 'CLT with FRP' samples. It should be noted that the term 'surface temperature' is not entirely accurate due to the crudity of the thermocouple fixing and the slight in-depth offset of the thermocouple tip by approximately 1 mm.

CLT CLT with FRP

Figure 2. Embedded surface thermocouple.

The samples that were tested as 'CLT' without glass fibre reinforcement were not processed further. The preparation of the remaining samples, 'CLT with FRP', will be outlined in the following.

3.1.1 Application of GFRP

Unidirectional glass fibre mat with a measured weight per unit area of 640 g/m² was cut into 130 mm wide and 1.5 m long strips with the fibres running in the longitudinal direction, i.e. individual fibre bundles being 1.5 m long. This length was chosen so the fibres would be anchored with resin at the unexposed "cold" back of the samples during the heat exposure tests.

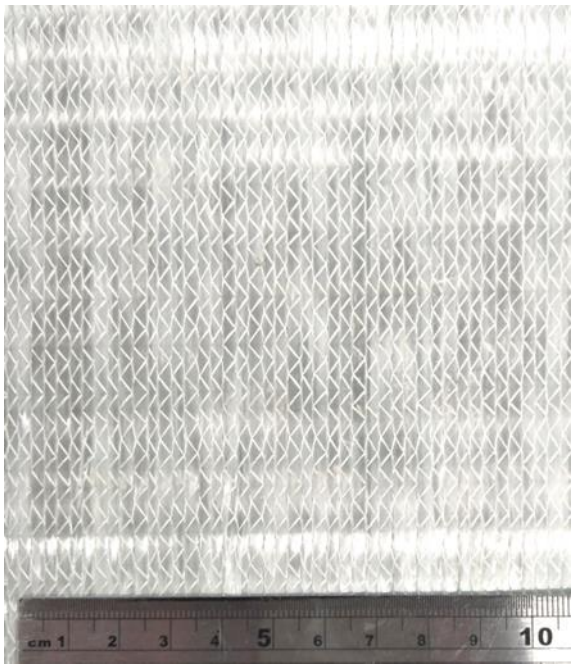

Figure 3. Unidirectional glass fibre mat.

Ampreg 22 Epoxy resin, prepared with slow hardener (mixed in a weight ratio of 100:28) was used to bond the glass fibre mat strips to the surface of the CLT column. As epoxy resins experience loss of bond with timber at temperatures below the pyrolysis temperature of wood (see section 2.3), the glass fibre mat was additionally fixed with metal staples of 8 mm leg length to ensure anchorage after loss of integrity of the resin. The staples were applied in the top, bottom and back face of the column, while the glass fibre mat was held under tension to keep it as tightly attached to the timber surfaces as possible. The 'CLT with FRP' samples were left to cure at ambient conditions for seven days to ensure full bond strength before any experiments were undertaken. Figure 4 shows the cured 'CLT with FRP' samples.

Figure 4. Cured 'CLT with FRP' samples without insulation (Top and bottom left and middle) and with insulation (Bottom right).

3.1.2 Sample Insulation

To ensure a repeatable area of incident heat flux and to hinder heat penetration of unknown magnitude above and below the area of constant heat flux, the top and bottom of each column were insulated. The radiant panel used to expose the samples to high heat fluxes (see section 3.2) supplies a uniform heat flux over a limited surface area, which was estimated for different heat fluxes by Chowdhury [49][f] as 250 mm high and 130 mm wide.

Three layers of 3 mm ceramic fibre paper were wrapped around the top and bottom 270 mm of the samples. They were wrapped with aluminium tape at the bottom end of the column. At the top end, the ceramic fibre paper was fixed at the back of the sample with aluminium tape. The front was covered with several layers of aluminium foil as aluminium tape at the top did not withstand exposure at high heat fluxes. A picture of the insulation and the resulting exposed surface is shown in Figure 4. The same insulation was also used on the sides of the sample with holes to insert the thermocouples.

A series of exploratory tests showed a high influence of the heat received by the sides on the in-depth temperature measurements. Side-insulation was applied to ensure better agreement with the assumption of one-dimensional in-depth heat transfer. It also helped to avoid re-ignition observed for FRP samples after the end of the test, which was not part of the scope of this thesis.

3.2 Test setup

The thermochemical and mechanical degradation of timber and adhesives are interdependent processes (see section 2.1). The structural capacity and integrity degrades as a function of temperature increase which can, in turn, promote faster heat transfer, e.g. due to cracking. Bond failuers caused by high temperatures as well as

[f] Unfortunately, a calibration with a heat flux gauge could not be conducted as planned due to the restricted lab access after the Covid-19 outbreak.

mechanical failures can both promote char fall off. It was therefore decided to study the potential of GFRP to hinder char fall off and improve the fire performance of CLT in a holistic approach. A twofold case can be made for the choice of a bending load for this experimental series. Firstly, bending was found to induce stresses in the adhesive layer promoting debonding in the adhesive and the adhesive-timber bi-material interface. Therefore bending can be argued to present a worst-case loading scenario for char fall off. Moreover, structurally-reinforcing GFRP is applied to a surface under tension in a non-fire design.

The CLT columns were tested in the loading frame developed by Chowdhury [49] at the University of Queensland shown in Figure 5 and Figure 7. The support connection was changed to a pin-pin support as shown in Figure 6 that was connected with an eccentricity to induce bending of the specimen. The CLT was tested under loading to acknowledge the influence of mechanically induced stresses on the thermal decomposition on engineered timber and the potential impacts on char fall off. A gas-fired radiant panel, placed at a carefully calibrated distance from the exposed surface of the sample, was ignited to supply a heat flux to the exposed sample surface. Right after ignition, the radiant panel takes a few seconds to heat up[g]. The afterwards resulting steady incident radiant heat flux can be treated as approximately constant over time, as the flow of natural gas was supplied from a pipe. Surface heat fluxes of 20 kW/m² and 50 kW/m² were chosen for this experimental series to investigate the impact of different heat fluxes. While both values were high enough to achieve flaming and are typical of compartment fire scenarios, 20 kW/m² is below the critical value for self-extinction of timber, 50 kW/m² is above (see section 2.1).

[g] A calibration of the radiant panel over time with a heat flux gauge was planned to determine the exact duration of the initial increase in heat flux, fluctuations over time and possible variations across the theoretically estimated area of constant heat flux. Unfortunately, restrictions in the usage of the laboratory facilities after the Covid19 outbreak made that impossible for the time being.

Figure 5. Loading frame designed by Chowdhury [49]**, with new pin-pin support.**

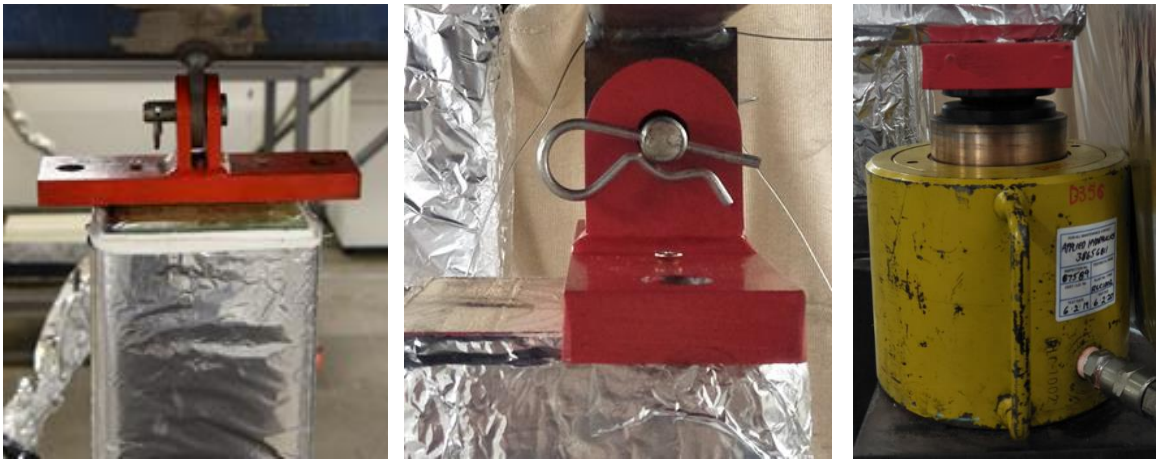

Figure 6. Pin-pin support.

It should be noted that as the cross-section and load-bearing capacity of the CLT specimen are expected to change throughout the test as the heat travels through the timber (see section 2.1). Consequently, the position of the neutral axis will move and thereby change the eccentricity of the loading axis. This effect would decrease the

deformation, i.e. bring the column back towards its initial straight shape.

On the other hand, the heating of a single face of the mechanically restricted timber will cause thermal stresses within the column. These are expected to increase the bending deformation, i.e. increase the deflection of the column and bring it closer towards the radiant panel. Detailed analysis of the measured displacement data would provide insight into the outcome of the superposition of these two effects. While this analysis is outside of the scope of this thesis, its potential effect on the char fall off and temperature evolution is expected to be relevant.

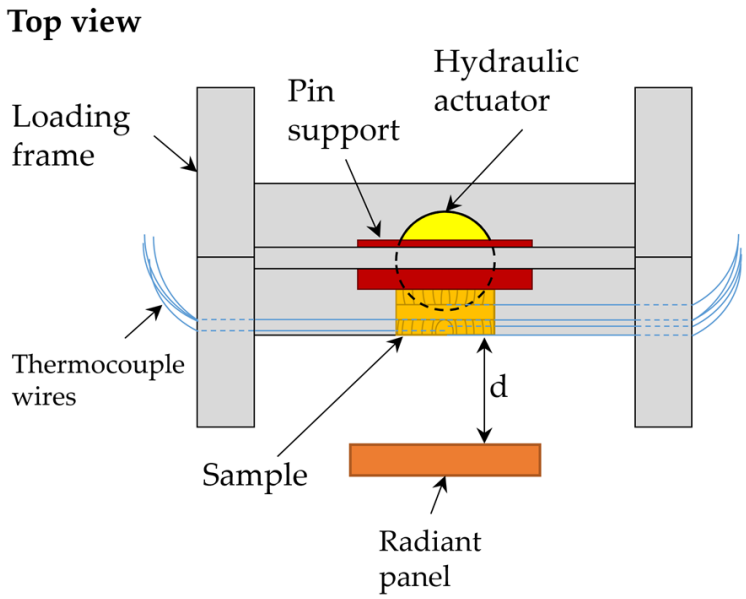

Figure 7. Schematic of the test setup.

3.3 Instrumentation

K-type thermocouples of 1.5 mm diameter were inserted into the CLT columns through drilled holes (see section 3.1). The end of each hole was of the same diameter as the thermocouple to ensure good contact with minimal air gaps. Five thermocouples were placed at different depths from the exposed surface to capture the temperature gradient throughout the first 40 mm. A schematic of the exact positioning of the thermocouples can be found in Appendix I . While aiming at the best resolution of the temperature gradient, especially near the moving char front, the disturbance caused by the thermocouples themselves had to be minimized. These thermocouples were all

right near the vertical centreline of the exposed area to measure as far away from edge effects as possible (meaning edge effects from the unexposed sides of the sample as well as from the unexposed top and bottom). To reduce the conduction effect of the thermocouples and ensure temperature measurements mostly undisturbed by the instrumentation, the thermocouples were inserted from both sides and slightly above and below the vertical centreline. To investigate possible variation in temperature evolution over height, four more thermocouples were placed at different height at a depth of 20 mm from the exposed surface, i.e. along the glue line. This additional temperature data was intended to verify whether the centreline thermocouples were providing representative data for the whole exposed height and to be able to quantify the error of the local measurements.

The thermocouples were inserted from the side of the sample, i.e. parallel to the exposed surface, to reduce the effect of conduction along the thermocouple. As the metallic thermocouples have a higher conductivity than the timber and adhesive, they experience increased heat flow along their length. This can cause a cooling effect at the tip of the thermocouple itself, and reduce the reading of that thermocouple. It can also disturb the heat transfer throug the sample and the resulting temperature field. Thermocouples inserted from the back of a timber sample are exposed to a large temperature gradient within the timber along their length which induces increased heat transfer from the hotter tip to the colder parts of the thermocouple up to where the thermocouple shaft is in ambient air. This effectively cools the thermocouple tip and reduces the measured temperature, as thermocouples measure their own temperature at the welded tip. This temperature was deemed not representative of the timber temperature due to the above-described phenomena. Thermocouples inserted from the side were expected to experience a lower temperature difference within the wood and therefore experience less conduction along their length. As a result, the temperature evolution in the depth of the timber would be disturbed less. The temperature evolution in depth was the main focus of these measurements. Therefore,

a lower disturbance of relevant data and more accurate measurements were expected from thermocouples inserted from the side than from the back and it was decided to insert them from the side.

The disadvantages of inserting thermocouples from the sides is that they potentially hold the char in place longer by acting as a barrier for underlying char pieces, which will make visual observations of char fall off less accurate. Moreover, it is more difficult to estimate the final position of the tip of the hole with respect to the exposed surface than for holes drilled from the back. To minimize the risk of a large offset and to compensate for not being able to quantify the offset, all thermocouple holes were drilled with a drilling robot as described in section 3.1.

It should be noted that for the comparative study herein, while it is important to reduce any measurement errors and disturbances caused by instrumentation to achieve measurements that are as realistic as possible, the main focus can lay on the repeatability of errors for both sample types.

3.4 Testing procedure

A constant load of 39 kN was applied to the samples with an electrically controlled hydraulic actuator. This load was chosen to create significant bending of the member. It was however much lower than critical loads for sudden structural failures. Observation of structural behaviour and the exact calculation of this load is out of the scope of this thesis.

Using the vertically oriented gas-fired radiant panel, a constant heat flux was applied to the surface of the mechanically loaded sample. Piloted ignition of the exposed surface of the CLT column was attempted with a hand-held torch burner every 30 seconds from ignition of the radiant panel until the sample showed sustained flaming.

The samples remained exposed to the heat flux until the second glue line at 40 mm depth from the surface reached 100 °C. Then the radiant panel was switched off,

which marked the end of the test. Immediately afterwards, cold water was sprayed on the CLT to extinguish any flaming or smouldering combustion and minimize further thermal decomposition.

In a preliminary study, samples with GFRP reinforcement showed smouldering in the char layer after the end of the test which eventually led to reignition of the sample. The flaming post-reignition continued to consume the remaining CLT cross-section. Investigation of this effect was out of the scope of this thesis. Therefore, for all experiments presented herein, additional insulation was used on the sides of the sample to prevent oxygen inflow. Moreover, right after the end of each test, all remaining combustion was extinguished with water spray.

A minimum amount of 250 ml of water was used for every sample. Water was sprayed until each thermocouple showed readings below 300 °C, corresponding to the pyrolysis temperature (see section 2.1). The insulation layers were removed from the sample immediately to allow faster cooling. Once the samples returned to ambient temperatures, the remaining weight and uncharred depths of the CLT sections were measured. The blunt-ended depth probe of a dial calliper was used to measure char dephts. Several measurements were undertaken for each sample in the 20 cm^2 around the centre point of the exposed area. Each individual measurement was performed in the centre of a char blister.

Table 4 presents the experimental matrix. All tests were performed with the same boundary conditions, load, heated area and sample geometry. The different heat fluxes applied in different tests can be found in the table. Three repetitions were performed for each testing condition. The testing duration allowed for the second glue line to reach 100 °C. This value was chosen to allow maximum times to observe heating and char fall off of the first lamella while avoiding the thermal profile to increase beyond the moisture evaporation at the second glue line.

Table 4. Experimental matrix.

Sample type	Incident heat flux	Test number
CLT	20 kW/m²	1
		2
		3
	50 kW/m²	4
		5
		6
CLT with FRP	20 kW/m²	7
		8
		9
	50 kW/m²	10
		11
		12

3.5 Thermogravimetric Analysis

Thermogravimetric analysis (TGA) was used to quantify the thermal decomposition, measured as mass loss, as a function of temperature. Tests were carried out in a pure nitrogen atmosphere (150 ml/min; three tests) and in air (21 % oxygen; three tests). Samples (6 to 9 mg) were heated from 50 °C to 900 °C at a rate of 20 °C/min. The obtained data per atmosphere was averaged and plotted together with an envelope showing the maximum and minium obtained value. The difference in normalised mass over the corresponding difference in temperature between two subsequent measurements was plotted to show the derivative thermogravimetry plot.

3.6 Methods of analysis

The following section presents a numerical model that was employed to determine the individual influence of different properties of the GFRP-timber composite system when heated. This analysis was undertaken as an attempt to understand how the GFRP was influencing the propagation of the thermal wave to result in the observed data measured in the experiments. A detailed explanation of the preceeding data processing of the experimental can be found in Appendix II.

3.6.1 Heat transfer model

The previous chapter highlighted the characteristics of the heating of timber. Due to the complex properties of the material, the modelling of the burning of timber is a challenging process. Different models were presented that attempt the modeling of heat transfer through wood, with some including temperature-dependent properties or pyrolysis reactions. Reska and Torero [24] highlighted the importance of moisture evaporation and the focus of this thesis lies on the effect of the char layer and char fall off on the propagation of the thermal wave. Detailed modeling of chemical reactions was shown to be unnecessary to predict heating trends relatively accurately [24].

Herein, the aim of modeling the heat transfer through timber was to investigate the impact of the char layer on the heating of the underlying cross-section. Therefore, a finite difference model was chosen that accounts for the change in properties between virgin timber, dried timber and char. This model was presented by Osorio [44] and important aspects will be reproduced in the following. The adjustments that were made to adress the aims of this work will be highlighted explicitly. The simplified energy balance for different nodes is shown in Figure 8. It accounts for the incident heat flux at the surface by summing the external heat flux ($\dot{q}_e''$) together with the surface absorptivity (a) (which was assumed to be 0.9 based on the value used by Osorio [44]) and the surface losses, approximated with a total heat transfer coefficient (h_T). The in-depth heat transfer is modelled as pure conduction. The resulting formulas applied to model the heat transfer through the timber section are indicated in Figure 8 and presented in Appendix III .

Figure 9 schematically shows the different zones and according temperatures assumed throughout the heated timber section. Below 100 °C, virgin timber is assumed with a density of 463 kg/m³ that was measured for the Radiata Pine CLT. Between 100 °C and 385 °C lies dry wood with 95 % of the initial density. Above 385 °C, wood is assumed to be fully charred, with 20 % of its initial density remaining. The distance between x_1 and x_2 (i.e. the thickness of the pyrolysis region) as well as the

distance between x_3 and x_4 (i.e. the region of moisture evaporation) were assumed to be infinitely thin.

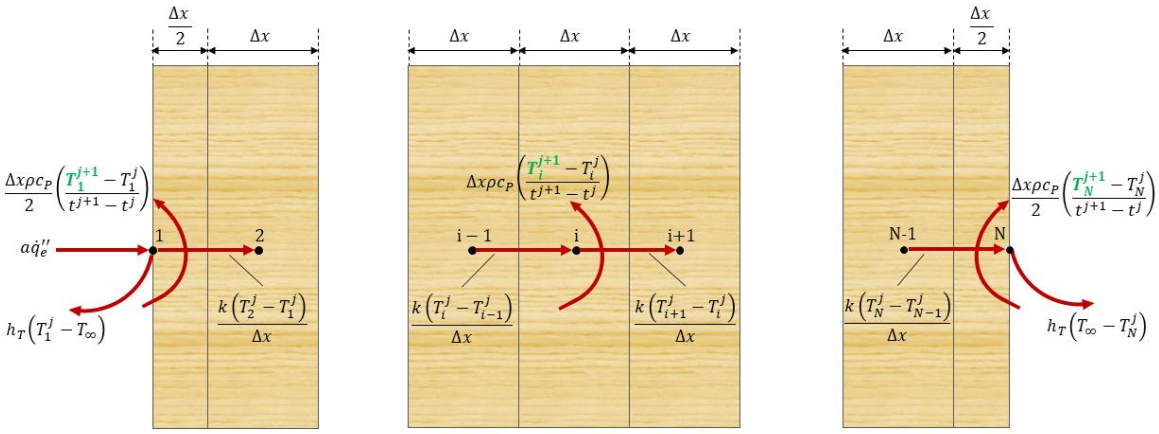

Figure 8. Energy balance at the surface node exposed to an external heat flux (left), internal nodes (middle) and the node at the back face (right).

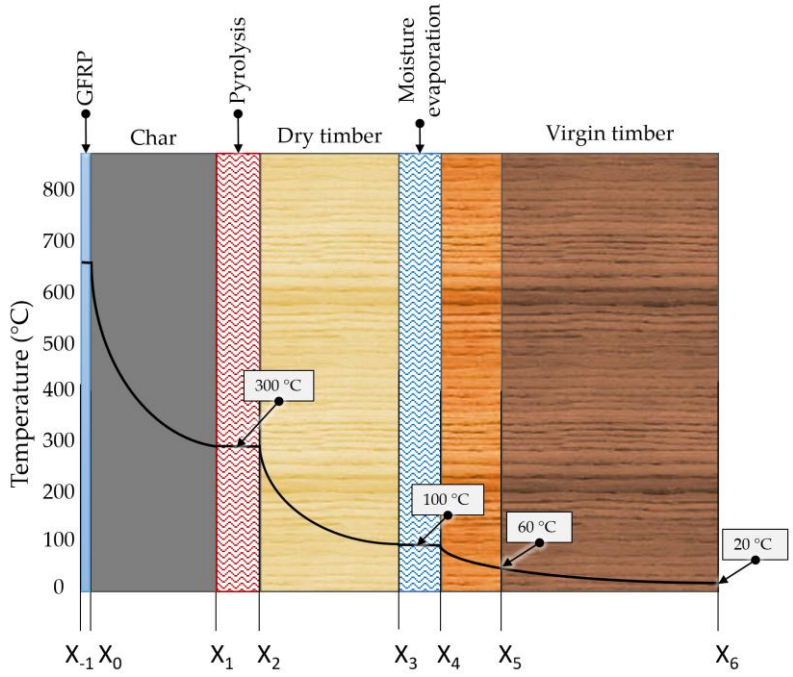

Figure 9. Temperature zones throughout the heated GFRP-timber composite system.

The temperature dependency of different properties of timber has been presented in Chapter 2 . The influence of temperature on conductivity (k) and specific heat capacity (c_P) has been accounted for in the model by using the following

equations [44] and the input parameters given in Table 5.

$$k(T) = k_0(T) * \left(\frac{T}{T_r}\right)^{n_k(T)} \quad 5$$

$$c_P(T) = c_{P_0}(T) * \left(\frac{T}{T_r}\right)^{n_{c_P}(T)} \quad 6$$

Table 5. Input values for the calculation of temperature-dependent thermal conductivity and specific heat capacity in virgin timber, dry timber and char.

	Temperature (°C)	Thermal conductivity (W/mK)		Specific heat capacity (J/kgK)	
		k_0	n_k[44]	c_{P_0}	n_{c_P}[44]
Virgin timber	< 100 °C	0.13 [33]	0.185	1600 [33]	0.406
Dry timber	100 ≤ T < 385 °C	0.1235 (95% of virgin timber [44])	0.594	1520 (95% of virgin timber [44])	0.66
Char	> 385 °C	0.071 [33]	0.435	1000 [33]	0.283

Each scenario was modeled for both a low external heat flux of 20 kW/m² and for 50 kW/m². The total heat transfer into the timber, simplified combining convective and radiative heat transfer to the solid surface, is a function of the surface temperature (T_S). The total heat transfer coefficient (h_T) was calculated with the following equation [44].

$$h_T = 0.0761 T_S[°C] + 9.5761 \quad 7$$

To investigate and possibly quantify the effect of different properties of and phenomena caused by the GFRP when added to the matrix of heated timber, the above presented model was developed further. The aim was to understand the mechanisms causing experimentally observed differences in heating of CLT with and without FRP that will be presented in Chapter 4 Schematics of the different investigated configurations are depicted in Table 6.

A Base Case was developed in which the exact formulation of the model presented above was implemented as a reference scenario. Then the heat transfer through an "inert" timber section was modeled to investigate the impact of changing timber properties at elevated temperatures. For this model, the properties of virgin

timber that were presented previously where used for all local temperatures.

Table 6. Schematics of the modelled configurations with indications of the boundary conditions.

Model Name	Schematic
0 Base Case	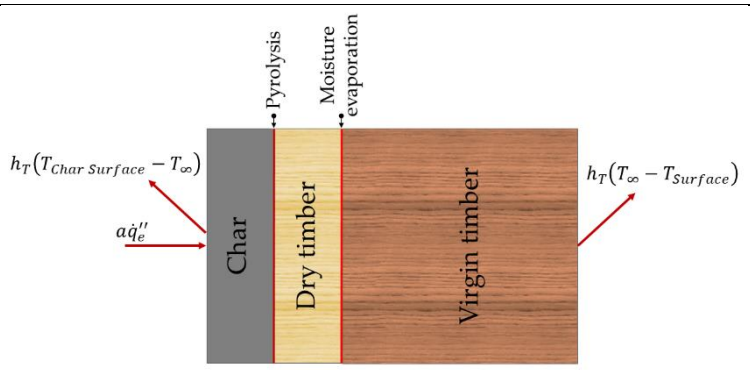
1 "Inert" virgin timber (No char or dry timber properties)	
2 Glass fibre layer	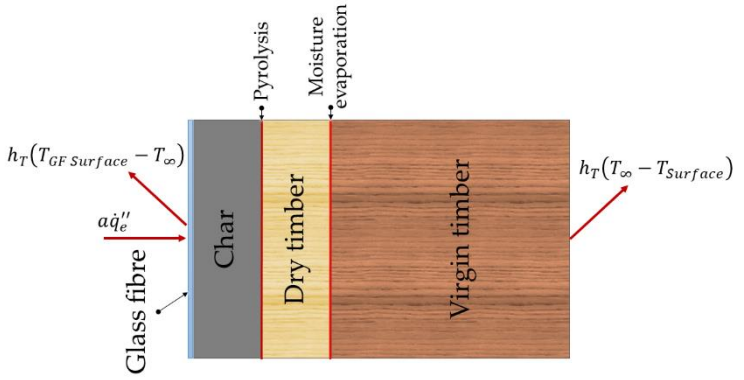
3 Air gap	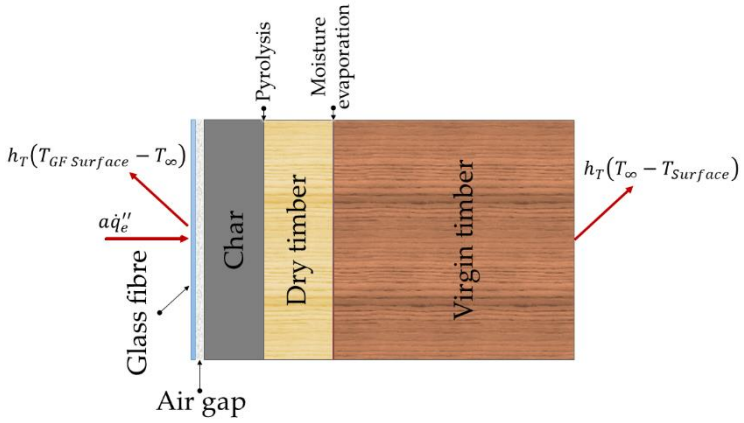

In a third model, a glass fibre layer was added on top of the timber surface. The alterations made to the model to predict the incident heat flux and heat transfer on the

glass fibre-timber interface are shown in Figure 10. For the first node on the surface of the GFRP, only the material properties were changed from timber properties to glass fibre properties. The equation describing the heat transfer to node 2 was altered to simulate the conduction through GFRP, while neglecting conduction through timber to avoid the complexity of modeling heat transfer through two different materials.

$$T_2^{j+1} = T_2^j + \frac{\Delta t}{\Delta x^2 * \rho_{CLT}(T) * c_{P\,CLT}(T)} \left[2k_{GF}(T) * \left(T_1^j - T_2^j\right) - k_{CLT}(T) * \left(T_2^j - T_3^j\right)\right] \quad 8$$

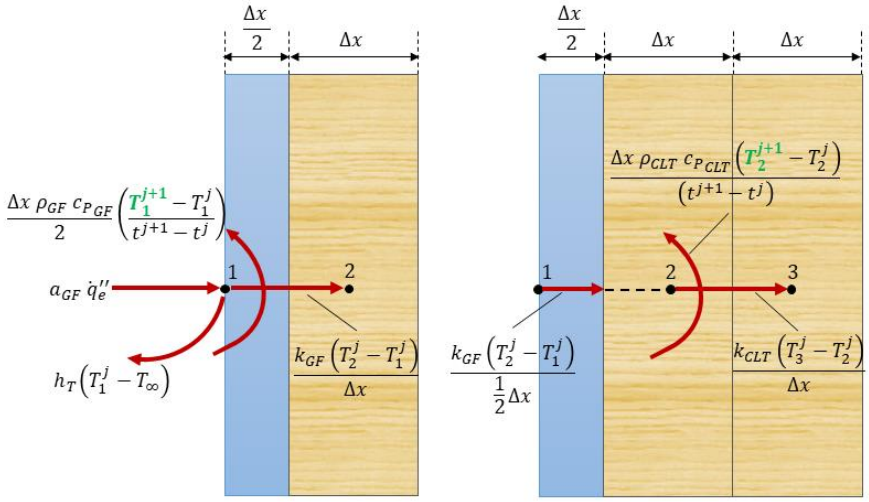

Figure 10. Alteration of model for series of materials (Glass fibre (GF) and CLT) for Node 1 (Left) and Node 2 (Right).

The materials properties used as input values are listed in Table 7. The model was used to analyse the impact of the inert glass fibre layer on the heat transfer into and within the underlying timber. The model does not account for the matrix material, as the epoxy resin is expected to be consumed early by the fire. The properties of the glass fibre layer were assumed to be temperature independent.

As a range ob absorptivity values for glass fibre was found, two calculations were performed for 0.75 and 0.95, representing the lower and upper range of values found in literature. Then an absorptivity of 0.9, equal to that previously used for timber, was assigned to the glassfibre to investigate the impact of its other properties

independently from this uncertain variable. The glass fibre layer was modelled with a thickness of 1 mm, which is approximately twice as thick as the glass fibre layer used in the experimental study. Therefore, estimated effects of the modeled glass fibre layer will be an overprediction.

Table 7. Input parameters used to model the glass fibre layer.

Thermal conductivity of glass fibre	0.1 W/mK [50]
Specific heat capacity	800 J/kgK [51]
Density	2550 kg/m^3 [51]
Absorptivity of glass fibre	0.75 and 0.95 [52]; 0.9 [44]

Lastly, an air gap of constant thickness was modeled between the glass fibre layer and the surface of the underlying timber based on an approach presented by Peng [53]. Air gap thicknesses ($\delta_{air\ gap}$) of 1 mm, 10 mm and 100 mm were modeled. The main assumption was that the air gap would be narrow enough to ignore heat transfer by convection (which might be approximately true for 1 mm and probably introduces a significant error through simplification for 10 mm and 100 mm). The resulting heat transfer through the air gap ($\dot{q}''_{air\ gap}$) is then represented by the following formula, that depends on the temperature at the back face of the glass fibre mat (T_2) and the surface temperature of the underlying CLT (T_3).

$$\dot{q}''_{air\ gap}(T) = \frac{k_{air\ gap}(T) * (T_2 - T_3)}{\delta_{air\ gap}} \quad 9$$

The equivalent thermal conductivity used to express the total heat flux through the air gap ($k_{air\ gap}$) is the sum of the radiative and conductive heat flux through the air gap that are calculated as proposed by Janssens [54] and Peng [53].

$$k_{air}(T) = 0.024 + 7.05 \times 10^{-5} T_{air} - 1.59 \times 10^{-8} T_{air}^2 \quad 10$$

$$k_{rad}(T) = 4\sigma(T_{air} + 273)^3 * \delta_{air\ gap} * \left(\frac{1}{\varepsilon_{GF}} + \frac{1}{\varepsilon_{CLT}} - 1\right)^{-1} \quad 11$$

The air temperature in the gap was estiamted as the average between T_2 and T_3. The emissivities of both materials were assumed to be unity which resulted in maximum radiative heat fluxes.

The surface node was calculated as presented repeatedly above, using material properties of the glass fibre layer. To eliminate the unknown variable of absorptivty at the exposed surface, a value of 0.9 was assumed again, equal to the absorptivity of the timber. The following equations were used to predict the temperature at the back face of the glass fibre layer (T_2^{j+1}) and the front surface of the CLT (T_3^{j+1}).

$$T_2^{j+1} = T_2^j + \frac{2\Delta t}{\Delta x_{GF}\rho_{GF}c_{P\,GF}}\left[k_{GF}\frac{\left(T_1^j - T_2^j\right)}{\Delta x_{GF}} - \dot{q}''_{Air\ gap}(T)^j\right] \quad 12$$

$$T_3^{j+1} = T_3^j + \frac{2\Delta t}{\Delta x_{CLT}\rho_{CLT}c_{P\,CLT}}\left[\dot{q}''_{Air\ gap}(T)^j - k_{CLT}\frac{\left(T_3^j - T_4^j\right)}{\Delta x_{CLT}}\right] \quad 13$$

Chapter 4 Results

Qualitative and quantitative observations regarding the thermal effect of char fall off on the heating of cross-laminated timber will be presented in the following. First, the thermal decompositon of the cross-laminated timber product used in this project will be quantified with thermogravimetric analysis to highlight characteristic temperatures and phases of decomposition. Then follows a comparative study of medium-scale CLT column tests under radiant heating. The residual weight and thickness of CLT sections with and without FRP will be compared. Visually observed char fall off will be assessed qualitatively. The times until the first char fall off event in each CLT test will be shown with the corresponding glue line temperatures. In the following, in-depth temperature measurements will be analysed in detail to quantify the effect of char fall off on the temperature evolution within the heated timber sections. The resulting differences in time taken to reach temperatures that will affect the structural capacity as well as pyrolysis temperatures at specific depths will be presented. The rate of heating for different samples types and under different heat fluxes will also be compared. Lastly, a numerical model will be employed to assess the impact of selected parameters on the differences in in-depth heating when char fall off was hindered by a layer of GFRP. Qualitative agreements between the experimental results and numerical analysis will be highlighted, pointing towards possible phenomena behind the reported observations.

4.1 Thermogravimetric analysis

The thermal decomposition of the Radiata Pine CLT samples tested in the TGA as explained in section 3.5 clearly shows the three dominating phases (see Figure 11 and Figure 12). Drying happened until 100 °C, followed by a heating phase with no thermal decomposition resulting in mass loss until just below 250 °C. Pyrolysis is the thermal decomposition of timber into char and pyrolysis gases and requires heat input but no oxygen (see section 2.1). A rapid increase in mass loss was found. Here the two

curves for the inert nitrogen atmosphere and air start to diverge: More rapid mass loss can be seen in the presence of oxygen. While the Nitrogen atmosphere only shows two peaks (drying and pyrolysis), char oxidation causes the third peak around 450 °C in the air atmosphere in Figure 12. It can be seen in Figure 11 that no further mass loss was seen above 500 °C. The remaing 6 % of mass are most likely caused by non-combustible impurities in the timber or the TGA process. The approximately 15 % difference between the final mass in air and in nitrogen is the mass of char that (theoretically) fully decomposes in air and cannot oxidise in an inert atmosphere. The overlap of the pyrolysis and char oxidation peaks in air in Figure 12, that prevents the curve from decreasing back to zero between the peaks, clearly shows that both processes take place simultaneously. Char oxidation is likely to start together with pyrolysis but continues at higher temperatures up to 550 °C in air.

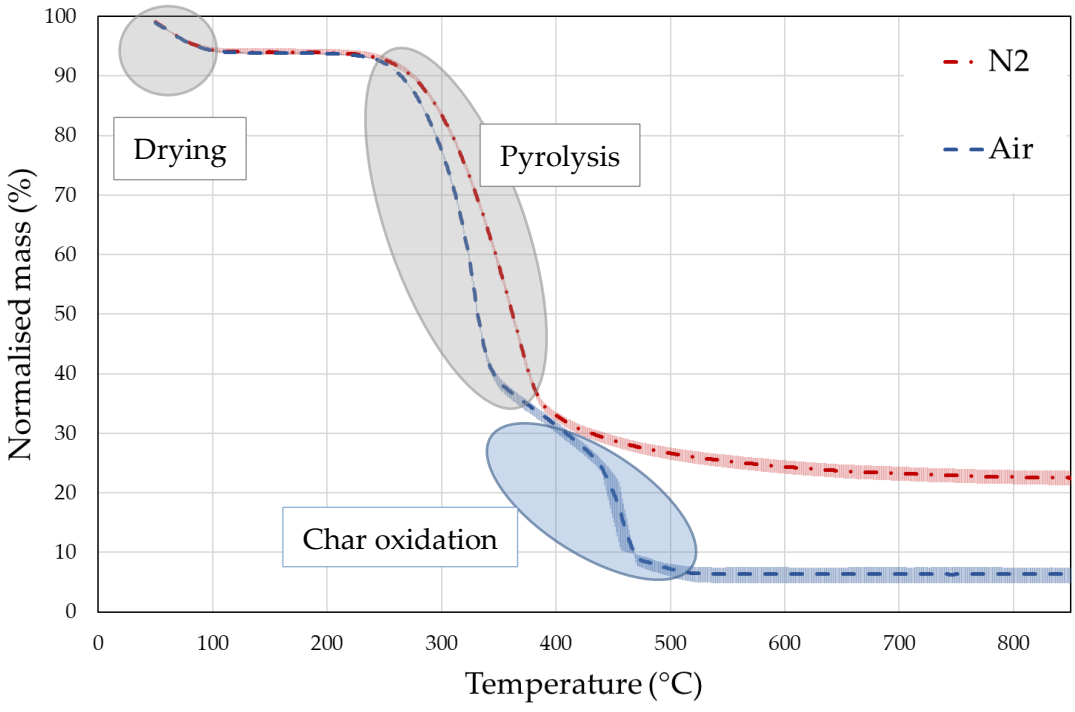

Figure 11. Thermal decomposition of Radiata Pine CLT as mass loss (%) over temperature.

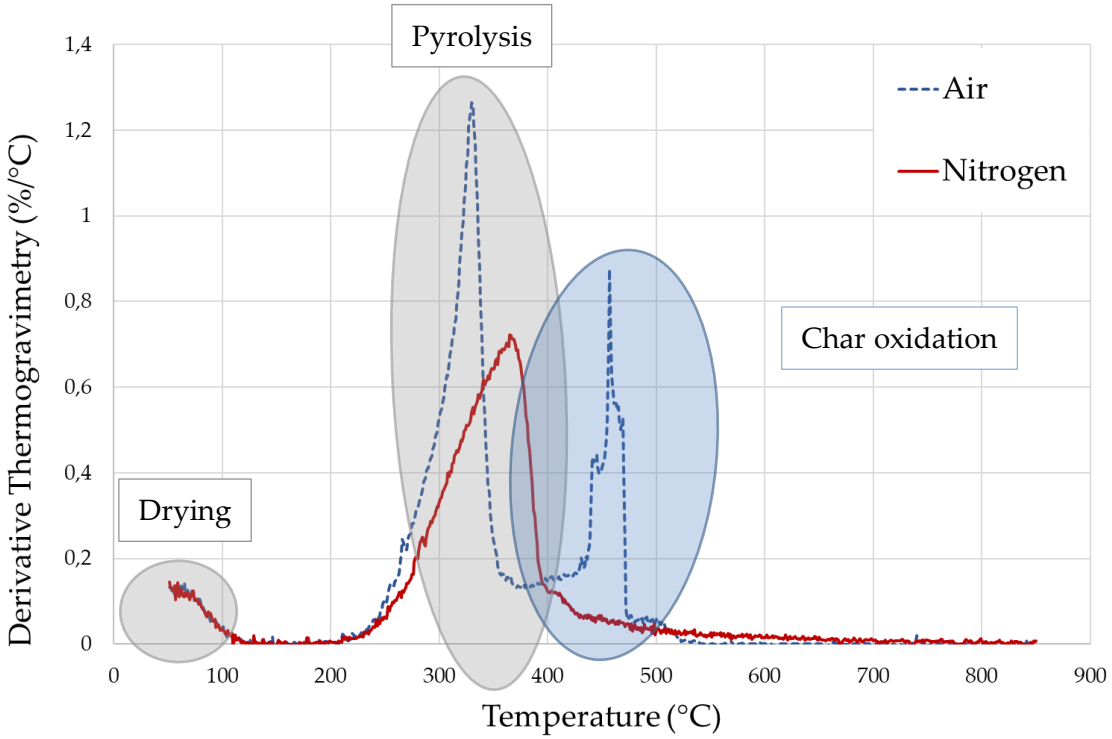

Figure 12. Mass loss rate with highlighted drying, pyrolysis and char oxidation over different, partly overlapping temperature ranges.

4.2 Medium-scale tests of load-bearing CLT columns exposed to radiant heating

A comparative experimental study was performed with medium-scale CLT columns. The columns were tested with and without a layer of glass fibre reinforced polymer on the exposed surface to hinder char fall off in the former. This allowed for investigation of the effect of char fall off on the propagation of the thermal wave within the timber sections. Char fall off was observed visually and a record of fallen char pieces is available in Appendix IV . In-depth temperatures were measured at different positions over the duration of each test. While the following section mostly analyses average temperatures from the three repetitions performed for each condition and sample type, the idividual temeperature measurements of each functioning thermocouple can be found in Appendix V .

4.2.1 Residual CLT weight and thickness

The averaged residual weight of CLT as a percentage of the initial mass of the CLT columns tested with and without glass fibre reinforced polymer is shown in Figure 13. Columns with FRP had additional 4 % of CLT-mass after tests at 20 kW/m² and 2 % at 50 kW/m². Regarding the nature of the test setup and uncertainties related to the measurement, the timber itself, the radiant panel and other factors, this is a very small difference that could be attributed to many factors and does in itself not necessarily show any effect of the GFRP layer. In comparison, Figure 14 shows the measured uncharred depths. It should be pointed out that this measurement refers to the remaining cross section of timber that could not be manually penetrated with a calliper. This data was not presented reversely as "charred depth" as large amounts of cross section were not only charred but also oxidised or fell off and were therefore entirely lost. It cannot be asumed that the difference between the initial depth of the section minus the here presented remaining cross section is a char layer sitting on top of the remaining timber. In fact, the char layer still attached to the cross section of CLT without FRP at the end of the test was between 4 mm and 15 mm thick (respectivly 3.2 % and 12 % of the initial depth of the cross section).

These plots show that the GFRP results in a reduction of loss of mass and cross-section from the CLT columns at a low and at a high heat flux. The change in thermal penetration differs however and shows a much more significant effect at the low heat flux. The experimental conditions seem to cover a range that overall shows the same trend but differing magnitude of the impact of GFRP. The following sections aim to explain the observed differences in residual weight and charring. They will investigate the effect caused by the glass fibre layer preventing char fall off. Identifying the governing parameters of the change in heat transfer will help to understand the implications of the char being held in place for the burning and residual structural capacity of timber.

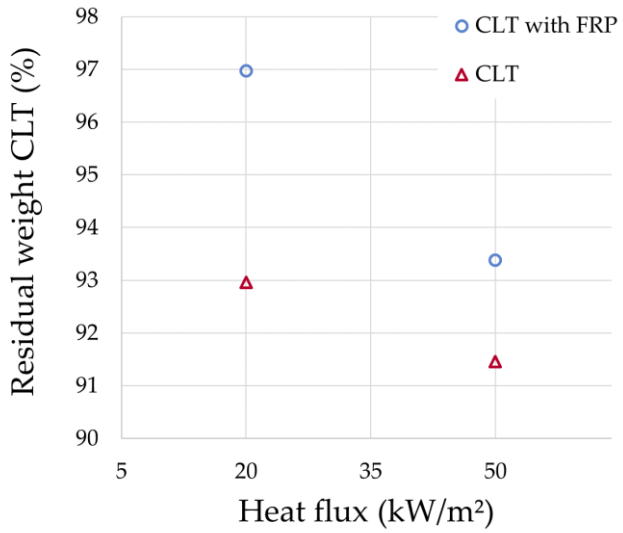

Figure 13. Averaged residual sample weight at the end of the test.

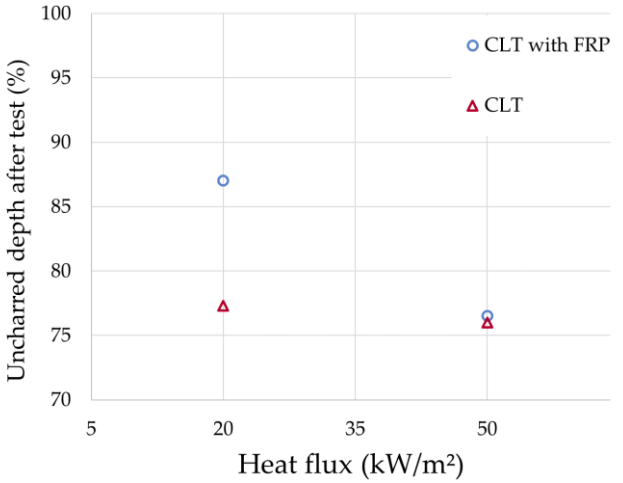

Figure 14. Averaged measured uncharred depth at the end of the test.

4.2.2 Visual observation of char fall off

Char fall off was only observed for pure CLT columns, not for CLT columns with FRP. After removing the glass fibre reinforced sample from the test setup, detachment of some char pieces from the underlying timber was seen. However, none of the pieces fell out of the matrix of the composite column during the test. At 50 kW/m², some parts of the glass fibre mat tore, potentially due to reduced tensile strength at elevated temperature or increased bending due to loss of cross section or a combination of both. Nevertheless, the glass fibre layer was still holding the char pieces in place for the

whole duration of each test and no char fell off. Exemplary pieces of fall-off from the tests with CLT without FRP are depicted in Figure 15. It can be seen that char pieces were of a wide range of shapes and sizes, from several centimeters to less than a milimeter. The thicknesses varied as well from a few milimetres to values near the thickness of the first lamella (20 mm).

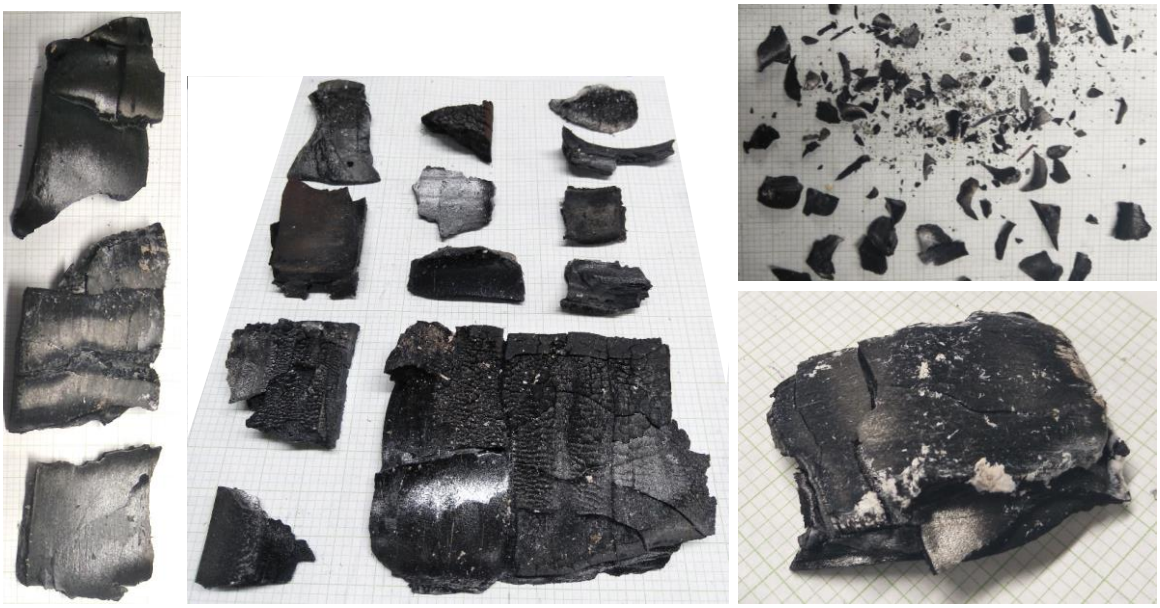

Figure 15. Exemplary pieces of fallen off char from exposed CLT columns without FRP (underlying grid paper with 2 mm-squares for reference).

Table 8 lists the times from the start of heat exposure to the first observed char fall off for CLT columns without FRP. Generally, char fall off was seen earlier at 50 kW/m² than at 20 kW/m². Test 4 with 50 kW/m² showed however an exception as char fall off happened after 1336 s compared to only 1258 s at 20 kW/m² for Test 3. Therefore it cannot generally be stated that char fall off happens later for lower heat fluxes. The three tests at 20 kW/m² show a higher variation of time to char fall off of almost 15 minutes. Less than 5 minutes lie between the earliest and latest first char fall off at 50 kW/m² heat exposure.

The measured temperature at the first glue line at the time when char fall off is also listed in Table 8. Values are highly scattered from 144 °C to as high as 812 °C. Char fall off never happened when 300 °C were measured at the glue line. PUR, the adhesive

used to bond the different lamellae for the investigated CLT, was described to significantly lose strength at temperatures between 50 °C and 150 °C [4]. Only one of the four tests showed char fall off with a glue line temeprature that falls within this range. Four of six samples showed char fall off at much higher temperatures.

Table 8. Time to char fall off for CLT samples and respective measured glue line temperatures.

Test	Heat flux	Time to first char fall off	Temperature at 1st glue line at char fall off	
1	20 kW/m²	1651 s	257 °C	
2		2216 s	531 °C (After end of test)	
3		1258 s	144 °C	Min
4	50 kW/m²	1336 s	(Thermocouple error)	
5		1059 s	431 °C	
6		1137 s	812 °C	Max

While char fall off was observed across the whole exposed surface area, the line temperatures listed in Table 8 were measured in a single point in the first glue line. It is possible that the temperatures in the glue line in the location of char fall off differed from the measured temperatures listed in Table 8. Figure 16 and Figure 17 show the range of temperature measurements across the five thermocouples placed in the first glue line [h] which show a repetitive general trend. The variation between the measurements increases at higher temperatures. At 20 kW/m², a significant increase of the range of measurements can be seen after 1000 s around 120 °C. At 50 kW/m², the variation is already higher than at 20 kW/m² below 100 °C and less than 300 s. It increases rapidly around 600 °C after overcoming the plateau of 100 °C.

[h] See section 3.3 and Appendix I for details on the thermocouple positioning. Individual thermocouples measurements at other depths, also for samples with FRP, can be found in Appendix V .

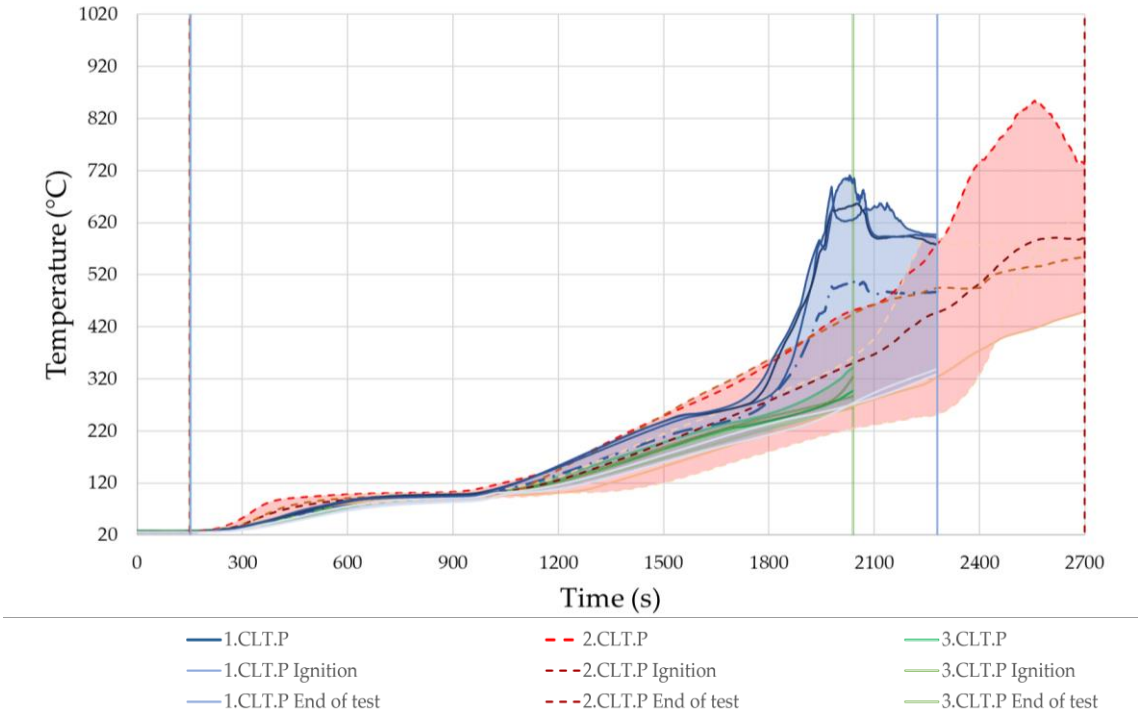

Figure 16. Temperature at the first glue line (20 mm in depth) of three different CLT samples at 20 kW/m² heat exposure (blue: Test 1, red: Test 2, green: Test 3).

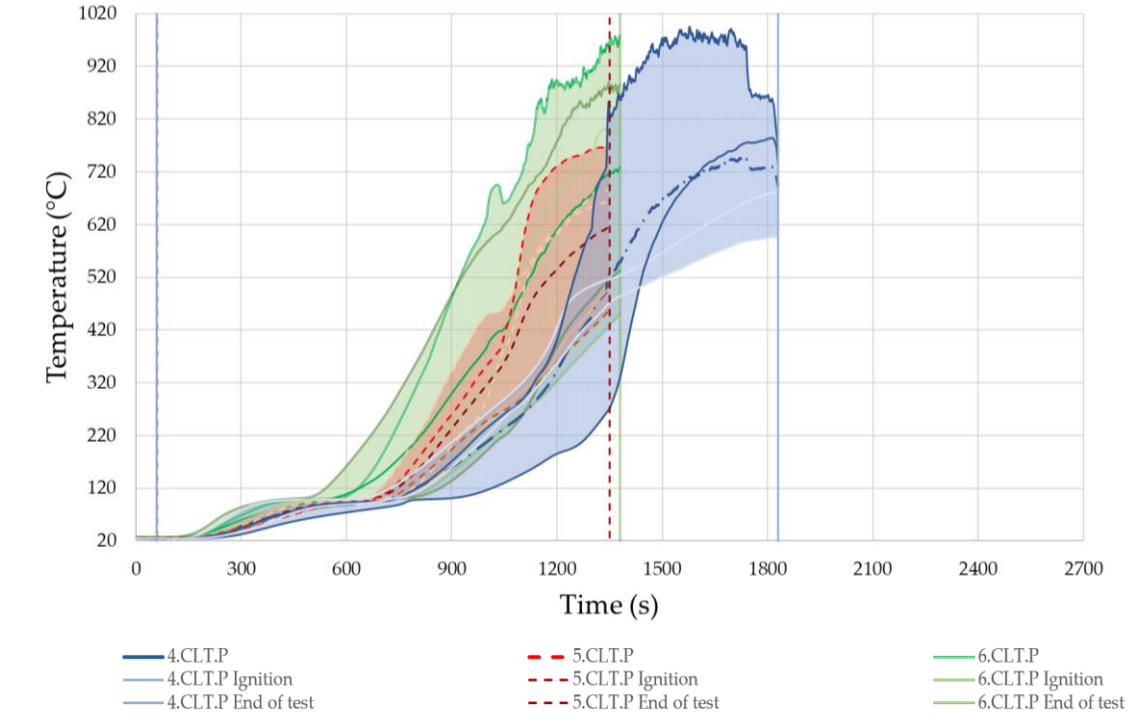

Figure 17. Temperature at the first glue line (20 mm in depth) of three different CLT samples at 50 kW/m² heat exposure (blue: Test 4, red: Test 5, green: Test 6).

4.2.3 Comparative study of in-depth temperature evolution in CLT with and without FRP

The following section will further investigate and compare the heating in depth of the medium-scale CLT columns with and without GFRP. Figure 18 and Figure 19 show the measured temperature evolution at different depths. Differences in the time taken to reach specific temperatures will be shown with Figure 22. The latter also shows the differences in rate of heating between CLT columns with and without glass fibre reinforced polymer. The temperature gradient within the timber section at different times can be found in Appendix VI .

Figure 18 and Figure 19 show the average temperature evolution measured by the in-depth thermocouples for the four conditions studied. Blue curves correspond to CLT columns with a surface layer of GFRP while red curvevs represent the CLT columns without FRP. Light coloured curves represent tests at 20 kW/m² while dark blue and dark red curves show data from tests at 50 kW/m². Maximum temperatures within a range of 780 °C to 950 °C were measured at the surface of the CLT without FRP exposed to 50 kW/m² (see Figure 18). Thereby this condition reached the highest temperatures among all four conditions not only at the surface but also five, fifteen and twenty milimetres in depth (see Figure 19). The lower temperatures measured for CLT at 20 kW/m² clearly show the influence of the incident heat flux at the surface. For samples with FRP, this influence seems to decrease with increasing depth while it remains similar for the CLT, except for the largest depth of 40 mm. The discontinuity in the data indicates the loss of cross section and subsequent exposure to the gas phase and incident radiative heat flux that was also visually observed. A rapid temperature increase of 100 °C to 250 °C can be seen right after high temperature values above 650 °C or 700 °C at all depths within the first lamella of CLT without FRP at 50 kW/m²,

Samples with FRP generally show narrower error envelopes than CLT samples without FRP. The fluctuation of error envelopes suggest that thermocouples were measuring a gas phase temperature, indicating a loss of the solid phase at shallower

depths than the thermocouple position. One thermocouple still measuring solid phase temperatures while the other was already emerged in the gas phase can be one factor increasing the error envelope. Both observations indicate higher repeatability between tests of CLT with FRP and less stochastic behaviour than for CLT without FRP.

Figure 18 shows the temperature history measured by the surface thermocouples. This corresponds to the surface of the CLT column, which is behind the glass fibre reinforced polymer for columns made of CLT with FRP. Therefore, this plot directly shows the influence of the FRP layer itself on the heat transfer at the CLT surface. For both heat fluxes, a delay in the temperature increase can be seen for CLT with FRP compared to pure CLT samples. In contrast, the maximum average temperatures are comparable: At 50 kW/m², CLT with FRP reached around 780 °C after 1000 seconds. That is only slightly lower than the steady state value of over 800 °C measured at the CLT sample from 250 s. CLT with FRP at 20 kW/m² reached temperatures aof almost 600 °C, which is above the steady state value of ca. 550 °C at the CLT surface. These results indicate that the glass fibre layer itself delays but does not reduce the heat transfer into the CLT.

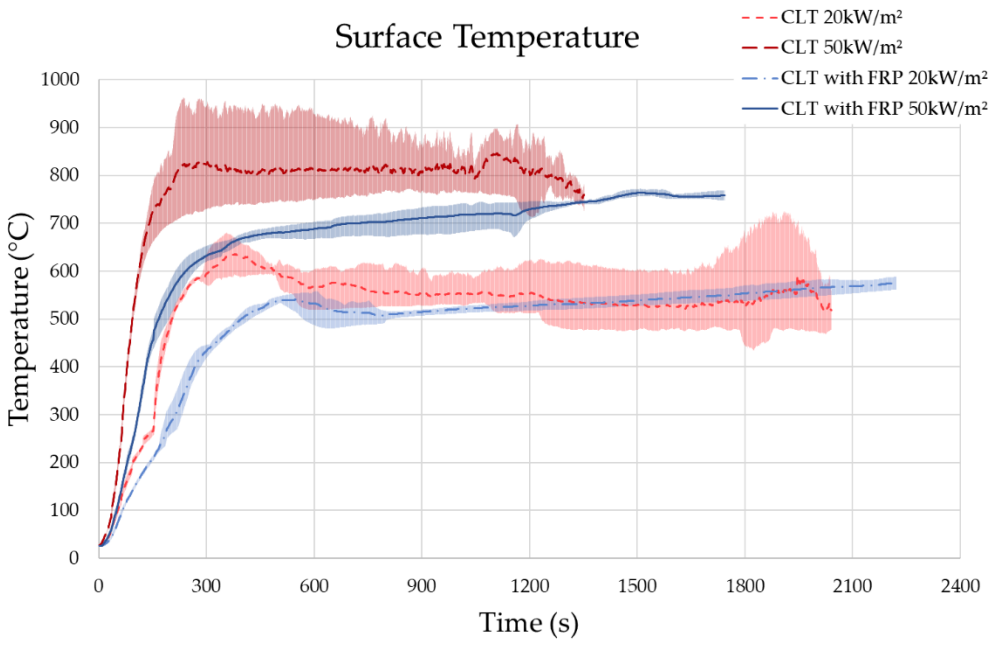

Figure 18. Temperature evolution at the CLT surface.

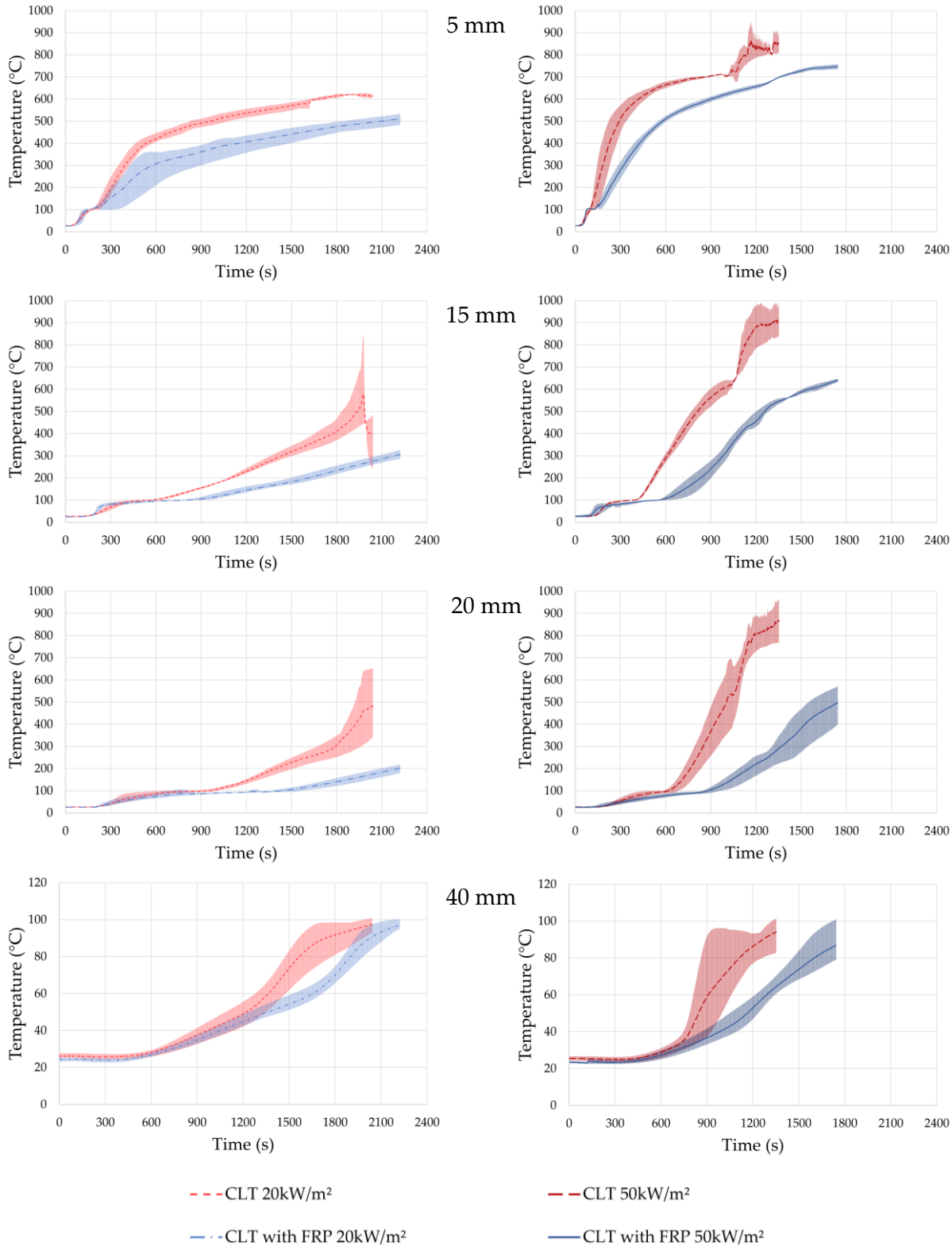

Figure 19. Temperature evolution at depths from 5 mm to 40 mm measured from the exposed surface (Left: 20 kW/m² incident heat flux; Right: 50 kW/m² incident heat flux).

All in-depth plots within the first lamella show a faster initial temperature increase for the CLT with FRP. It can probably be seen most clearly in the graphs at 15 mm depth. After this initially more rapid increase, a longer plateau around 100 °C can be seen for samples with FRP (see also Figure 21). Chemically unbound moisture evaporates during this plateau (see section 2.1).

The temperature evolution directly following the evaporation of moisture has been analysed in more detail. The slope of the temperature increase between 120 °C and 280 °C at different depths is indicated in Figure 21. These values are not intended to be a representative measurement but only to quantify the differences in heating between different conditions in this experimental study. The largest variation between testing conditions and sample types can be seen at or near the surface. The difference decrease with increasing depth, until at 40 mm, all curves show effectively the same slope. The higher heat flux of 50 kW/m² results in a larger difference between CLT and CLT with FRP than the low heat flux. Throughout al depths up to the first glue line, CLT without FRP at 50 kW/m² has the highest slope. CLT with FRP at 50 kW/m² shows more similarity with CLT at 20 kW/m² than with CLT at 50 kW/m².

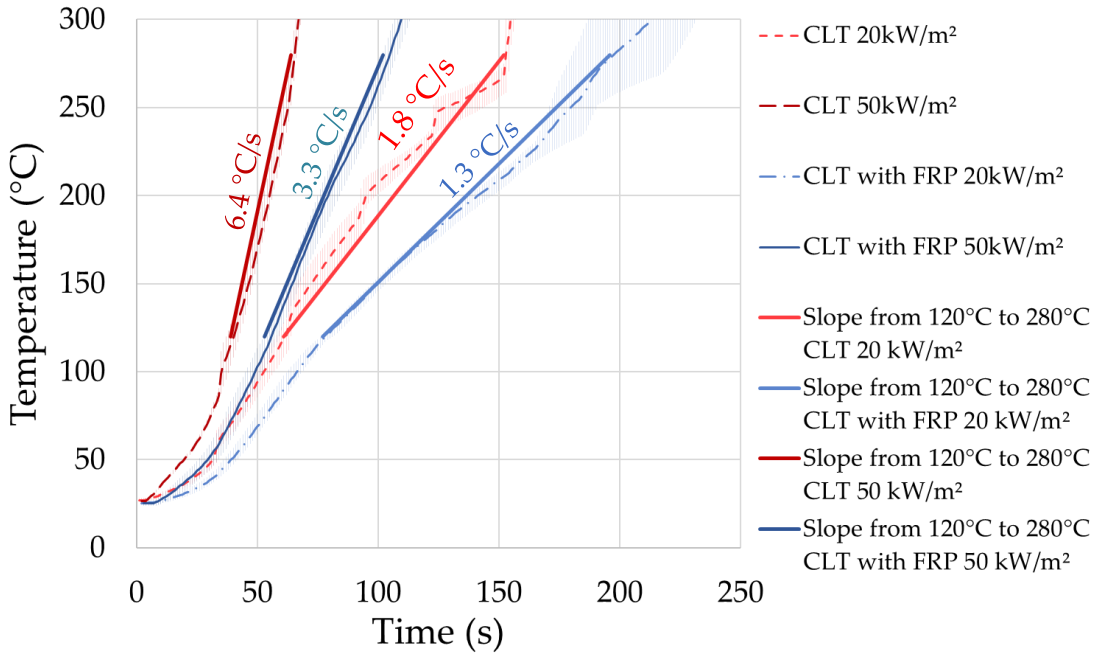

Figure 20. Slopes of temperature increase from 120 °C to 280 °C at the surface.

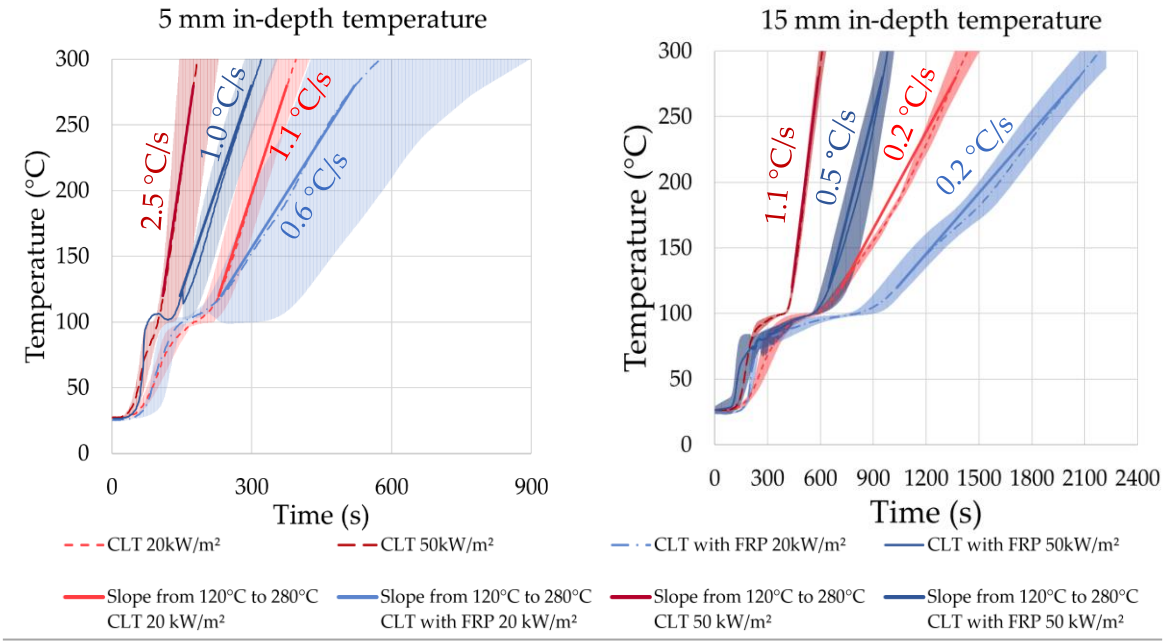

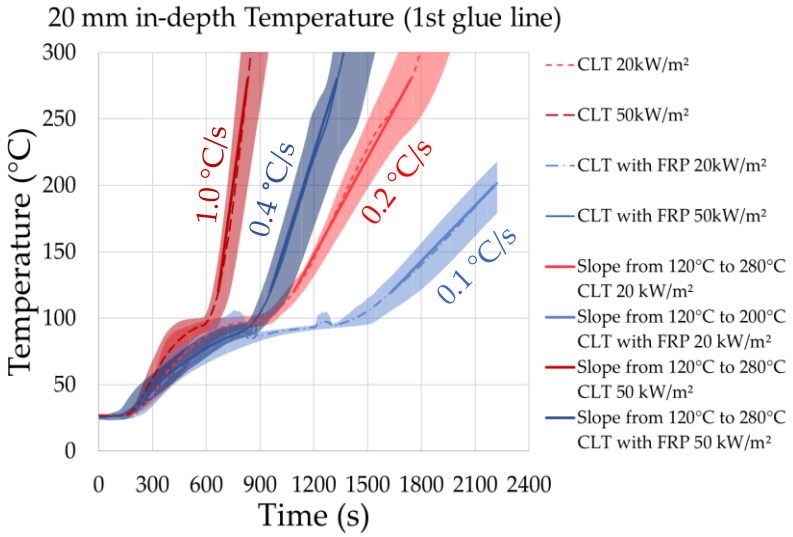

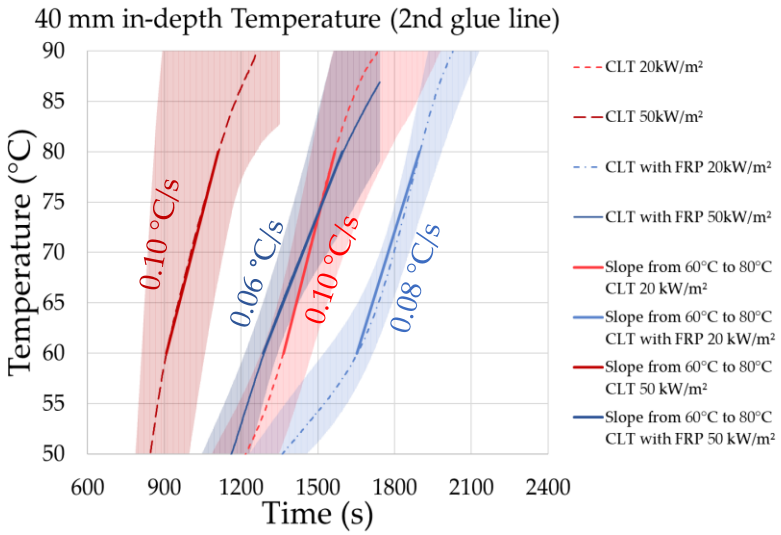

Figure 21. Slopes of temperature increase from 120 °C to 280 °C at different depths.

Timber has been shown to already irreversibly lose structural capacity from temperatures around 60 °C. A temperature of 300 °C is often seen as indicating the position of the pyrolysis front (see section 2.1).The time taken to reach 60 °C and 300 °C and at certain depths is shown in the lower and upper plot respectively in Figure 22. While depth of 40 mm reached 60 °C within the duration of the test, only a depth of 15 to 20 mm was heated to 300 °C. The measurement on the surface of the CLT is plotted at 1 mm in depth to account for the small indentation to make the thermocouple tips flush with the surface and initially measure solid phase temperatures.

Both plots show clear differences between CLT columns with and without FRP. With FRP, longer times are required at all depths to reach 300 °C, with a much larger absolute difference between heating times at deeper depths. The surface and 5 mm in depth show very similar times to reach 60 °C for samples with and without FRP, and no clear trend can be seen at 15 mm in depth as to whether FRP influences the heating process. At 20 mm however the same trend as for heating to 300 °C can already be seen with samples with FRP taking longer to reach 60 °C than CLT without FRP. This difference becomes much more significant at 40 mm.

The results presented in the previous sections show that the glass fibre layer is affecting the thermal decomposition by changing the propagation of the thermal wave within the underlying CLT. CLT with FRP was shown to have two to four percent higher residual weight of CLT at the end of the test for both applied heat fluxes. However, the remaining cross-section was only larger for CLT with FRP tested at 20 kW/m². CLT with and without FRP tested at 50 kW/m² showed the same residual uncharred depth.

Initially, samples with GFRP layer heated faster than bare CLT in depths of 5 mm and 15 mm below the exposed surface. This effect resulted in the samples with GFRP reaching the plateau around 100 °C slightly earlier. After this minor effect, that was seen within the first 300 seconds of the experiments, this plateau that marks the evaporation of moisture in the timber, tended to be elongated for samples with FRP.

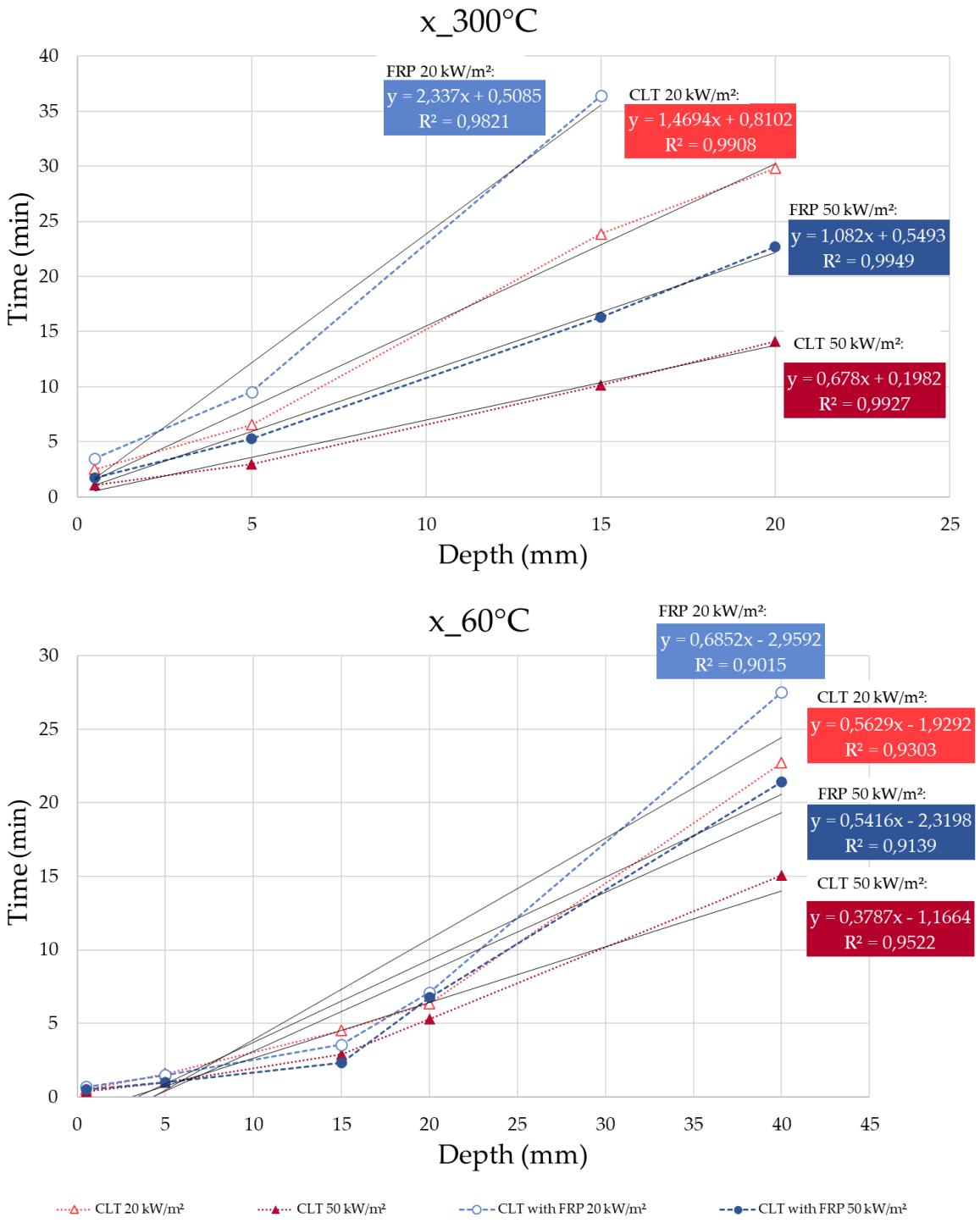

Figure 22. Times to reach 300 °C (Top) and 60 °C (Bottom) at specific in-depth positions within the CLT.

Temperatures in samples without FRP began to increase again earlier. At the surface and shallow depths, the slope of temperature increase was higher for samples without FRP. The difference of slope was found throughout the thickness of the first

lamella, with the difference in slopes between sample types and external heat fluxes decreasing with depth. At 40 mm, i.e. at the second glue line, all sample types at all heating conditions showed very similar slopes of temperature increase but with an aparent delay in time for the samples with FRP.

The observed changes in thermal decomposition, loss of cross-section and thermal propagation raise the question how the GFRP layer affects the heat transfer within the underlying CLT. The epoxy matrix is believed to be consumed by combustion reactions very early during the burning of the column. The inert glass fibre layer was however seen to remain on front of the CLT surface, even after some parts of the mat tore at high heat fluxes. Char fall off was observed for CLT without FRP at both heat fluxes but at neither heat flux for CLT with FRP. A list of hypotheses was developed regarding possible causes for the observed differences in thermal propagation between samples with and without glass fibre reinforced polymer.

A. The change in properties of the char compared to the virgin timber could create a higher thermal resistance. This affects the heat transfer in-depth as the glass fibre layer is mechanically holding the char in place (as compared to the loss of cross-section due to char fall off observed for samples without a glass fibre layer).
B. The volume of the char layer, independent of its exact thermal properties, could serve as an additional thermal mass. With the glass fibre layer preventing char fall off, given a finite amount of incident energy, longer times will be required to reach high temperatures in the underlying timber.
C. The glass fibre layer itself could be creating an additional thermal resistance due to its material properties and thickness.
D. The air gap formed between the glass fibre and the surface of CLT (char or timber) after the initial surface regression could be creating an insulation effect for the underlying CLT (char and timber).
E. The glass fibre mat could be preventing mass transfer of oxygen from the

surrounding atmosphere to the char layer and thereby reduce the heat flux from the oxidising char layer into the underlying timber.

This list of hypotheses is not a complete list of possible causes. Other factors could be causing the observed changes. Some of the above presented possibilities have been analysed with a numerical model. The obtained results will be presented in the following section.

4.3 Numerical analysis of the heat transfer in a heated timber section

The impact of different properties of the glass fibre layer itself and the char layer, mechanically constrained to stay attached to the CLT surface, were analysed with a numerical tool. For both incident heat fluxes, calculations were carried out for four general scenarios, two of which were repeated with variations to see the impact of a specific variable. See section 3.6.1 for a detailed explanation of the different modeled cases that were developed based to verify some of the hypotheses presented above. A high and a low heat flux were used for the numerical analysis based on the experimental data showing different results depending on the heating condition. Table 9 and Table 10 list the results at 20 kW/m² and 50 kW/m² external heat flux respectively. As a performance criterion, the time for the pyrolysis front, assumed to be the 300 °C-isotherm, to reach 20 mm was chosen. Then the times to reach 60 °C at 40 mm were found as this temperature was shown to mark the onset of irreversible loss of structural capacity (see section 2.1). The depths were chosen as the positions of the first and second glue line in the experimental study as temperature data from the test was recorded there and because the previously observed effect on these depths was different. In parenthesis, the difference from each model compared to the base case is indicated.

For both heat fluxes, all modeled cases show closer agreement for the time to reach 60 °C at 40 mm depth than for the times to reach 300 °C at 20 mm. The resulting

times to reach 300 °C at 20 mm for different modeled cases lie closer together at 50 kW/m² than at 20 kW/m². This implies larger effects of the analysed properties closer to the surface and at lower heat fluxes.

Table 9. Numerical results for different models: Times to reach specific temperatures at certain depths with 20 kW/m² external heat flux.

	Time (s) to reach 300 °C at 20 mm	Time (s) to reach 60 °C at 40 mm
Model		
0 (Base Case)	6,763	1,720
1 ("Inert" virgin timber)	7,523 (+11%)	1,728 (+0.5%)
2 (Glass fibre layer with Base Case)		
2.1 (GF with a=0.75)	12,385 (+83%)	1,849 (+7%)
2.2 (GF with a=0.90)	6440 (-5%)	1734 (+1%)
2.3 (GF with a=0.95)	5,662 (-16%)	1,688 (-2%)
3 (Glass fibre layer with Air Gap and Base Case)		
3.1 1mm air gap	7196 (+6%)	1,820 (+6%)
3.2 10 mm air gap	8,299 (+23%)	2,009 (+17%)
3.3 100 mm air gap	8,533 (+26%)	2,048 (+19%)

Table 10. Numerical results for different models: Times to reach specific temperatures at certain depths with 50 kW/m² external heat flux.

	Time (s) to reach 300 °C at 20 mm	Time (s) to reach 60 °C at 40 mm
Model		
0 (Base Case)	1,580	1,223
1 ("Inert" virgin timber)	1,936 (+23%)	1,308 (+7%)
2 (Glass fibre layer with Base Case)		
2.1 (GF with a=0.75)	1,892 (+20%)	1,310 (+7%)
2.2 (GF with a=0.90)	1541 (-3%)	1,237 (+1%)
2.3 (GF with a=0.95)	1456 (-8%)	1216 (-1%)
3 (Glass fibre layer with Air Gap and Base Case)		
3.1 1mm air gap	1,694 (+7%)	1,274 (4%)
3.2 10 mm air gap	1,793 (+13%)	1,326 (+8%)
3.3 100 mm air gap	1,808 (+14%)	1,335 (+9%)

The assumption of inert timber that does not degrade or change properties at elevated temperatures shows 11 % and 23 % longer times for the first glue line to reach 300 °C at 20 and 50 kW/m² respectively. The effect is lower at deeper depths which is likely indicating the progression of drying and charring in depth in the base case that the model is compared to.

As the exact absorptivity of the glass fibre mat was unclear, the highest (0.95) and lowest value (0.75) were analysed. The absorptivity defines the incident heat flux into the composite section. It determines the fraction of the external heat flux that gets transferred into the solid. At 20 kW/m², a lower absopivity achieved the largest improvement of all cases at 20 mm depth (+83%). A significant improvement (+20%) can also be seen at 50 kW/m². Similar to the experimental results, the effect in depths in less concise and very similar for both heat fluxes (+7%). Therefore the absorptivity seems likely to be a factor in the observed differences between the temperatures in CLT with and without FRP in the experiments. However, further tests are necessary to verify the exact emissivity of the glass fibre mat.

To remove absorptivity as a variable, it was set to 0.9, equal to the absorptivity of timber. This case shows that thin layer of glass fibre itself does not strongly effect the heat transfer within the timber section. The resulting negative values could be attributed to the simplified way of modeling the conduction through the bi-material interface of glass fibre and timber. However, it is clear that the impact of the glass fibre as such is negligible at all depths and heat fluxes.

The air gap that forms between the glass fibre and the charred timber surface has a significant impact on the heat transfer once it reaches a consiberable thickness. Its impact approaches however a maximum value, as an unrealistic air gap of 100 mm only showed a minor improvement compared to a more realistic gap of 10 mm. The development of an air gap over time would have to be investigated more closely to accurately quantify the impact on the heat transfer process.

Figure 23 and Figure 25 visualise the heated depths calculated in the heat transfer model for the different cases. Figure 23 compares the depths that reached 300 °C in the time that it took the 300 °C isoterm in the Base Case to reach the first glue line (20 mm). Using the same approach, Figure 25 depicts the depths heated to 60 °C at the time that the 60 °C-isotherm required in the Base Case to reach the second glue line (40 mm). Figure 24 and Figure 26 visualise the experimental data in a similar manner for

comparison.

The different magnitude of the analysed properties with respect to each other but also at different heat fluxes can be seen in Figure 23. Figure 25 shows clearly that all tested properties have either no or a positive effect on the propagation of the 60 °C-isotherm. None of the properties investigated in isolation show the same effect as the experimental results in Figure 24 and Figure 26. This implies that different effects happen simultaneously or that other phenomena are occuring that have not been analysed.

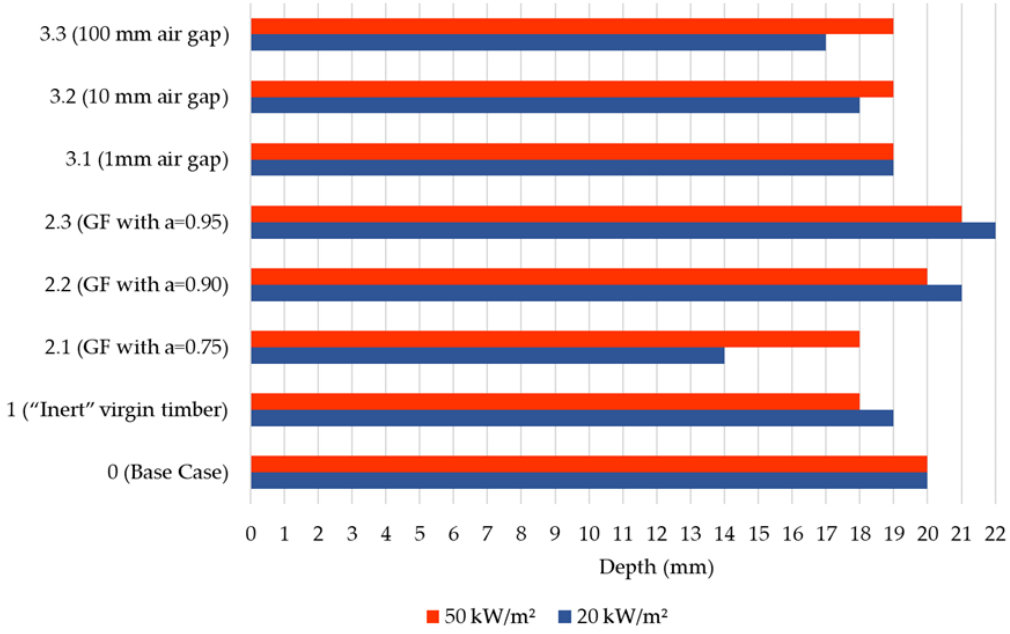

Figure 23. Position of 300 °C-isotherm at time step when 1st glue line of Base Case reaches 300 °C.

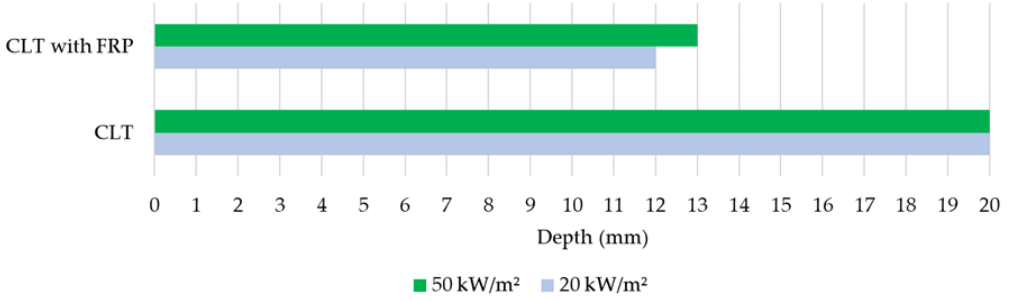

Figure 24. Position of 300 °C-isotherm at time when 1st glue line of CLT reaches 300 °C (Experimental data).

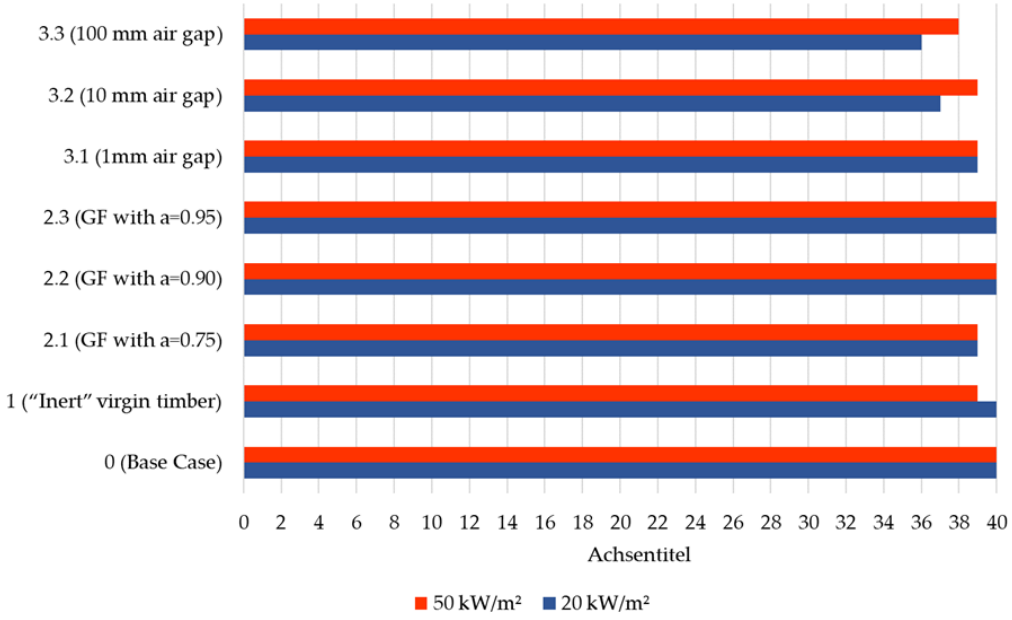

Figure 25. Position of 60 °C-isotherm at time step when 2nd glue line of Base Case reaches 60 °C.

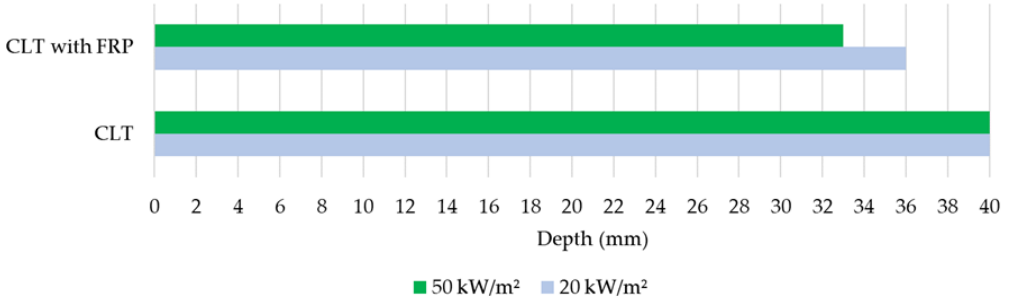

Figure 26. Position of 60 °C-isotherm at time when 2nd glue line of CLT reaches 60 °C (Experimental data).

Chapter 5 Discussion

The results presented in the previous chapter demonstrated that the chosen experimental method allowed to show, quantify and investigate differences between external heat fluxes of varying magnitude and between CLT with and without glass fibre reinforcement. Results were also shown to be relatively repeatable regarding the observed trends and the effect of the FRP on the residual weight, uncharred depth and char fall off. Additional sources information like Thermogravimetric Analsys and thermocouple measurements allowed further insights into the phenomena of interest, like the temperature development in-depth over time.

The applied thin layer of GFRP was shown to prevent char fall off under all testing conditions, which affected the in-depth heating of the underlying CLT section. The glass fibre layer held detached char pieces within the matrix of the composite material, thereby providing a thermal barrier for the underlying timber. This shows that preventing char fall off has a significant positive impact on the heat transfer within the timber. While the effect was larger at lower heat fluxes, the resulting temperature distribution within the timber was also improved at high heat fluxes. From a reversed point of view, the obtained results show that the influence of char fall off on the thermal decomposition and burning of timber is important and cannot be ignored. The loss of char was shown to greatly affect the propagation of the thermal wave and further decomposition of the timber.

The results of the numerical model imply, in agreement with the experimental results, larger immediate effects of char fall off closer to the surface and at lower heat fluxes. The numerical model helped to quantify the influence of some timber and glass fibre properties on the in-depth heat transfer. The thermal resistance of the glass fibre layer itself was negligible, while the surface absorptivity had a significant effect on the observed differences in temperatures between CLT with and without FRP.

The numerical results prove that char does not inherit improved insulation properties compared to virgin timber. Charring thus increases the heating in depth

compared to virgin timber. It is of course not possible to hinder virgin timber from undergoing thermal decomposition into dry and charred timber at elevated temperatures. Therefore, it would be favourable to keep the timber at low temperatures for as long as possible to ensure better insulation of deeper depths. This would also positively affect residual structural integrity. However, keeping charred sections in place will still provide an insulating effect similar to that of the original timber section whereas char fall off continuously exposes underlying timber. As a result, the rate of heating, in-depth temperatures and the heated depth increase. This leads to higher mass loss and reduced depths of the residual cross-section. These results imply that the structural capacity of engineered timber in fire conditions will be largely affected by char fall off. The consequences for the mechanical behaviour of timber members need to be evaluated but were not analysed herein.

By promoting faster and more in-depth thermal decomposition of a larger amount of timber cross-section, char fall off also likely to affect the contribution of the timber structure itself to the fire. Increased production of combustible pyrolysis gases in the timber will provide a higher fuel load to compartment fires in exposed timber structures. In the early stages of a fire, this can intensify the burning and decrease the time available for safe evacuation. It can also extend the duration of a fire, which in turn promotes larger in-depth heating of structural members. This can endanger structural integrity and compartmentation, leading to failure of the fire safety strategy and putting lifes of fire service personnel and property at risk.

There are likely other phenomena introduced by the GFRP system that have not yet been investigated which reduce char depths, prevent char fall off and contribute to the changed thermal behaviour. Moreover, different processes could be interdependent and promote or hinder each other, which cannot be seen from the numerical analysis that investigated different properties in isolation. An air gap between the GFRP and the char layer was found to have significant potential to improve the thermal insulation of the underlying timber. The phenomena creating this

gap, like char oxidation, and the potential impacts of it, need to be investigated futher in the future to create a deeper understanding of the relevent mechanisms. Insights into the different cohesive and adhesive failure modes in engineered timber at elevated temperatures seem to be essential. Understanding the prevalent causes for char fall off on a micro-scale seems to be essential to identify the critical conditions for char fall off in general, which could be critical stresses, temperatures and their interactions.

It was shown that isotherm positions cannot predict char fall off, as no systematic correlation between glue line temperatures and char fall off was seen. Therefore the propagation of the 300 °C-isotherm, often used to indicate the pyrolysis front, is no direct indication for char fall off. Moreover, the degradation of adhesive properties with temperature, seen in isolation, cannot be used as a direct indicator to predict char fall off. Four out of six samples showed char fall off at glue line temperatures far higher than the expected softening temperature of PUR.

The highly scattered times to the first observation of char fall off and the high variability in temperatures at the first glue line further highlight that char fall off cannot easily be predicted. Char fall off was proven to be an extremely complicated problem that at present is not yet understood sufficiently and thus cannot be solved with tools that are currently available. Therefore, to date, no numerical model can account for the phenomenon of char fall off, that was however found to be highly relevant. As char fall off was found to largely affect the burning of engineered timber, and the progression of heat within the cross section, no modeling approach known to the author is able to accurately predict the response of engineered timber in fire conditions.

Chapter 6 Conclusions

An experimental study was conducted in which loaded cross-laminated timber columns under a constant bending load were exposed to a radiant heat flux. The aim of the research was to investigate the effect of char fall off on the heat transfer within engineered timber. Therefore, some specimen were equipped with a layer of glass fibre reinforced polymer (GFRP) to prevent char fall off. This allowed for a comparative study of the impact of char fall off resulting in differences in residual weight of the CLT columns, remaining depth of the cross-section, and the evolution of in-depth temperatures.

All bare CLT samples showed char fall off, while no char fall off was observed for any sample with GFRP reinforced surface. Char fall off was shown to increase the mass loss by 4 % at 20 kW/m² and by 2 % at 50 kW/m². At 20 kW/m², the char front progressed about 10 % further in depth for samples that showed char fall off. No significant difference was found between the remaining uncharred depths of columns tested under 50 kW/m².

The time to the first char fall off event varied from ca. 17 minutes to 37 minutes from first heat exposure and tended to be shorter at higher heat exposure. Temperatures measured at the first glue line at the times of first char fall off showed no clear trend and ranged between 144 °C and 812 °C, while the thermocouple measurements were shown to follow relatively repeatable trends.

Initial heating in-depth up to temperatures of around 100 °C was slightly faster (<1 min) for samples with GFRP than for bare CLT. The following plateau, characteristic for evaporation of moisture within the timber, was approximately twice as long for CLT with FRP at depths between 5 and 20 mm. The following temperature increase was more rapid for samples at 50 kW/m². This was most succinct at the surface with a 3.5-times steeper slope for CLT without FRP and a 2.5-times steeper slope for CLT with FRP compared to samples exposed to 20 kW/m². Throughout the duration

of the tests, CLT samples without FRP that experienced char fall off showed higher temperatures at all depths than CLT with FRP. CLT reached maximum average temperatures of 900 °C throughout the initial thickness of the first lamella. The maximum temperature for CLT with FRP was 750 °C at the surface and 5 mm in depth, while further in depth only lower temperatures were reached. The tests were stopped when the second glue line reached 100 °C which was later for all samples with FRP than for CLT samples that showed char fall off.

It was shown with a numerical model that the thermal resistance of the glass fibre layer itself only had a minor effect on the heat transfer within the timber. The absorptivity of the surface material directly exposed to the external radiant heat flux showed a significant impact on the temperature evolution at 20 mm in depth. An absorptivity of 0.75 almost doubled the time to reach 300 °C compared to a value of 0.9. An air gap between the glass fibre and the charred timber surface also affected the temperature by up to 26 %. However, none of the timber and glass fibre properties analysed in isolation showed the same impact on heated depths as found from the experimental data (-7 mm ±0.5 for 300 °C and -5.5 mm ±1.5 for 60 °C). It can therefore be concluded that the whole composite system that is preventing char fall off is causing the experimentally measured effect on the propagation of the thermal wave within the timber. Moreover, other phenomena that have not been investigated herein could affect the propagation of the thermal wave.

Numerical modeling of the thermal degradation and burning of timber is highly complex. A good model needs to account for all relevant phenomena that significantly affect the decomposition of timber. As presented herein, char fall off has a strong influence on the thermal response of timber exposed to radiant heating, both mechanically and for the resulting fire dynamics. The mechanisms behind char fall off are, however, only poorly understood. Therefore all numerical tools developed to date do not or not accurately account for char fall off and consequently cannot predict the response of engineered timber products exposed to fire conditions in a reliable

manner. Suitable research methods aiming at refining the understanding of char fall off need to be developed to enable robust and resilient fire safety designs of engineered timber structures.

References

[1] M. H. Ramage *et al.*, "The wood from the trees: The use of timber in construction," *Renewable and Sustainable Energy Reviews*. 2017, doi: 10.1016/j.rser.2016.09.107.

[2] D. Barber, "Tall Timber Buildings: What's Next in Fire Safety ?," *Fire Technology*. 2015, doi: 10.1007/s10694-015-0497-7.

[3] A. Law and R. M. Hadden, "We need to talk about timber," *Struct. Eng.*, 2020.

[4] F. Wiesner, "Structural behaviour of cross-laminated timber elements in fires," The University of Edinburgh, 2019.

[5] A. I. Bartlett, R. M. Hadden, and L. A. Bisby, "A Review of Factors Affecting the Burning Behaviour of Wood for Application to Tall Timber Construction," *Fire Technology*. 2019, doi: 10.1007/s10694-018-0787-y.

[6] E. Barbero, J. Davalos, and U. Munipalle, "Bond Strength of FRP-Wood Interface," *J. Reinf. Plast. Compos.*, 1994, doi: 10.1177/073168449401300905.

[7] L. Schmidt and D. Fernando, "Fire behaviour of a timber composite with GFRP reinforcement compared to unreinforced laminated timber," in *Advanced Composites in Construction, ACIC 2019 - Proceedings of the 9th Biennial Conference on Advanced Composites in Construction 2019*, 2019.

[8] D. Drysdale, *An Introduction to Fire Dynamics: Third Edition*. 2011.

[9] R. Stürzenbecher, K. Hofstetter, and J. Eberhardsteiner, "Structural design of Cross Laminated Timber (CLT) by advanced plate theories," *Compos. Sci. Technol.*, 2010, doi: 10.1016/j.compscitech.2010.04.016.

[10] L. Hasburgh, K. Bourne, P. Peralta, P. Mitchell, S. Schiff, and W. Pang, "Effect of adhesives and ply configuration on the fire performance of Southern pine cross-laminated timber," in *WCTE 2016 - World Conference on Timber Engineering*, 2016.

[11] R. Brandner, G. Flatscher, A. Ringhofer, G. Schickhofer, and A. Thiel, "Cross laminated timber (CLT): overview and development," *Eur. J. Wood Wood Prod.*,

vol. 74, no. 3, pp. 331–351, 2016, doi: 10.1007/s00107-015-0999-5.

[12] R. M. Foster and M. H. Ramage, "Briefing: Super tall timber - Oakwood Tower," *Proc. Inst. Civ. Eng. Constr. Mater.*, 2017, doi: 10.1680/jcoma.16.00034.

[13] M. F. L. Mallo and O. Espinoza, "Cross-Laminated Timber vs. Concrete/steel: Cost comparison using a case study," in *WCTE 2016 - World Conference on Timber Engineering*, 2016.

[14] M. Green and E. Karsh, "The Case for Tall Wood Buildings," *mgb Archit. + Des.*, 2012.

[15] L. Lowden and T. Hull, "Flammability behaviour of wood and a review of the methods for its reduction," *Fire Sci. Rev.*, 2013, doi: 10.1186/2193-0414-2-4.

[16] V. Babrauskas, "Ignition of wood: A review of the state of the art," *J. Fire Prot. Eng.*, 2002, doi: 10.1177/10423910260620482.

[17] A. Frangi, M. Fontana, M. Knobloch, and G. Bochicchio, "Fire behaviour of cross-laminated solid timber panels," in *Fire Safety Science*, 2008, doi: 10.3801/IAFSS.FSS.9-1279.

[18] E. Mikkola, "Charring Of Wood Based Materials," *Fire Saf. Sci.*, 1991, doi: 10.3801/iafss.fss.3-547.

[19] R. H. White and M. A. Dietenberger, "Wood Products: Thermal Degradation and Fire," in *Encyclopedia of Materials: Science and Technology*, 2001.

[20] S. Poncsák, D. Kocaefe, M. Bouazara, and A. Pichette, "Effect of high temperature treatment on the mechanical properties of birch (Betula papyrifera)," *Wood Sci. Technol.*, 2006, doi: 10.1007/s00226-006-0082-9.

[21] F. Browne, "Theories of the combustion of wood and its control," *United states Dep. Agric. For. Serv. Rep. No. 2136*, 1958.

[22] P. Reszka, "In-Depth Temperature Profiles in Pyrolyzing Wood," The University of Edinburgh, 2008.

[23] R. Emberley, A. Inghelbrecht, Z. Yu, and J. L. Torero, "Self-extinction of timber," *Proc. Combust. Inst.*, vol. 36, no. 2, pp. 3055–3062, 2017, doi:

10.1016/j.proci.2016.07.077.

[24] P. Reszka and J. L. Torero, "In-depth temperature measurements in wood exposed to intense radiant energy," *Exp. Therm. Fluid Sci.*, 2008, doi: 10.1016/j.expthermflusci.2007.11.014.

[25] A. Law and R. Hadden, "Burnout means Burnout." SFPE, 2017.

[26] A. Bartlett, R. Hadden, L. Bisby, and B. Lane, "Auto-extinction of engineered timber as a design methodology," in *WCTE 2016 - World Conference on Timber Engineering*, 2016.

[27] R. Emberley, T. Do, J. Yim, and J. L. Torero, "Critical heat flux and mass loss rate for extinction of flaming combustion of timber," *Fire Saf. J.*, vol. 91, pp. 252–258, Jul. 2017, doi: 10.1016/j.firesaf.2017.03.008.

[28] R. Crielaard, J. W. van de Kuilen, K. Terwel, G. Ravenshorst, and P. Steenbakkers, "Self-extinguishment of cross-laminated timber," *Fire Saf. J.*, vol. 105, no. January, pp. 244–260, 2019, doi: 10.1016/j.firesaf.2019.01.008.

[29] C. Gorska, J. P. Hidalgo, and J. L. Torero, "An Experimental Study of Medium-Scale Compartment Fire Tests With Exposed Cross Laminated Timber," in *IFireSS 2017 – 2nd International Fire Safety Symposium*, 2017.

[30] A. Inghelbrecht, "Evaluation of the burning behaviour of wood products in the context of structural fire design," The University of Queensland, Ghent University, 2014.

[31] A. Frangi and M. Fontana, "Charring rates and temperature profiles of wood sections," *Fire Mater.*, 2003, doi: 10.1002/fam.819.

[32] A. I. Bartlett, A. Chapman, C. Roberts, F. Wiesner, R. M. Hadden, and L. A. Bisby, "Thermal and flexural behaviour of laminated bamboo exposed to severe radiant heating," in *WCTE 2018 - World Conference on Timber Engineering*, 2018.

[33] R. M. Hadden *et al.*, "Effects of exposed cross laminated timber on compartment fire dynamics," *Fire Saf. J.*, 2017, doi: 10.1016/j.firesaf.2017.03.074.

[34] A. I. Bartlett, R. M. Hadden, L. A. Bisby, and A. Law, "Analysis of cross-

laminated timber charring rates upon exposure to nonstandard heating conditions," in *Fire and Materials 2015 - 14th International Conference and Exhibition, Proceedings*, 2015.

[35] K. L. Friquin, "Material properties and external factors influencing the charring rate of solid wood and glue-laminated timber," *Fire Mater.*, 2011, doi: 10.1002/fam.1055.

[36] T. T. Lie, "Method for Assessing the Fire Resistance of Laminated Timber Beams and Columns.," *Can. J. Civ. Eng.*, vol. 4, no. 2, pp. 161–169, 1977, doi: 10.1139/l77-021.

[37] R. Emberley *et al.*, "Description of small and large-scale cross laminated timber fire tests," *Fire Saf. J.*, 2017, doi: 10.1016/j.firesaf.2017.03.024.

[38] C. Miao, D. Fernando, M. T. Heitzmann, and H. Bailleres, "GFRP-to-timber bonded joints: Adhesive selection," *Int. J. Adhes. Adhes.*, 2019, doi: 10.1016/j.ijadhadh.2019.05.007.

[39] Lavender CE Pty Ltd, "Guide to Reinforcements." [Online]. Available: www.lavender-ce.com. [Accessed: 06-Apr-2020].

[40] D. Fernando, J. G. Teng, J. Gattas, and M. Heitzmann, "Hybrid fibre-reinforced polymer–timber thin-walled structural members," *Adv. Struct. Eng.*, 2018, doi: 10.1177/1369433217739709.

[41] L. A. Bisby and M. Green, "Fire Performance of FRP Systems for Infrastructure : A State-of-the-Art Report NRC Publications Archive (NPArC)," no. October 2015, 2005, doi: 10.4224/20377587.

[42] K. Richter and R. Steiger, "Thermal stability of wood-wood and Wood-FRP bonding with polyurethane and epoxy adhesives," *Adv. Eng. Mater.*, 2005, doi: 10.1002/adem.200500062.

[43] P. K. Mallick, *Fiber-reinforced composites: Materials, manufacturing, and design, third edition*. 2007.

[44] A. F. Osorio, J. P. Hidalgo, and P. D. Evans, "Enhancing the fire performance of

engineered mass timber and its implications to the fire safety strategy," *WCTE 2018 - World Conf. Timber Eng.*, no. Lvl, 2018.

[45] M. N. Fardis and H. H. Khalili, "FRP-encased concrete as a structural material," *Mag. Concr. Res.*, 1982, doi: 10.1680/macr.1982.34.121.191.

[46] F. Richter and G. Rein, "A multiscale model of wood pyrolysis in fire to study the roles of chemistry and heat transfer at the mesoscale," *Combust. Flame*, vol. 216, pp. 316–325, 2020, doi: 10.1016/j.combustflame.2020.02.029.

[47] C. Lautenberger and C. Fernandez-Pello, "A model for the oxidative pyrolysis of wood," *Combust. Flame*, vol. 156, no. 8, pp. 1503–1513, 2009, doi: 10.1016/j.combustflame.2009.04.001.

[48] F. P. Incropera, D. P. DeWitt, T. L. Bergman, and A. S. Lavine, *Fundamentals of Heat and Mass Transfer(6th edition)*. 2007.

[49] P. Chowdhury, "Experimental study of char fall-off phenomenon in CLT under fire," The University of Queensland, 2019.

[50] Y. El-Hage, S. Hind, and F. Robitaille, "Thermal conductivity of textile reinforcements for composites," *J. Text. Fibrous Mater.*, vol. 1, p. 251522111775115, 2018, doi: 10.1177/2515221117751154.

[51] "AZO Materials." [Online]. Available: https://www.azom.com/properties.aspx?ArticleID=764.

[52] A. J. Stretton, "Radiation heat transfer," in *SFPE Handbook of Fire Protection Engineering, Fifth Edition*, 2016.

[53] L. Peng, G. Hadjisophocleus, J. Mehaffey, and M. Mohammad, "Predicting the Fire Resistance of Wood–Steel–Wood Timber Connections," *Fire Technol.*, vol. 47, no. 4, pp. 1101–1119, 2011, doi: 10.1007/s10694-009-0118-4.

[54] M. Janssens, "Thermo-physical properties for wood pyrolysis models," in *Pacific timber engineering conference*, 1994.

Appendix I Thermocouple positions

The positioning of the in-depth thermocouples used in the medium-scale experimental study with CLT with and without GFRP is shown in Figure 27.

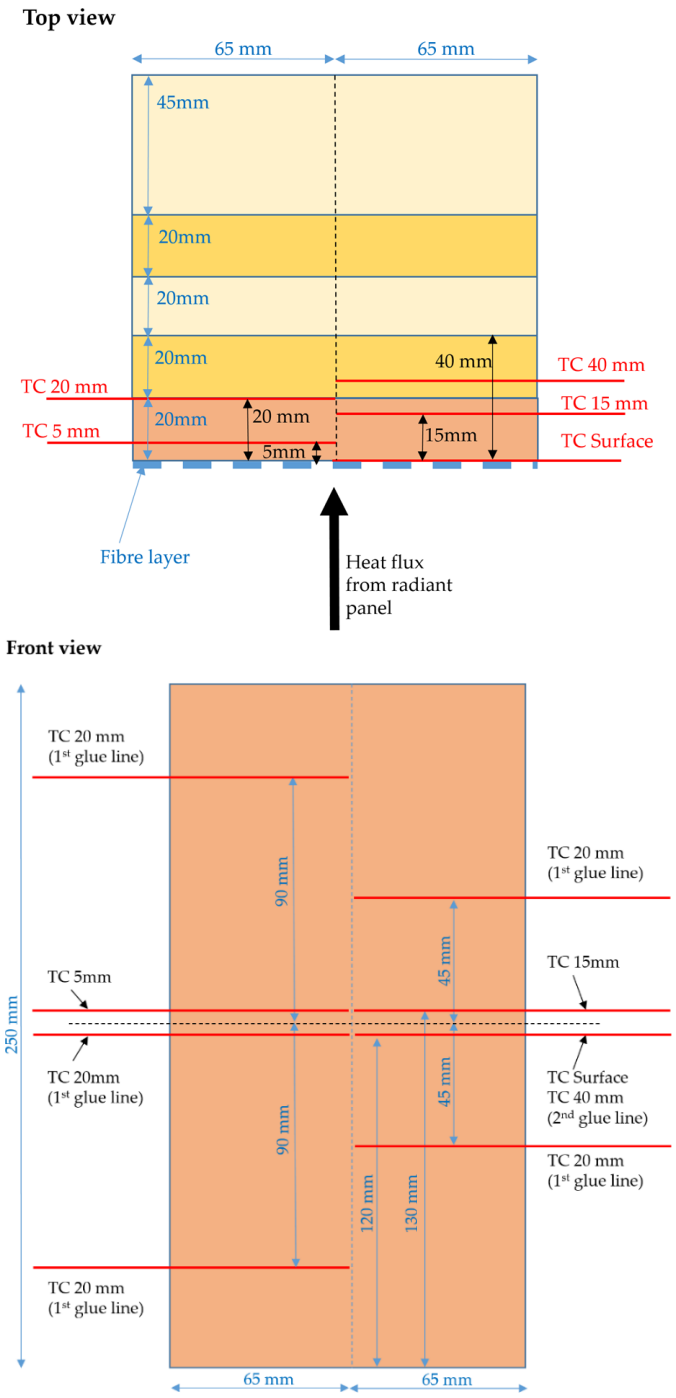

Figure 27. Thermocouple positions in the exposed area (Top: Top view, Bottom: Front view). Surface TC: CLT without FRP: indentation in timber surface, CLT with FRP: between FRP and timber surface.

Appendix II Data analysis

All data recorded during the experimental test series was carefully reviewed and processed. Therefore each set of thermocouple data was plotted individually over time to determine outliers caused by broken thermocouples, poor connections or similar. Table 11 lists the thermocouple data from all tests that had to be removed from the analysis to avoid misleading and wrong results.

Table 11. Discarded thermocouple measurements.

Test	Thermocouple position	From	To	Reason
1 (CLT)	Surface	0 s	1945 s	Sudden temperature drop (indicating thermocouple failure or falling of the thermocouple out of the heated CLT section)
	5 mm	0 s	1621 s	Sudden temperature drop (indicating thermocouple failure or falling of the thermocouple out of the heated CLT section)
4 (CLT)	5 mm 15 mm 20 mm	0 s	End	Anomalous data
10 (CLT with FRP)	5mm	0 s	End	Faulty connection of the thermocouples
11 (CLT with FRP)	Surface 5 mm	0 s	150 s	The initial surface temperature and temperature at 5mm depth were accidentally increased above ambient because the radiant panel was switched on too early. After 150 seconds, the thermocouples at 0mm and 5mm align with other test data. Thermocouples at greater depths did not seem to be affected, probably due to the short duration of the accidental pre-heating period.
12 (CLT with FRP)	15 mm	1286 s	End	Sudden temperature drop (indicating thermocouple failure or falling of the thermocouple out of the heated CLT section)
	40 mm	0 s	119 s	Anomalous data

The timeline of each test was corrected with t_{new}=0 s at the moment of ignition of the radiant panel (see section 3.2 for details on the test setup). All data after the end of

the test, i.e. when the radiant panel was switched off, was removed from further analysis.

The average temperature over time of the three repetition tests of the same sample type ('CLT' or 'CLT with FRP') at the same incident radiant heat flux (20 kW/m² or 50 kW/m²) was calculated for each thermocouple position. A time step of one second was selected for this average. For every average temperature, the minimum and maximum temperature at each time step was also determined to create error envelopes for each graph, indicating that a range of temperatures was measured rather than singular values.

Appendix III Heat transfer model

Node numbers i = 2,3,4…N-1 (with Δx = distance between neighbouring nodes)

j = time step (with Δt = duration of time step)

x=0

$$T_1^{j+1} = T_1^j + \frac{2\Delta t}{\Delta x * \rho(T) * c_P(T)}\left(a\dot{q}_e'' - h_T\left(T_1^j - T_\infty\right) + \frac{k(T)}{\Delta x}\left(T_2^j - T_1^j\right)\right)$$

With k, rho, c of timber if no GFRP and k, rho, c of GF if with glass fibres.

0<x<L (L=x6)

$$T_i^{j+1} = T_i^j + \frac{\alpha(T) * \Delta t}{\Delta x^2}\left(T_{i-1}^j - 2T_i^j + T_{i+1}^j\right)$$

x=L (L=x6)

$$T_N^{j+1} = T_N^j + \frac{2\Delta t}{\Delta x * \rho(T) * c_P(T)}\left(\frac{k(T)}{\Delta x}\left(T_{N-1}^j - T_N^j\right) + h_T\left(T_\infty - T_N^j\right)\right)$$

The duration of time steps were chosen such that stability of the solution was achieved. The impact of the time step on the results was analysed and for time steps of less than 5 seconds, no effect was seen as long as stability of the solution was maintained.

Appendix IV Char pieces from exemplary tests.

The underlying grid consists of squares with 2 mm side length.

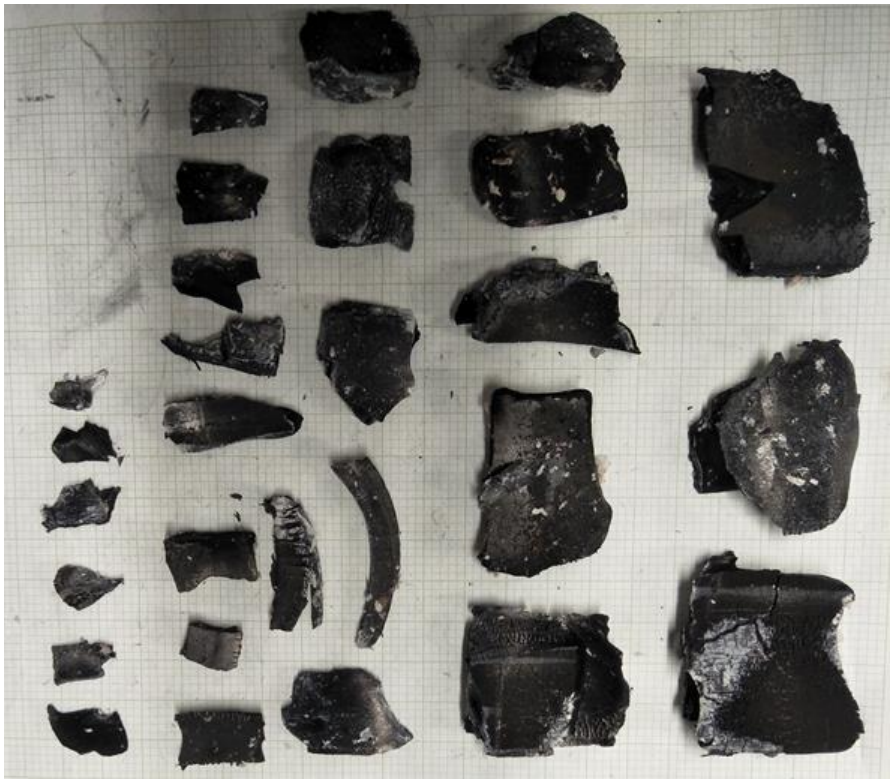

Figure 28. Fallen char from CLT without FRP at 20 kW/m² (1.CLT.P).

Figure 29. Fallen char from CLT without FRP at 20 kW/m² (2.CLT.P).

Figure 30. Fallen char from CLT without FRP at 50 kW/m² (5.CLT.P).

Figure 31. Fallen char from CLT without FRP at 50 kW/m² (6.CLT.P).

Appendix V Measured temperature evolution over time within the CLT sections.

The following plots show the individual thermocouple measurements that were presented as average curves in Figure 18 and Figure 19 and analysed further throughout Chapter 4 The labels used to distinguish between repetition tests are listed in Table 12.

Table 12. Experimental matrix with legend for sample labels.

Sample type	Incident heat flux[2]	Test number	Label
CLT	20 kW/m²	1	1.CLT.P
		2	2.CLT.P
		3	3.CLT.P
	50 kW/m²	4	4.CLT.P
		5	5.CLT.P
		6	6.CLT.P
CLT with FRP	20 kW/m²	7	1.FRP.P
		8	2.FRP.P
		9	3.FRP.P
	50 kW/m²	10	4.FRP.P
		11	5.FRP.P
		12	6.FRP.P

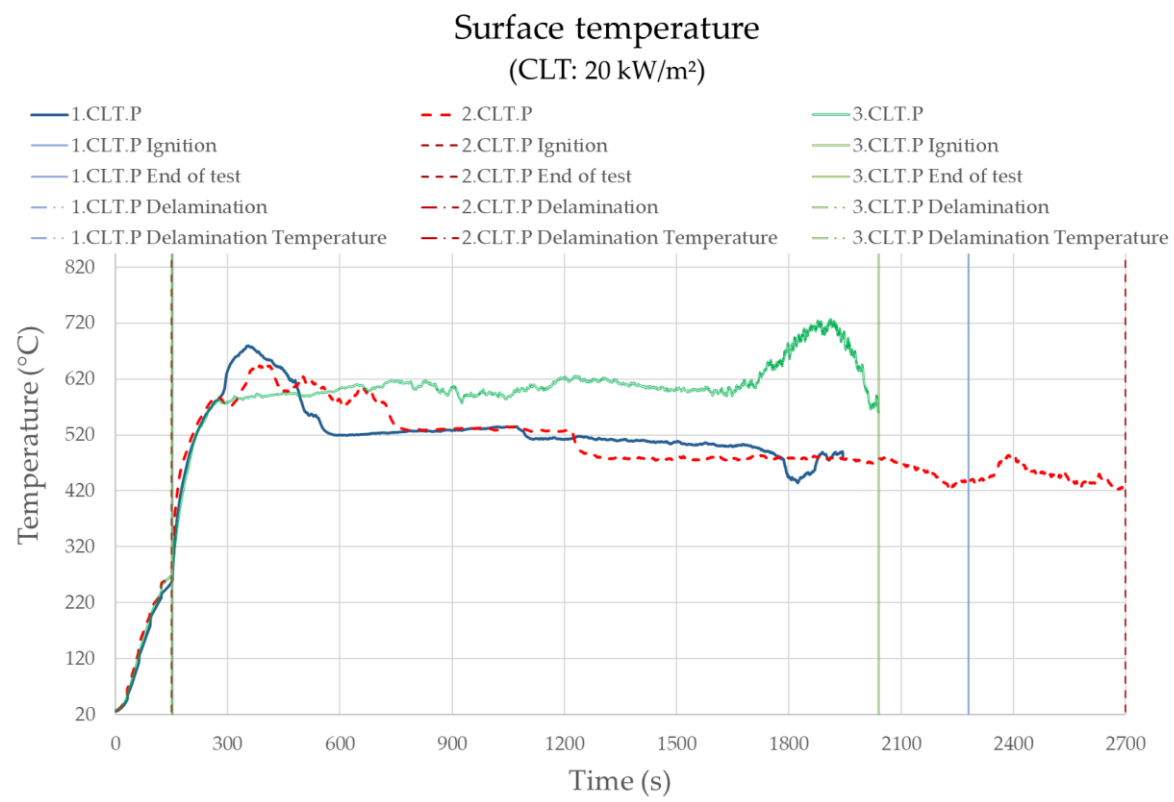
Surface temperature
(CLT: 20 kW/m²)
1.CLT.P
2.CLT.P
3.CLT.P
1.CLT.P Ignition
2.CLT.P Ignition
3.CLT.P Ignition
1.CLT.P End of test
2.CLT.P End of test
3.CLT.P End of test
1.CLT.P Delamination
2.CLT.P Delamination
3.CLT.P Delamination
1.CLT.P Delamination Temperature
2.CLT.P Delamination Temperature
3.CLT.P Delamination Temperature
Temperature (°C)
820
720
620
520
420
320
220
120
20
0
300
600
900
1200
1500
1800
2100
2400
2700
Time (s)

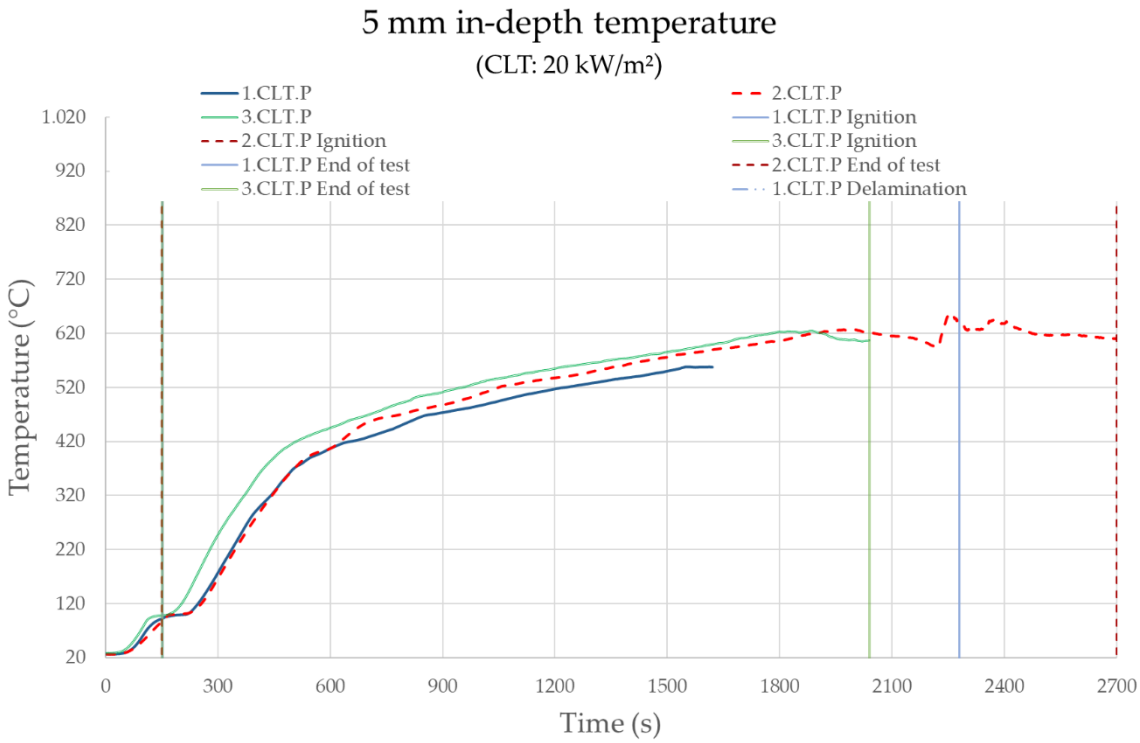
5 mm in-depth temperature
(CLT: 20 kW/m²)
1.CLT.P
2.CLT.P
3.CLT.P
1.CLT.P Ignition
2.CLT.P Ignition
3.CLT.P Ignition
1.CLT.P End of test
2.CLT.P End of test
3.CLT.P End of test
1.CLT.P Delamination
Temperature (°C)
1.020
920
820
720
620
520
420
320
220
120
20
0
300
600
900
1200
1500
1800
2100
2400
2700
Time (s)

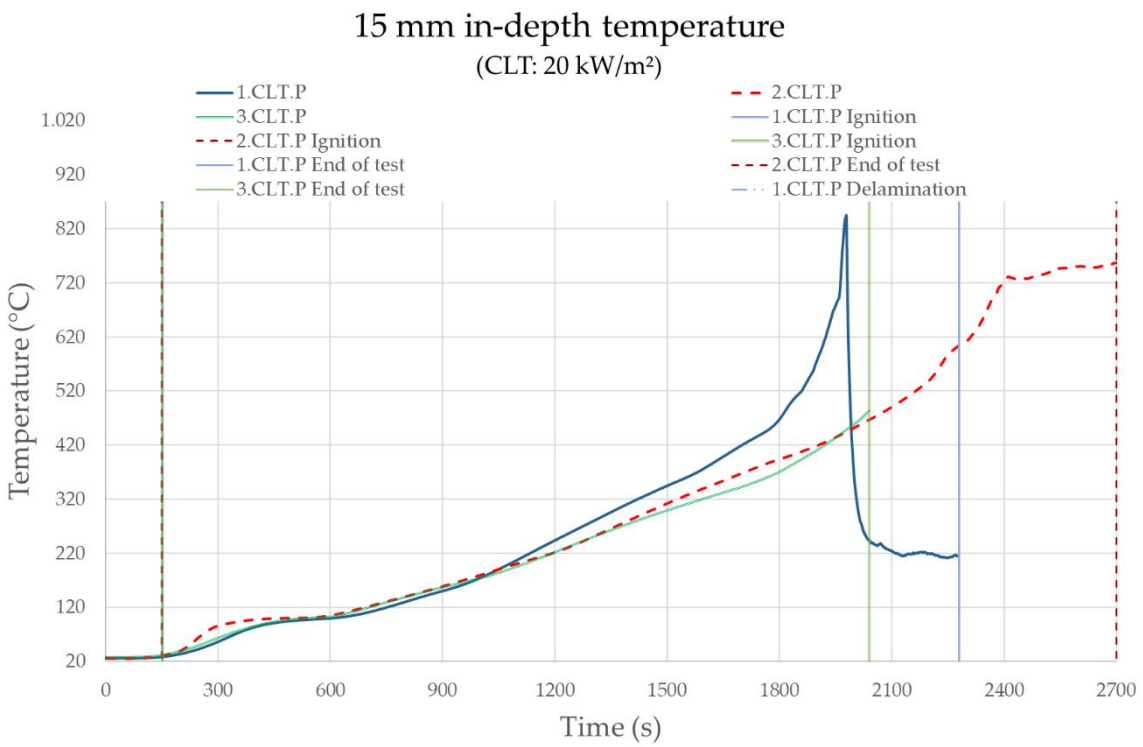
15 mm in-depth temperature
(CLT: 20 kW/m²)
1.CLT.P
2.CLT.P
3.CLT.P
1.CLT.P Ignition
2.CLT.P Ignition
3.CLT.P Ignition
1.CLT.P End of test
2.CLT.P End of test
3.CLT.P End of test
1.CLT.P Delamination
Temperature (°C)
Time (s)

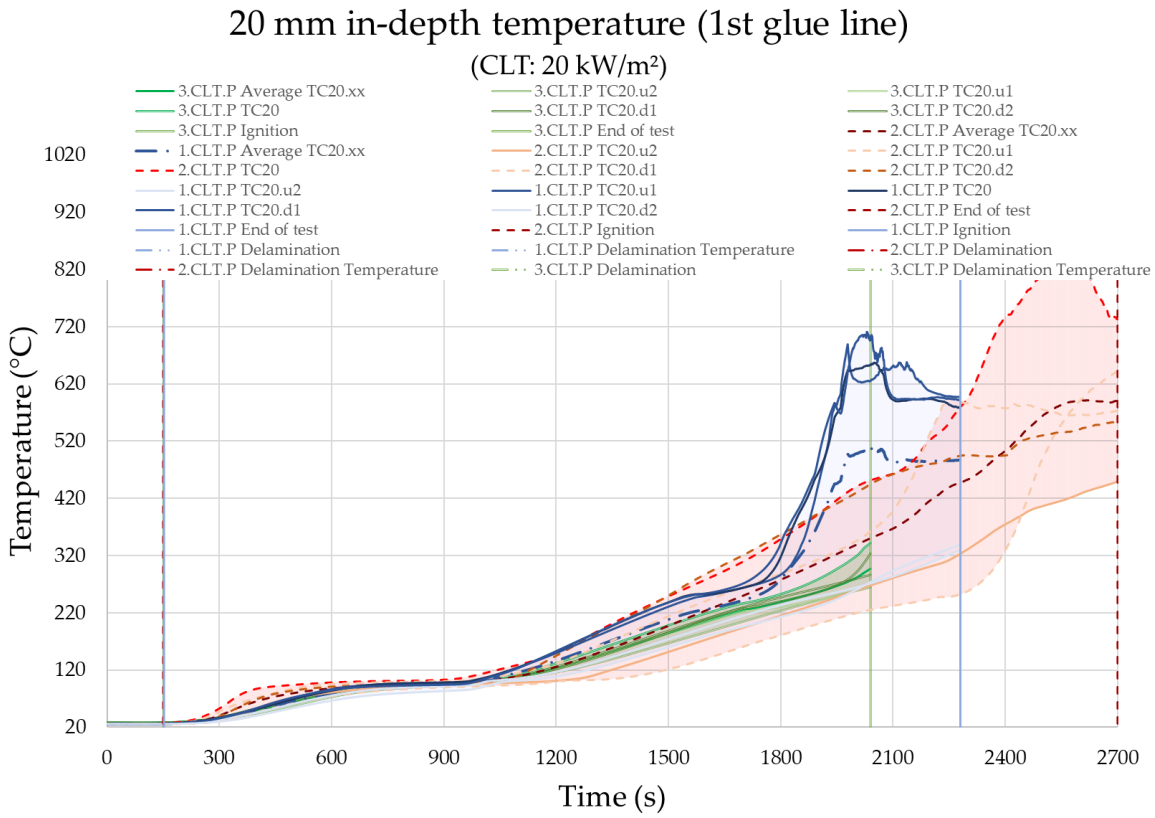
20 mm in-depth temperature (1st glue line)
(CLT: 20 kW/m²)
3.CLT.P Average TC20.xx
3.CLT.P TC20.u2
3.CLT.P TC20.u1
3.CLT.P TC20
3.CLT.P TC20.d1
3.CLT.P TC20.d2
3.CLT.P Ignition
3.CLT.P End of test
2.CLT.P Average TC20.xx
1.CLT.P Average TC20.xx
2.CLT.P TC20.u2
2.CLT.P TC20.u1
2.CLT.P TC20
2.CLT.P TC20.d1
2.CLT.P TC20.d2
1.CLT.P TC20.u2
1.CLT.P TC20.u1
1.CLT.P TC20
1.CLT.P TC20.d1
1.CLT.P TC20.d2
2.CLT.P End of test
1.CLT.P End of test
2.CLT.P Ignition
1.CLT.P Ignition
1.CLT.P Delamination
1.CLT.P Delamination Temperature
2.CLT.P Delamination
2.CLT.P Delamination Temperature
3.CLT.P Delamination
3.CLT.P Delamination Temperature
Temperature (°C)
Time (s)

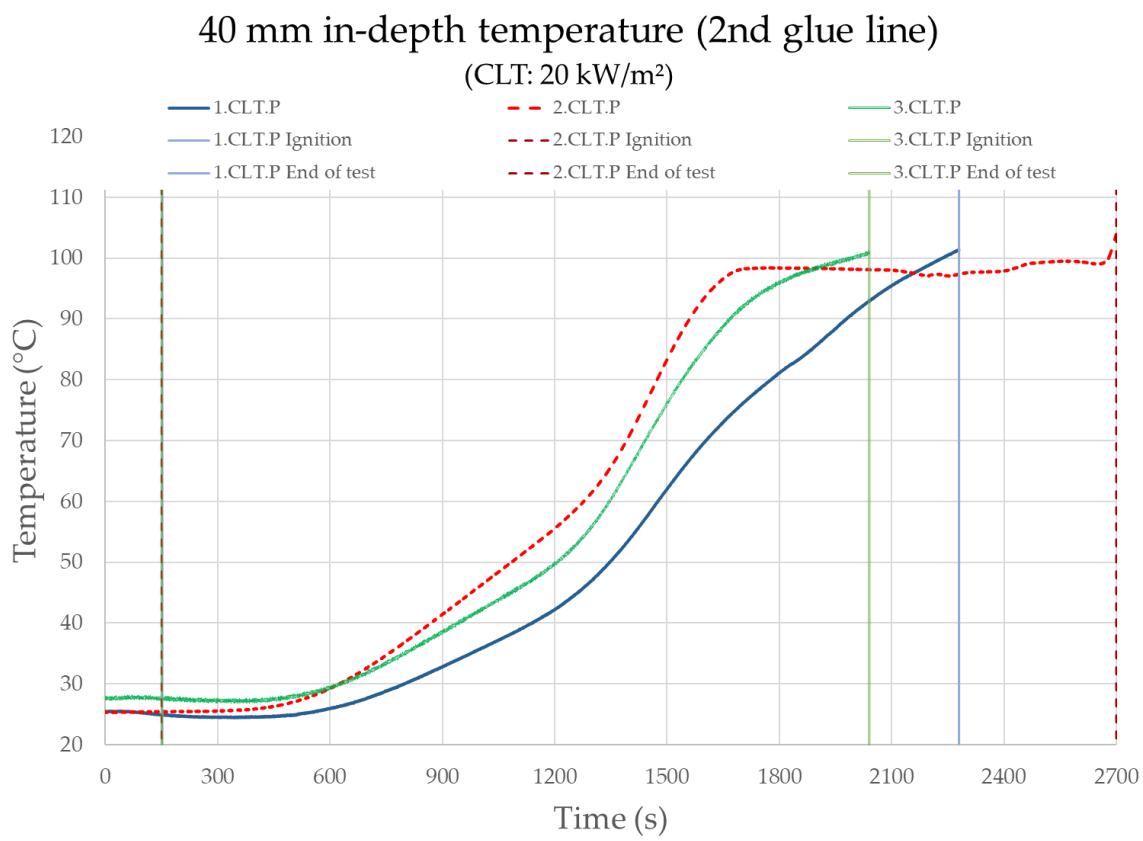
40 mm in-depth temperature (2nd glue line)
(CLT: 20 kW/m²)
1.CLT.P
2.CLT.P
3.CLT.P
1.CLT.P Ignition
2.CLT.P Ignition
3.CLT.P Ignition
1.CLT.P End of test
2.CLT.P End of test
3.CLT.P End of test
Temperature (°C)
Time (s)

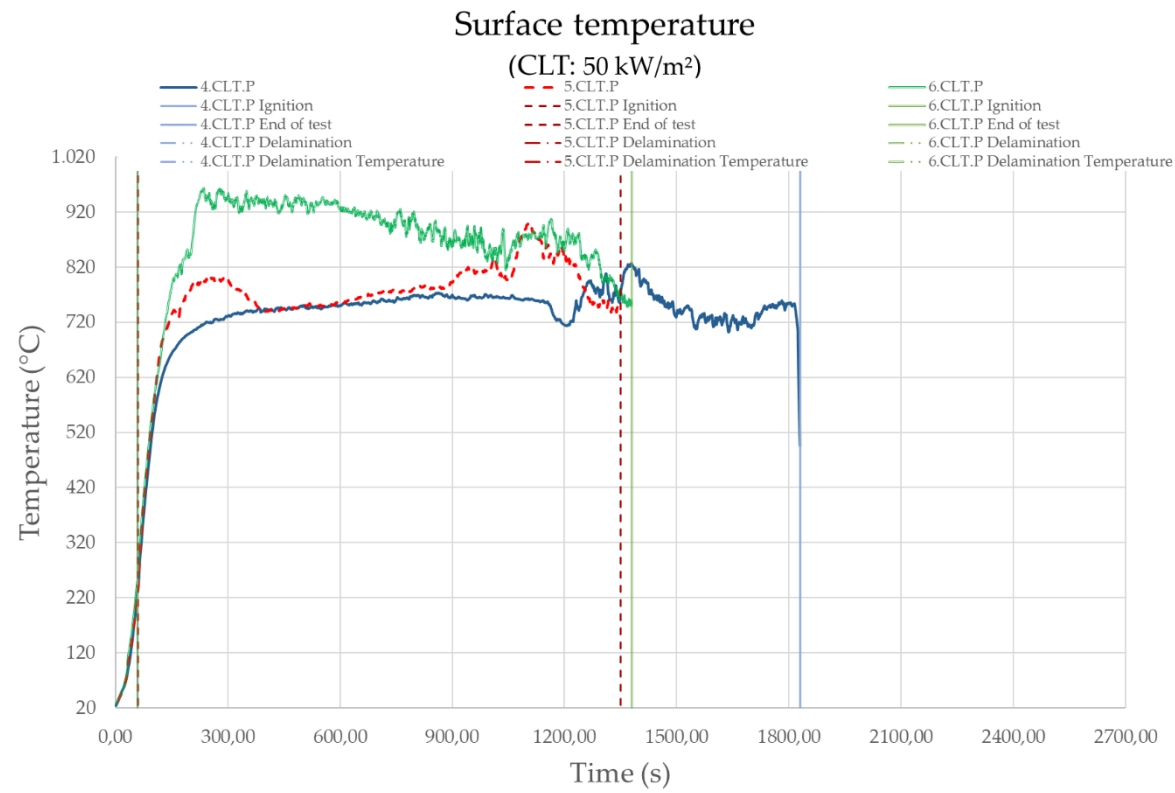
Surface temperature
(CLT: 50 kW/m²)
4.CLT.P
5.CLT.P
6.CLT.P
4.CLT.P Ignition
5.CLT.P Ignition
6.CLT.P Ignition
4.CLT.P End of test
5.CLT.P End of test
6.CLT.P End of test
4.CLT.P Delamination
5.CLT.P Delamination
6.CLT.P Delamination
4.CLT.P Delamination Temperature
5.CLT.P Delamination Temperature
6.CLT.P Delamination Temperature
Temperature (°C)
Time (s)

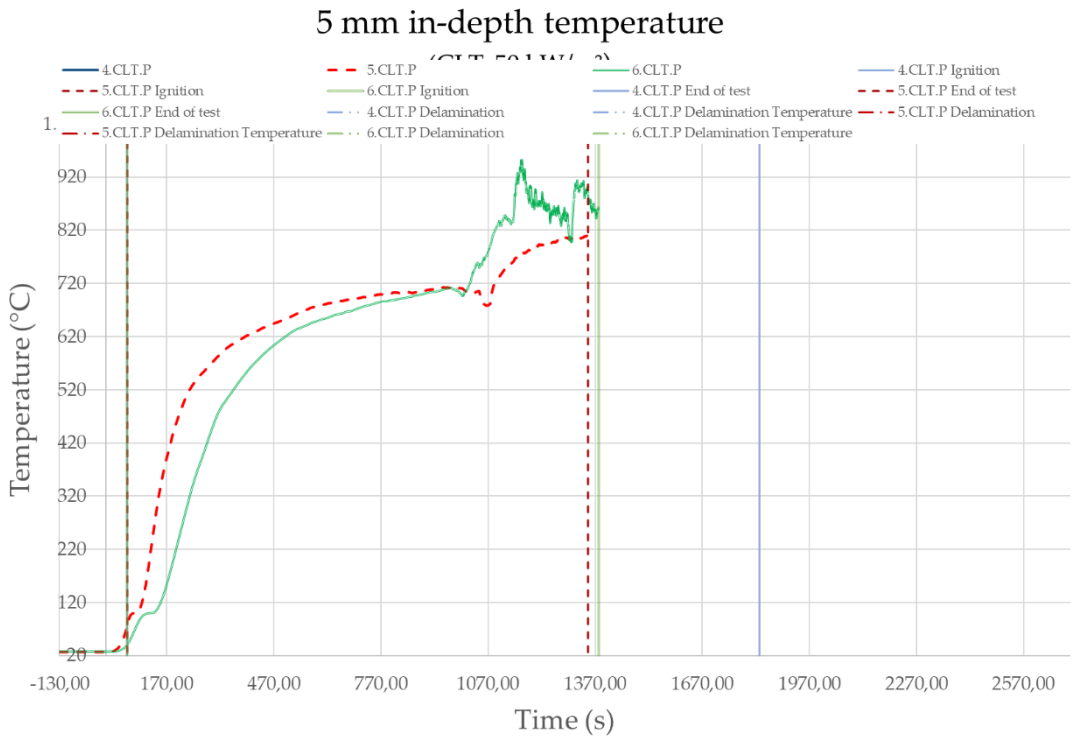
5 mm in-depth temperature
4.CLT.P
5.CLT.P
6.CLT.P
4.CLT.P Ignition
5.CLT.P Ignition
6.CLT.P Ignition
4.CLT.P End of test
5.CLT.P End of test
6.CLT.P End of test
4.CLT.P Delamination
5.CLT.P Delamination
6.CLT.P Delamination
4.CLT.P Delamination Temperature
5.CLT.P Delamination Temperature
6.CLT.P Delamination Temperature
Temperature (°C)
920
820
720
620
520
420
320
220
120
-130,00
170,00
470,00
770,00
1070,00
1370,00
1670,00
1970,00
2270,00
2570,00
Time (s)

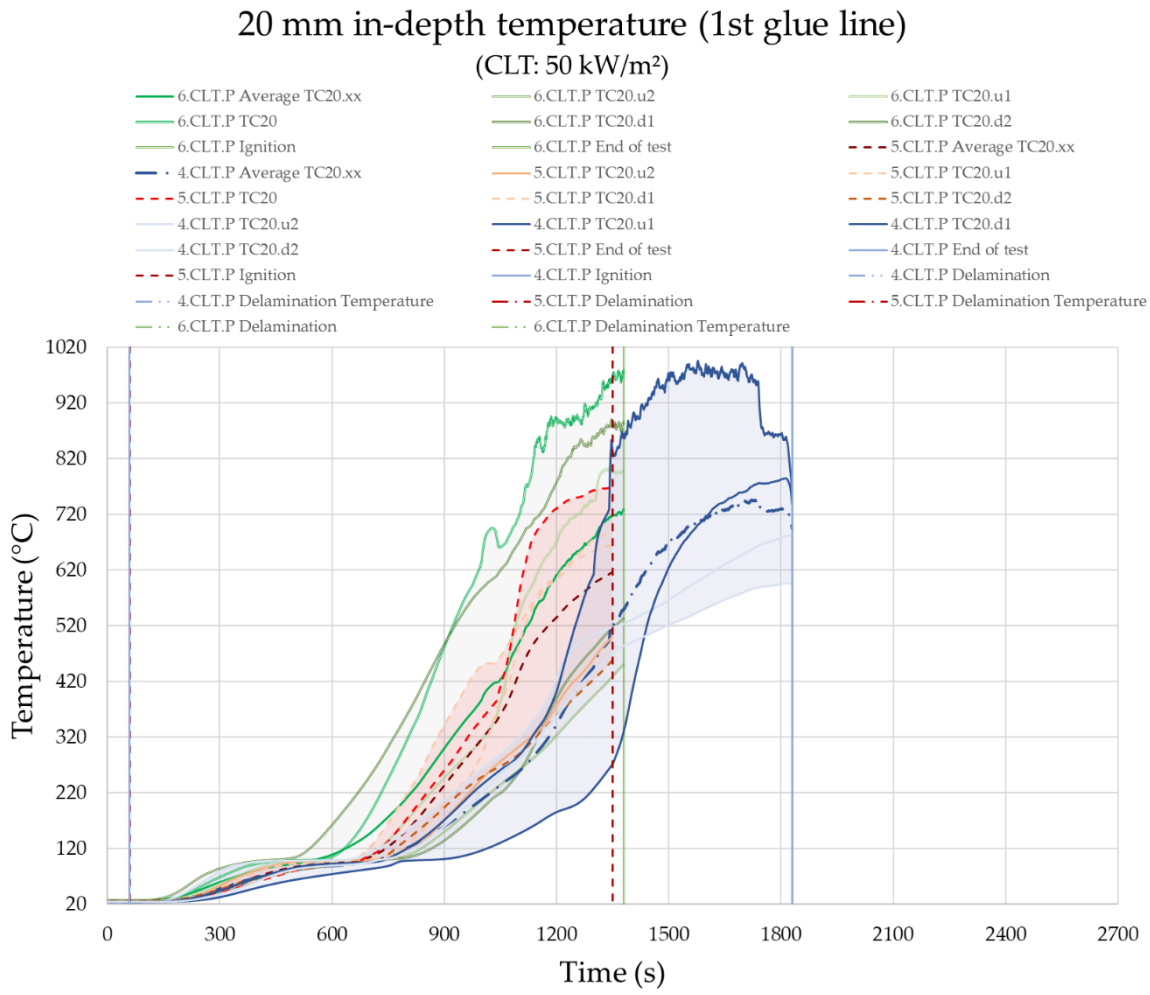
20 mm in-depth temperature (1st glue line)
(CLT: 50 kW/m²)
6.CLT.P Average TC20.xx
6.CLT.P TC20.u2
6.CLT.P TC20.u1
6.CLT.P TC20
6.CLT.P TC20.d1
6.CLT.P TC20.d2
6.CLT.P Ignition
6.CLT.P End of test
5.CLT.P Average TC20.xx
4.CLT.P Average TC20.xx
5.CLT.P TC20.u2
5.CLT.P TC20.u1
5.CLT.P TC20
5.CLT.P TC20.d1
5.CLT.P TC20.d2
4.CLT.P TC20.u2
4.CLT.P TC20.u1
4.CLT.P TC20.d1
4.CLT.P TC20.d2
5.CLT.P End of test
4.CLT.P End of test
5.CLT.P Ignition
4.CLT.P Ignition
4.CLT.P Delamination
4.CLT.P Delamination Temperature
5.CLT.P Delamination
5.CLT.P Delamination Temperature
6.CLT.P Delamination
6.CLT.P Delamination Temperature
Temperature (°C)
1020
920
820
720
620
520
420
320
220
120
20
0
300
600
900
1200
1500
1800
2100
2400
2700
Time (s)

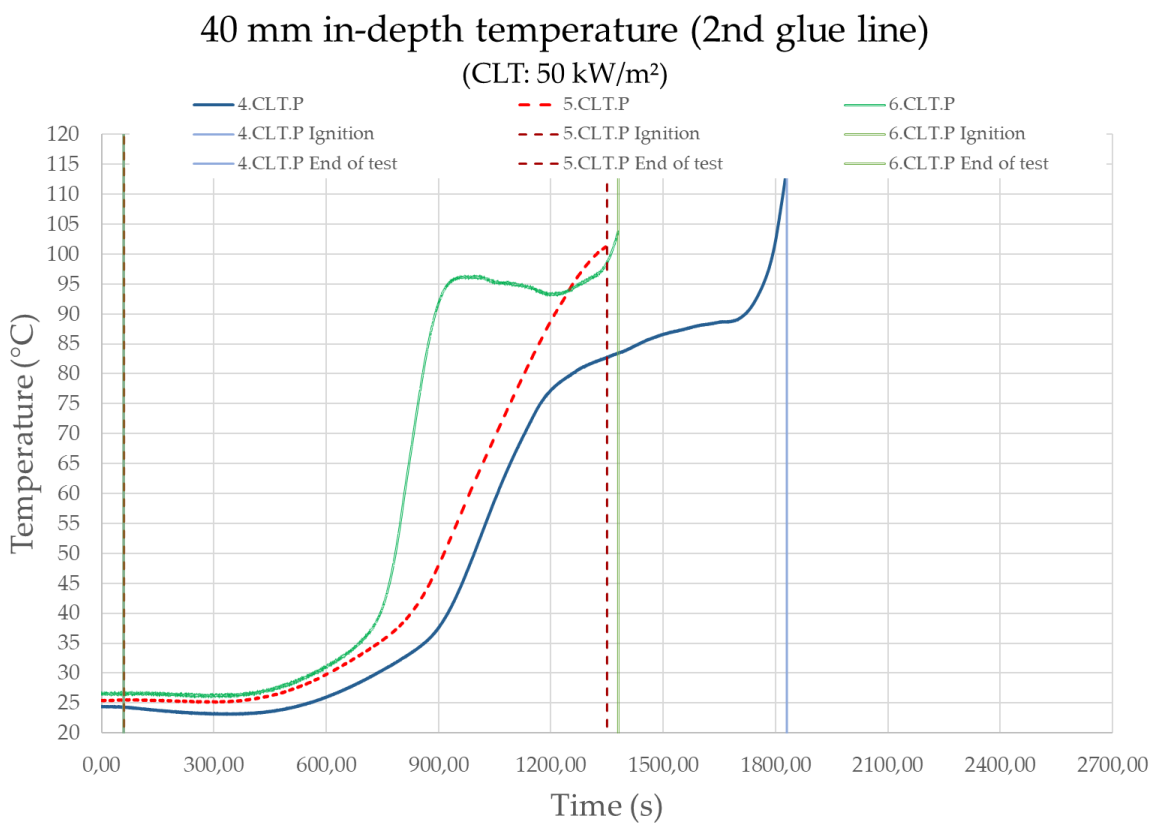
40 mm in-depth temperature (2nd glue line)
(CLT: 50 kW/m²)
4.CLT.P
5.CLT.P
6.CLT.P
4.CLT.P Ignition
5.CLT.P Ignition
6.CLT.P Ignition
4.CLT.P End of test
5.CLT.P End of test
6.CLT.P End of test
Temperature (°C)
Time (s)

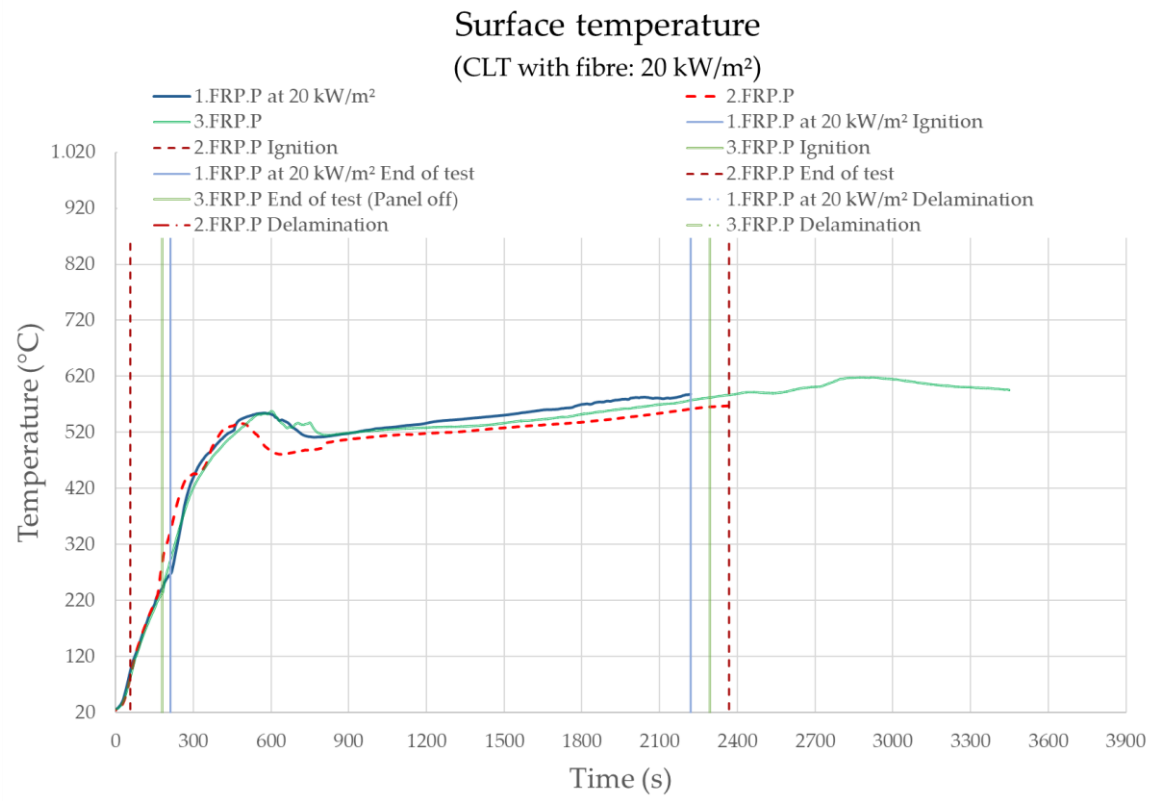
Surface temperature
(CLT with fibre: 20 kW/m²)
1.FRP.P at 20 kW/m²
2.FRP.P
3.FRP.P
1.FRP.P at 20 kW/m² Ignition
2.FRP.P Ignition
3.FRP.P Ignition
1.FRP.P at 20 kW/m² End of test
2.FRP.P End of test
3.FRP.P End of test (Panel off)
1.FRP.P at 20 kW/m² Delamination
2.FRP.P Delamination
3.FRP.P Delamination
Temperature (°C)
Time (s)

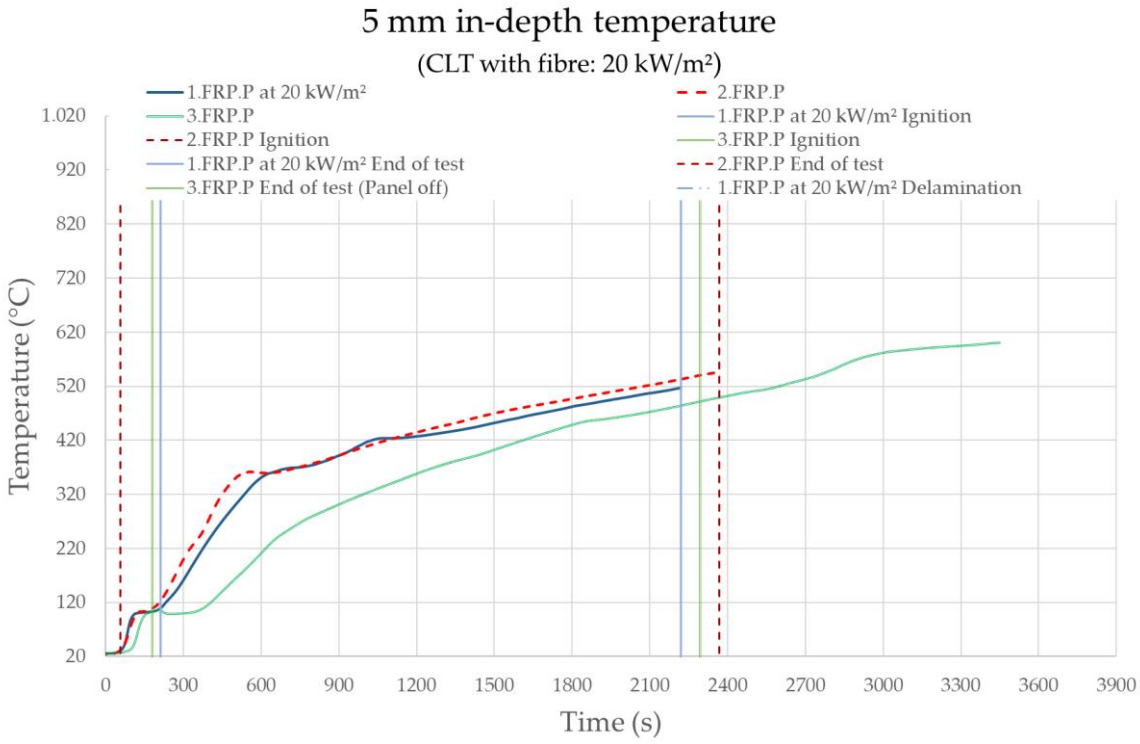
5 mm in-depth temperature
(CLT with fibre: 20 kW/m²)
1.FRP.P at 20 kW/m²
2.FRP.P
3.FRP.P
1.FRP.P at 20 kW/m² Ignition
2.FRP.P Ignition
3.FRP.P Ignition
1.FRP.P at 20 kW/m² End of test
2.FRP.P End of test
3.FRP.P End of test (Panel off)
1.FRP.P at 20 kW/m² Delamination
Temperature (°C)
1.020
920
820
720
620
520
420
320
220
120
20
0
300
600
900
1200
1500
1800
2100
2400
2700
3000
3300
3600
3900
Time (s)

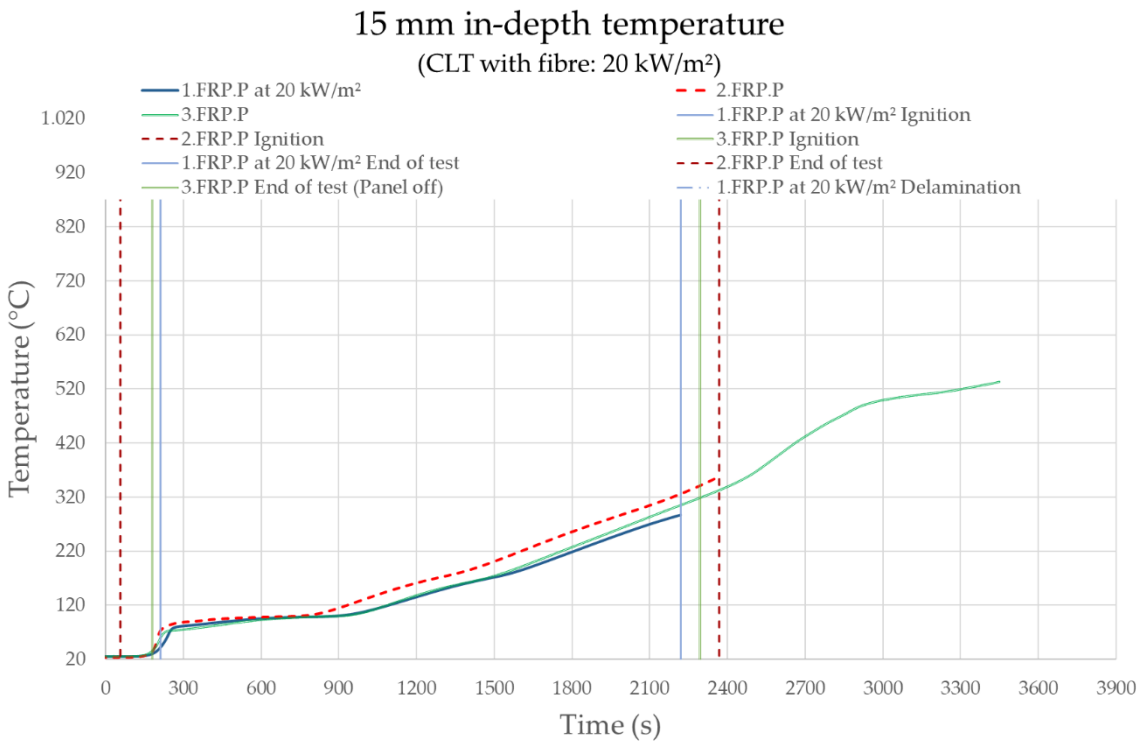
15 mm in-depth temperature
(CLT with fibre: 20 kW/m²)
1.FRP.P at 20 kW/m²
2.FRP.P
3.FRP.P
1.FRP.P at 20 kW/m² Ignition
2.FRP.P Ignition
3.FRP.P Ignition
1.FRP.P at 20 kW/m² End of test
2.FRP.P End of test
3.FRP.P End of test (Panel off)
1.FRP.P at 20 kW/m² Delamination
Temperature (°C)
1.020
920
820
720
620
520
420
320
220
120
20
0
300
600
900
1200
1500
1800
2100
2400
2700
3000
3300
3600
3900
Time (s)

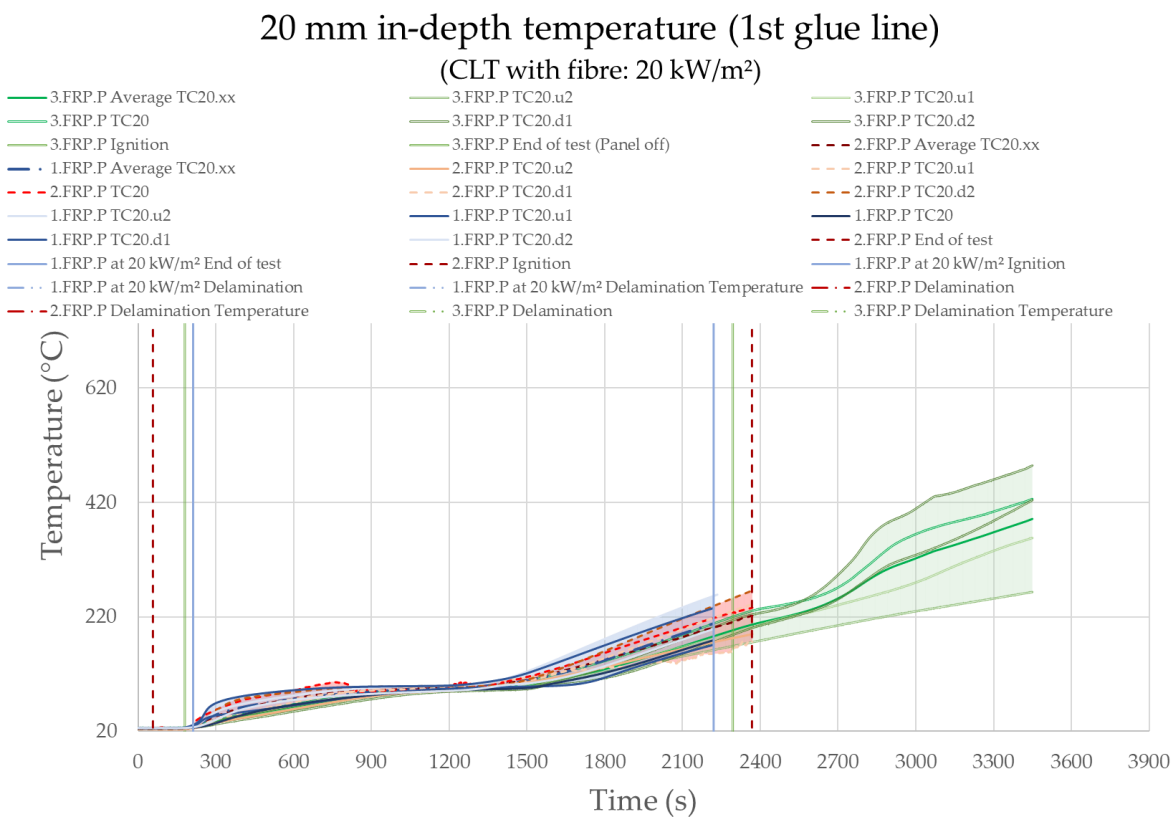
20 mm in-depth temperature (1st glue line)
(CLT with fibre: 20 kW/m²)
3.FRP.P Average TC20.xx
3.FRP.P TC20.u2
3.FRP.P TC20.u1
3.FRP.P TC20
3.FRP.P TC20.d1
3.FRP.P TC20.d2
3.FRP.P Ignition
3.FRP.P End of test (Panel off)
2.FRP.P Average TC20.xx
1.FRP.P Average TC20.xx
2.FRP.P TC20.u2
2.FRP.P TC20.u1
2.FRP.P TC20
2.FRP.P TC20.d1
2.FRP.P TC20.d2
1.FRP.P TC20.u2
1.FRP.P TC20.u1
1.FRP.P TC20
1.FRP.P TC20.d1
1.FRP.P TC20.d2
2.FRP.P End of test
1.FRP.P at 20 kW/m² End of test
2.FRP.P Ignition
1.FRP.P at 20 kW/m² Ignition
1.FRP.P at 20 kW/m² Delamination
1.FRP.P at 20 kW/m² Delamination Temperature
2.FRP.P Delamination
2.FRP.P Delamination Temperature
3.FRP.P Delamination
3.FRP.P Delamination Temperature
Temperature (°C)
620
420
220
20
0
300
600
900
1200
1500
1800
2100
2400
2700
3000
3300
3600
3900
Time (s)

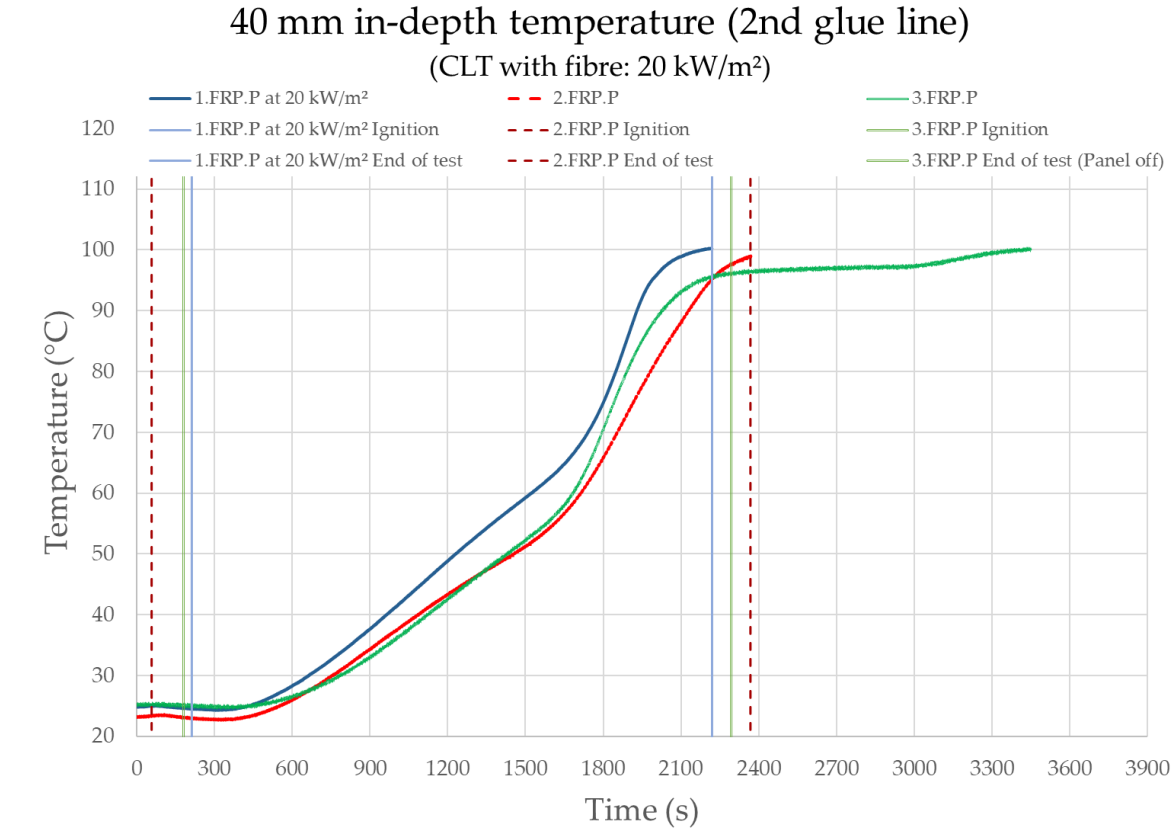
40 mm in-depth temperature (2nd glue line)
(CLT with fibre: 20 kW/m²)
1.FRP.P at 20 kW/m²
2.FRP.P
3.FRP.P
1.FRP.P at 20 kW/m² Ignition
2.FRP.P Ignition
3.FRP.P Ignition
1.FRP.P at 20 kW/m² End of test
2.FRP.P End of test
3.FRP.P End of test (Panel off)
Temperature (°C)
120
110
100
90
80
70
60
50
40
30
20
0
300
600
900
1200
1500
1800
2100
2400
2700
3000
3300
3600
3900
Time (s)

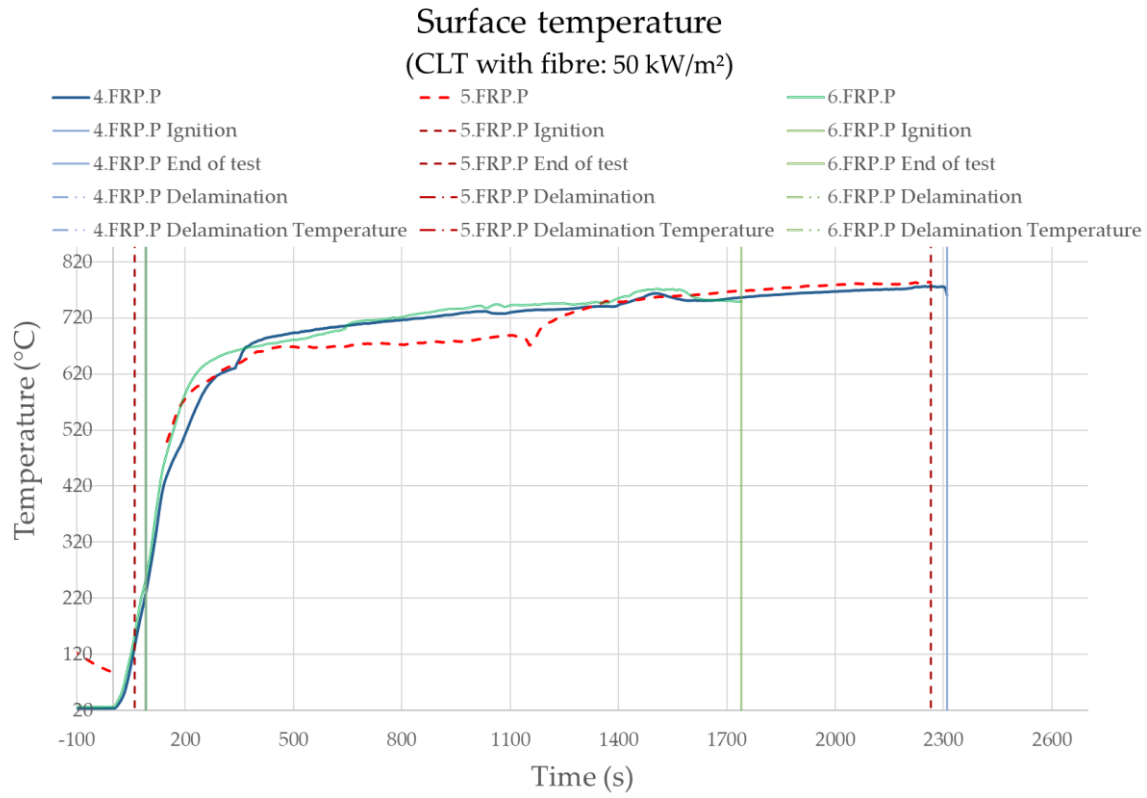
Surface temperature
(CLT with fibre: 50 kW/m²)
4.FRP.P
5.FRP.P
6.FRP.P
4.FRP.P Ignition
5.FRP.P Ignition
6.FRP.P Ignition
4.FRP.P End of test
5.FRP.P End of test
6.FRP.P End of test
4.FRP.P Delamination
5.FRP.P Delamination
6.FRP.P Delamination
4.FRP.P Delamination Temperature
5.FRP.P Delamination Temperature
6.FRP.P Delamination Temperature
Temperature (°C)
820
720
620
520
420
320
220
120
20
-100
200
500
800
1100
1400
1700
2000
2300
2600
Time (s)

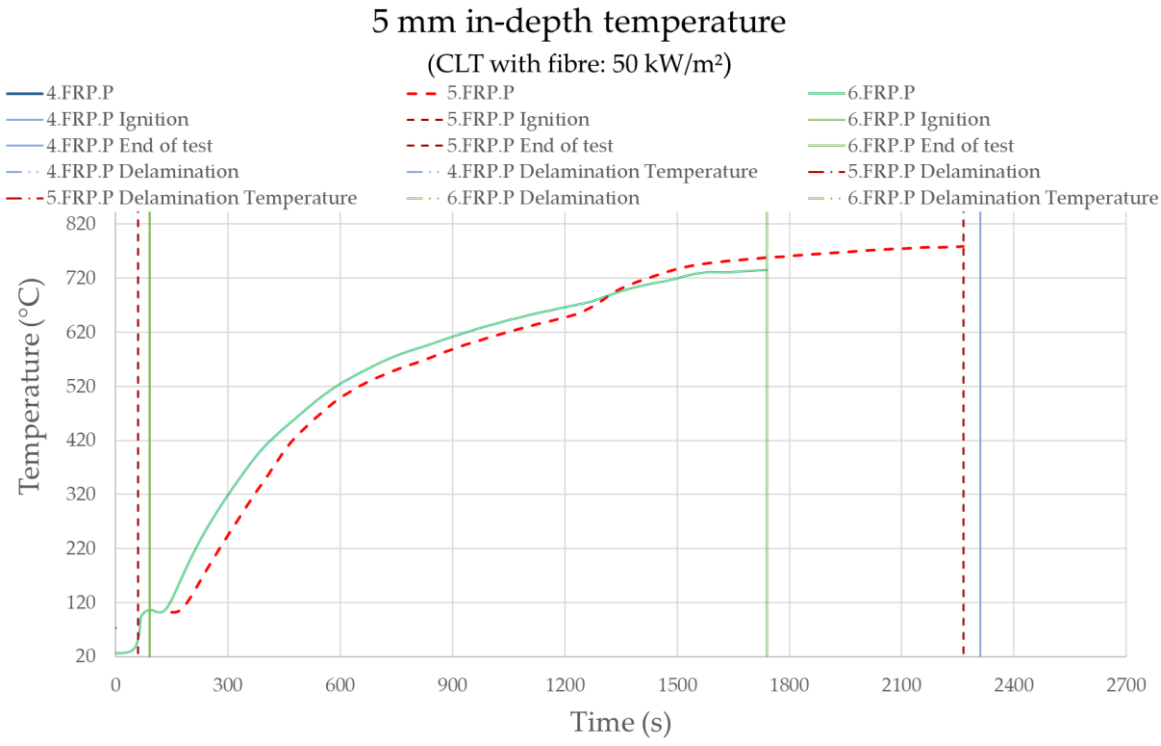
5 mm in-depth temperature
(CLT with fibre: 50 kW/m²)
4.FRP.P
5.FRP.P
6.FRP.P
4.FRP.P Ignition
5.FRP.P Ignition
6.FRP.P Ignition
4.FRP.P End of test
5.FRP.P End of test
6.FRP.P End of test
4.FRP.P Delamination
4.FRP.P Delamination Temperature
5.FRP.P Delamination
5.FRP.P Delamination Temperature
6.FRP.P Delamination
6.FRP.P Delamination Temperature
Temperature (°C)
820
720
620
520
420
320
220
120
20
0
300
600
900
1200
1500
1800
2100
2400
2700
Time (s)

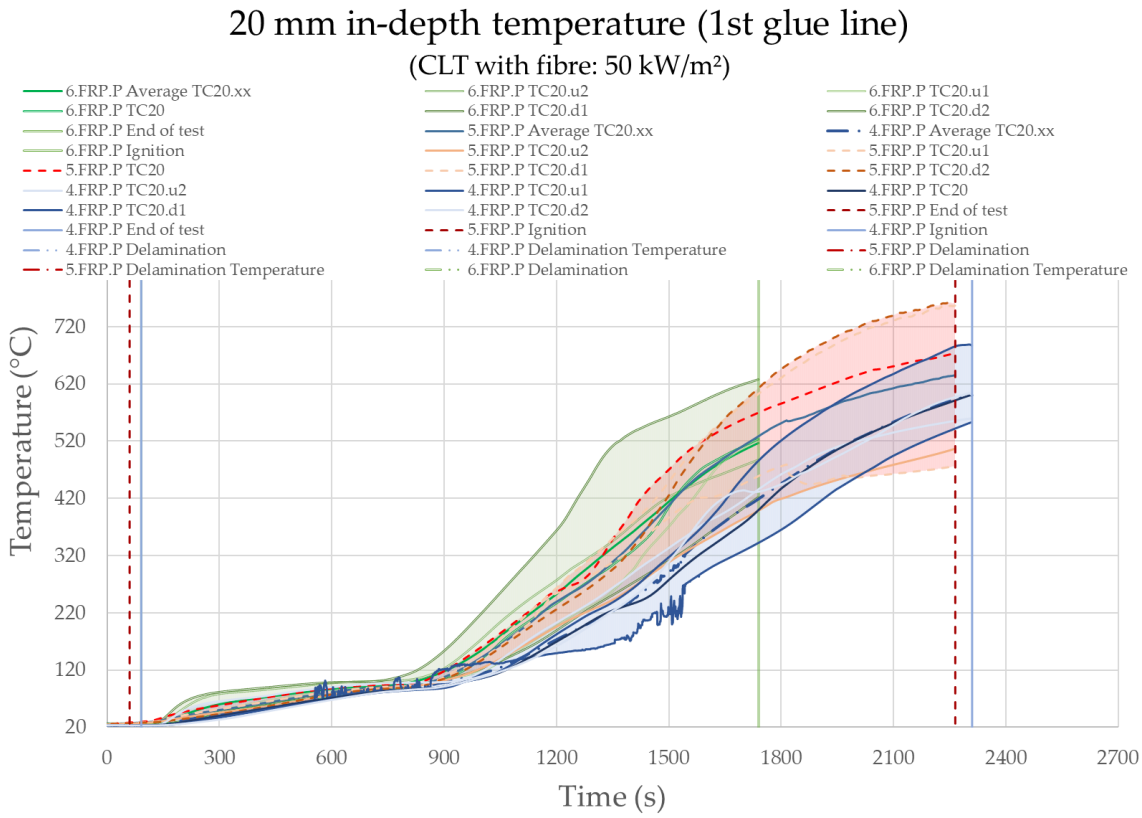
20 mm in-depth temperature (1st glue line)
(CLT with fibre: 50 kW/m²)
6.FRP.P Average TC20.xx
6.FRP.P TC20.u2
6.FRP.P TC20.u1
6.FRP.P TC20
6.FRP.P TC20.d1
6.FRP.P TC20.d2
6.FRP.P End of test
5.FRP.P Average TC20.xx
4.FRP.P Average TC20.xx
6.FRP.P Ignition
5.FRP.P TC20.u2
5.FRP.P TC20.u1
5.FRP.P TC20
5.FRP.P TC20.d1
5.FRP.P TC20.d2
4.FRP.P TC20.u2
4.FRP.P TC20.u1
4.FRP.P TC20
4.FRP.P TC20.d1
4.FRP.P TC20.d2
5.FRP.P End of test
4.FRP.P End of test
5.FRP.P Ignition
4.FRP.P Ignition
4.FRP.P Delamination
4.FRP.P Delamination Temperature
5.FRP.P Delamination
5.FRP.P Delamination Temperature
6.FRP.P Delamination
6.FRP.P Delamination Temperature
Temperature (°C)
720
620
520
420
320
220
120
20
0
300
600
900
1200
1500
1800
2100
2400
2700
Time (s)

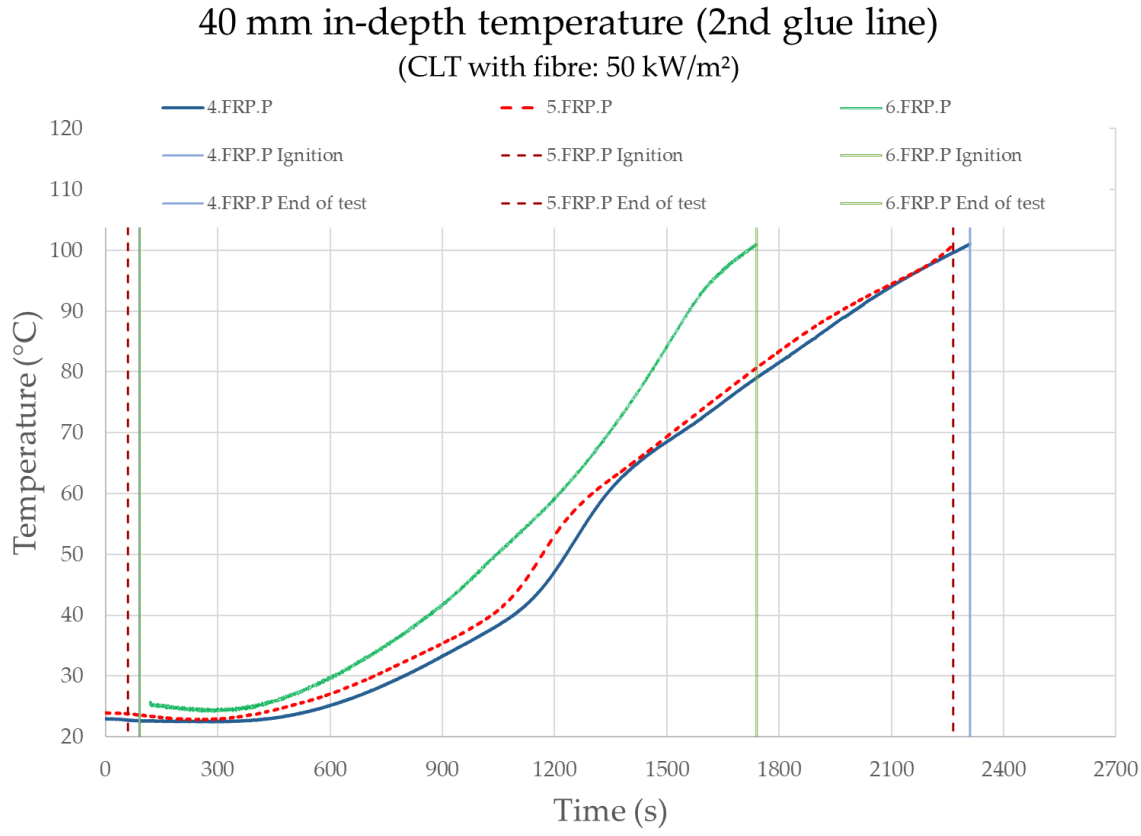
40 mm in-depth temperature (2nd glue line)
(CLT with fibre: 50 kW/m²)
4.FRP.P
5.FRP.P
6.FRP.P
4.FRP.P Ignition
5.FRP.P Ignition
6.FRP.P Ignition
4.FRP.P End of test
5.FRP.P End of test
6.FRP.P End of test
Temperature (°C)
120
110
100
90
80
70
60
50
40
30
20
0
300
600
900
1200
1500
1800
2100
2400
2700
Time (s)

Appendix VI Temperature gradient in the CLT section at different times

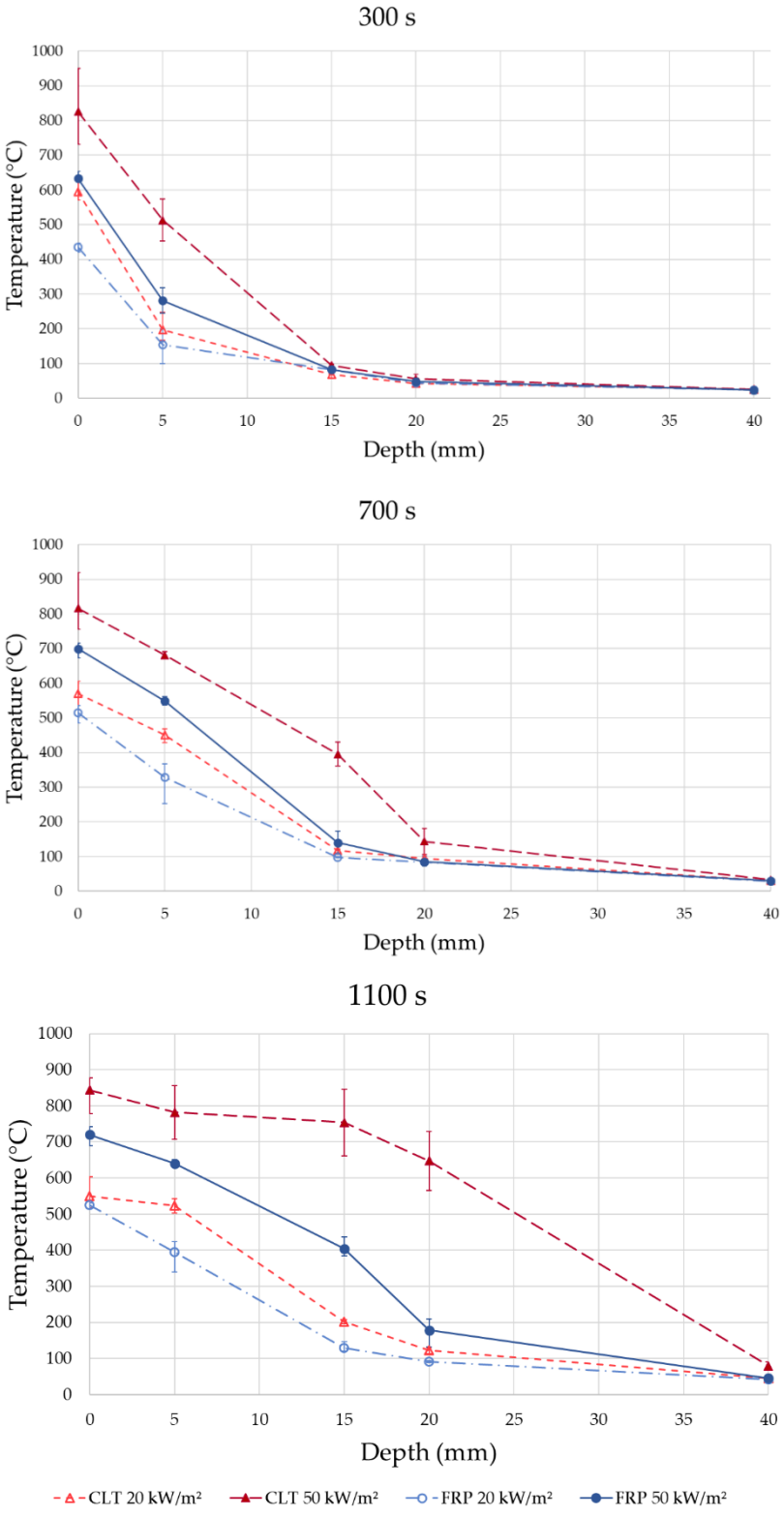

Figure 32. Temperature gradient within the timber section at different times.